INFORMATION TO USERS

This manuscript has been reproduced from the microfilm master. UMI films the text directly from the original or copy submitted. Thus, some thesis and dissertation copies are in typewriter face, while others may be from any type of computer printer.

The quality of this reproduction is dependent upon the quality of the copy submitted. Broken or indistinct print, colored or poor quality illustrations and photographs, print bleedthrough, substandard margins, and improper alignment can adversely affect reproduction.

In the unlikely event that the author did not send UMI a complete manuscript and there are missing pages, these will be noted. Also, if unauthorized copyright material had to be removed, a note will indicate the deletion.

Oversize materials (e.g., maps, drawings, charts) are reproduced by sectioning the original, beginning at the upper left-hand corner and continuing from left to right in equal sections with small overlaps.

ProQuest Information and Learning
300 North Zeeb Road, Ann Arbor, MI 48106-1346 USA
800-521-0600

University of Alberta

INTEGRATED METHODS FOR RAPID GENETIC ANALYSIS USING MICROFLUIDIC DEVICES

by

Golnaz Vahedi 

A thesis submitted to the Faculty of Graduate Studies and Research in partial fulfillment of the requirements for the degree of **Master of Science**.

Department of Electrical and Computer Engineering

Edmonton, Alberta

Spring 2005

Dedicated to Simin and Mahdi, my dear parents

Abstract

In this work, we developed novel techniques for genetic analysis of nuclear DNA and mitochondrial DNA on microchips. In the first chapter of this work, the background chapter, we explain various concepts used in the rest of the thesis. In the second chapter, we developed a method for mutation detection of PCR products and we integrated both labeling and denaturation of DNA on the chip. In the third chapter, we proposed a labeling method which may be capable of increasing the resolution of separations. Although the expected results were not obtained, the idea for on-chip labeling may increase the resolution and sensitivity of mutation detection techniques.

Mutations in mitochondrial DNA may play an important role in some diseases, such as Parkinson's and Alzheimer's. In the last chapter of the thesis, we introduced preliminary work toward the development of a novel mtDNA purification method that will be used in the analysis of the mitochondrial DNA. We also tried to develop a protocol used for sizing of mtDNA as the first step toward the on-chip characterization of mtDNA. Although the presented results in this chapter are promising, there are some issues to be resolved before this technique can be used in lab-on-a-chip technology.

Acknowledgements

I would like to thank Dr. Christopher Backhouse for his great guidance and support. I would also like to thank Dr. Koles and Dr. Glerum, the members of my defense committee. I am grateful to Dr. Dammika Manage and Alex Stickel for their ideas and assistance. I also thank the staff and students at the Backhouse lab for helping me through my research.

I would like to extend my thanks to my parents, for their endless love and support through years.

Contents

List of Tables

List of Figures

List of Abbreviations

A	Adenine
bp	base pair
C	Cytosine
CE	Capillary Electrophoresis
DNA	Deoxyribonucleic acid
DNAse	Deoxynuclease
dsDNA	Double-stranded DNA
FWHM	Full-width-half-max
G	Guanine
HA	Heteroduplex Analysis
ins	insertion
KSS	Kearns-Sayre Syndrome
LHON	Leber's hereditary optic neuropathy
LIF	Laser-induced fluorescence
LOC	Lab-on-a-chip
MERRF	Myoclonic epilepsy with ragged-red fibers
MELAS	Mitochondrial encephalopathy lactic acidosis and stroke-like episodes
mRNA	Messenger RNA
mtDNA	Mitochondrial DNA
PCR	Polymerase Chain Reaction
PDMA	Polydimethylacrylamide
PDMS	Polydimethyl siloxane
RNA	Ribonucleic Acid

SSCP	Single-stranded conformation polymorphism
ssDNA	Single-stranded DNA
RNAse	Ribonuclease
rRNA	Ribosomal RNA
T	Thymine
tRNA	Transfer RNA
TBE	Tris Borate with EDTA
WT	Wildtype

Chapter 1

Background

1.1 Nucleotides and Nucleic Acids

1.1.1 DNA Structure

One of the major kinds of macromolecules within cells is the nucleic acid. Nucleic acids, coming in two varieties: deoxyribonucleic acid (DNA) and ribonucleic acid (RNA), serve as the information storage devices of cells. DNA is often referred to as the hereditary material since the information that specifies what an organism is like can be copied and passed down to its descendants by DNA replication. The alternative form of nucleic acid, RNA, plays an intermediary role in converting the information contained in DNA into proteins [2].

Nucleic acids are long polymers of subunits called nucleotides. Each nucleotide consists of a sugar (deoxyribose), a nitrogen containing base attached to the sugar, and a phosphate group. Four different types of nucleotides have been found in DNA, which differ only in the nitrogenous base. They are given one-letter abbreviations as shorthand for the four bases: A for adenine, G for guanine, C for cytosine, and T for thymine. The deoxyribose sugar of the DNA backbone has 5 carbons and 3 oxygens. The carbon atoms are numbered 1, 2, 3, 4, and 5 to distinguish from the numbering of the atoms of the base rings. The hydroxyl groups on the 5- and 3- carbons link to the phosphate groups to form the DNA

backbone [2].

Watson and Crick first discovered the structure of DNA double helix in 1953 (Figure 1.1) [2]. Duplex DNA is a right-handed helix formed by two individual DNA strands aligned in an anti-parallel fashion. This means that one strand is oriented in the 5'–>3' direction and the other in the 3'–>5' direction. The two strands are held together by hydrogen bonds, a short, noncovalent, and directional interaction between a covalently bound hydrogen atom (donor) and a negatively charged acceptor atom. The negative charge (acceptor) is provided by electrons on a carbonyl oxygen (-C≡O) or the lone pair of electrons on nitrogen. Base stacking near the center of the cylindrical helix provides considerable stability to the double helix. The sugar and phosphate groups are on the outside of the helix and form a "backbone" for the helix [3].

Figure 1.1: Double-stranded DNA showing a double helix formed by two individual DNA strands aligned in an anti-parallel fashion

To fit into a chain, a large base must always be opposite a small one. A and T can pair

only with one another because of these size and bonding restrictions, similarly G and C pair with one another. This is called the complementary feature of dsDNA and it makes possible the precise duplication of the hereditary information [2].

Double helix DNA can be in three forms: A, B, and Z. A-form DNA is a form of DNA with tilted base pairs and has more base pairs per turn than does B-form DNA. The most common form B-DNA, which has about 10 bases per turn of the helix, is the right-handed helical form commonly found for DNA in solution.

A dominant feature of B-form DNA is the presence of two distinct grooves, a major and a minor groove. Proteins and other molecules can interact with DNA, recognizing double-stranded DNA by the phosphoribose backbone, and forming specific interactions based on the DNA sequence through access to the major and minor grooves. Most interactions occur in the major groove because of its size, and because there is an additional potential hydrogen bond donor from A-T residues in the major groove [3]. The groove in the A-DNA form is not as deep as in B-DNA, and the bases are much more tilted. The Z-DNA form is a left-handed helix that is very different from right-handed DNA forms. The Z-DNA can form under conditions that include high salt concentrations, the presence of certain divalent cations, or DNA supercoiling [3].

1.1.2 Physical Properties of Double-Stranded DNA

1.1.2.1 Ultraviolet Absorption by DNA

DNA absorbs ultraviolet (UV) light in a band centered around 260 nm [4]. The absorption profile of DNA can be used as a measure of the concentration and purity of a DNA sample. There is a relation between UV absorbance and nucleic acid concentration, which can be described by the Beer-Lambert equation (equation 1.1)

$$A = \varepsilon c l \tag{1.1}$$

where A is the absorption of a material, c is the concentration of DNA or RNA (in mol/L), l is the distance of the light path (in cm), and ε is the extinction coefficient which

is 6600 L/(mol.cm) for DNA [3]. Since the extinction coefficient for DNA is known, the unknown DNA concentration would be calculated following this formula.

Extinction coefficients vary with the type of nucleic acid. Nucleic acids have a peak absorbance in the ultraviolet range at about 260 nm. When the spectrophotometer has a path length of 1 cm, we define the optical density (O.D.) as:

$$O.D. = \varepsilon c \tag{1.2}$$

A pure solution of double stranded DNA at a concentration of 50 μg/ml has an absorbance at 260 nm equal to 1 and similarly a pure solution of RNA at a concentration of 40 μg/ml has an absorbance at 260 nm equal to 1 [4]. UV is absorbed by proteins maximally at 280 nm, therefore, the ratio of A_{260}/A_{280} is a measure of the purity of a DNA preparation and in general, a pure DNA sample will have an A_{260}/A_{280} ratio between 1.7 and 1.9 (DNA quality measurement is based on the fact that O.D. at 260 nm is twice that at 280 nm if the solution contains pure DNA).

At present, there is not sufficient information to reliably predict the extinction coefficients of DNA, RNA and dsRNA, and mixed double- and single-stranded structure [5]. The major disadvantage of the absorbance method is the inability to distinguish between DNA and RNA and the relative insensitivity of the assay (an A_{260} of 0.1 corresponds to a 5 μg/ml dsDNA solution).

1.1.2.2 Denaturation of Double-Stranded DNA

The double-stranded (ds) structure of DNA is remarkably stable. This stability is derived from two chemical forces: hydrogen bonding and base stacking interactions (section 1.1.1). In addition, water molecules cover the helix by forming a "shell of hydration" around the DNA. To melt the two strands or denature the DNA, all these stabilizing forces must be overcome. The two strands of DNA come apart readily on incubation at pH$\geq$12 or pH$\leq$2 due to ionization of the bases. Ionization results in a change in the hydrogen bond donor/acceptor properties of the bases, which will disrupt the normal A.T and C.G hydrogen bonds. In addition, the shell of hydration surrounding the DNA is disrupted at very

high or low pH by destabilizing the base stacking. Increasing the temperature of DNA also destabilizes the double helix by disrupting the hydrogen bonds and destroying the shell of hydration of DNA, leading to a loss of forces holding the two strands together and it results in the separation of the two strands [3].

The melting temperature of a dsDNA sequence, T_m, is the temperature at which 50% of the dsDNA melts to form single-stranded (ss)DNA. The main factors affecting T_m are salt concentration, DNA concentration, the presence of denaturants (formamide), DNA sequence and DNA length. Formamide reduces the melting temperature of DNA duplexes in a linear fashion (by $0.72^{\circ}C$ for each percent of formamide), and the melting temperature of hybrids in the presence of formamide can be calculated according to the following equation [6]:

$$T_m = 81.5 - 16.6 * \log M - (\%41.0)(G-C) - (\%72.0)(formamide) \qquad (1.3)$$

where T_m is the melting temperature in Celsius, M is the monovalent salt molarity, and (%G+C) is the percentage of guanine plus cytosine residues in DNA sample. A more detailed investigation of the effect of formamide on the melting temperature can be found in [6–10].

DNA denaturation can be monitored in many different ways. One method would be the measurement of a characteristic increase in the absorbance at 260 nm. Single stranded DNA has an approximately 40 % higher absorption than double stranded DNA, since the heterocyclic rings of the bases absorb more light if they are not piled up or connected by hydrogen bonds inside the double helix. Another method employs enzymes specific for single-stranded DNA [3].

1.1.3 DNA Supercoiling

Plasmid DNA, a small circular piece of DNA, is one of the most common genetic vectors used in molecular biology applications and it can exist in different topoisomers. A topoisomer is a topological form of DNA with the same sequence as another but differing in linking number (the number of times one strand crosses the other when the DNA is made

to lie flat on a plane). A covalently closed circular DNA molecule (cccDNA), called *form I* DNA, is negatively supercoiled (tending to unwind the helix), and is the natural form of a simple plasmid molecule purified from a bacterial cell. Covalently closed means that the two phosphodiester backbones are covalently continuous. If a cccDNA molecule contains a single nick (by breaking even one phosphodiester bond) in one of the strands, the supercoils are lost. The nicked or open circular molecule has been called *form II* DNA, they could also be called "relaxed" since there are no supercoils. Circular DNA would be unknotted by cleaving both strands; thus a linear DNA molecule, called *form III*, will be formed by breaking both phosphate backbones at the same point (or nearly the same point) along the helical axis [3]. These three isomers can be separated by electrophoresis in agarose gels [11–13].

One topological property of a DNA molecule is its *linking number*, L. The linking number is only changed by chemical or enzymatic cleavage breaking of the phosphodiester backbone. The topology of DNA is described by the simple equation:

$$L = W + T \tag{1.4}$$

where L is the linking number, T is the number of helical turns in the DNA, and W is the writhing number of DNA which describes the supertwisting or coiling of the helix in space. When a molecule is relaxed and contains no supercoils, the linking number is equal to the twist number since W=0. A rough estimate for the linking number of relaxed DNA is $L_0 = N/10.5$, where N is the number of base pairs in the DNA fragment. Negatively supercoiled DNA has a deficiency in the linking number compared with relaxed DNA, $L \leq L_0$. Underwinding results in more base pairs per helical turn and a decrease in the angle of twist. Positively supercoiled DNA (tending to wind the helix) is overwound with respect to the number of helical turns compared with relaxed DNA, $L \geq L_0$. Overwinding results in fewer base pairs per helical turn and an increase in the winding angle. DNA is a dynamic molecule that can exist in many states with different values of helical turns and supercoils. Although the linking number is not changing and must be an integer, the number of twists can vary in positive and negative increments with offsetting negative and positive changes

in the writhe number [3].

The level of negative supercoiling increases by increasing the temperature since changes in temperature affect the winding of dsDNA. Similarly, as temperature decreases, the twist angle in DNA increases, resulting in fewer base pairs per helical turn. The salt concentration also may influence the winding of the DNA. For higher concentrations of a monovalent cation Na^{+} or a divalent cation Mg^{+2}, writhe of plasmids in solutions increases [3].

1.1.4 A Vocabulary of Genetics

In this section, there are some brief descriptions for the genetic terms that have been used in the rest of the thesis.

Eukaryote: The eukaryotic cells contain a well-defined nucleus, bounded by a membrane, within which DNA is formed into distinct chromosomes [2].

Prokaryote: Prokaryotes are organisms whose cells lack organelles. There are no any specialized segregated structures such as nuclei, mitochondria, and chloroplasts in prokaryotes. Prokaryotic DNA is not arranged in chromosomes but forms a coiled structure called a nucleoid [2].

Chromosome: The interiors of eukaryotic cells are subdivided by membranes in a complicated way. The DNA of the cell is present within the nucleus, associated with protein, in units called chromosomes. Eukaryotic DNA is able to coil up into a highly condensed form during cell division because of its association with protein [2].

Gene: The basic unit of hereditary is called the gene. A gene is a sequence of DNA nucleotides on a chromosome that contains the information necessary to make a protein and so determines the nature of an individual's inherited traits [2].

Homozygous: Humans typically have two copies of each gene, and if the genetic information carried by the two copies is identical, it is called homozygous.

Heterozygous: If the genetic information carried by the two copies is different, it is called heterozygous.

Wild-type: Any genetic sequence that does not contain mutations (i.e. normal) is referred to as being wildtype. Wild-type samples are often used as controls in genetic analysis.

Mutation: Mutation is a rare change in the DNA of genes that ultimately creates genetic diversity.

SNP:

In two randomly selected human genomes, 99.9% of the DNA sequence is identical. The remaining 0.1% of DNA contains sequence variations. The most common type of such variation is called a single-nucleotide polymorphism, or SNP. SNPs are highly abundant, stable, and distributed throughout the genome. These variations are associated with diversity in the population, individuality, susceptibility to diseases, and individual response to medicine [14].

1.2 Microfluidic Devices

Microfluidic technologies are used for controlling the flow and reaction of minute amounts of liquids or gases in a miniaturised system [15]. Whole blood samples, bacterial cell suspensions, proteins, nucleic acids or antibody solutions and various buffers are commonly used in microfluidic devices. Microfluidic devices offer the ability to work with smaller reagent volumes, shorter reaction times, and the possibility of parallel operation [16]. Although the idea of miniaturizing analytical systems has been around for years, the technology to do so was not available until the development of photolithography for producing integrated circuits. The main idea was that if photolithography could create paths and control elements for electrons, it could also produce components for the control and mobilization of fluids [17–20]. In the same way that integrated circuits allowed for the miniaturization of computers from the size of a room to the size of a notebook, miniaturization has the potential to shrink a room full of instruments into a compact lab-on-a-chip [21].

Most microfluidic systems have two modes for transporting fluids: pressure-driven and electrokinetically-driven flow. Electrokinetic transport refers to the combination of electroosmotic and electrophoretic transport. In pressure-driven flow, movement of the fluid is provided with pumping through the device via positive displacement pumps, such as syringe pumps. In this flow, the velocity profile is parabolic (i.e. fastest in the middle of the channel) and the mean flow rate will depend on the channel cross-sectional area. An advantage of pressure driven flow, depending on the application, is that both charged and uncharged molecules can be moved without separation [22]. The electrokinetic flow and its velocity profiles will be discussed in next sections.

1.2.1 Electroosmosis

If the walls of a microchannel have an electric charge, an electric double-layer of opposite ions (in the microchannels) will form at the walls (Figure 1.2). When an electric field is applied along the channel, the ions in the double-layer move towards the electrode of opposite polarity. The electric double-layer creates motion of the fluid near the walls that

transfers via viscous forces into convective motion of the bulk fluid [22]. In other words, electroosmosis refers to the bulk movement of an aqueous solution passing a stationary solid surface due to an externally applied electric field. Electroosmosis requires the existence of a charged double-layer at the solid-liquid interface. In glass capillaries, surface silanol groups become deprotonated and therefore are negatively charged. This negatively charged surface attracts positive ions present in the flow [23], which will be discussed more in section 2.3.

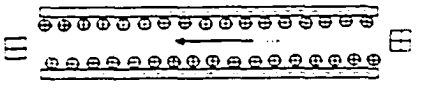

Figure 1.2: Electroosmotic flow made by electric double layer formation upon applying an electric voltage.

1.2.2 Electrophoresis

Electrophoresis, the commonly used form of microfluidic transport, is the method of separating large molecules (such as DNA fragments or proteins) from a mixture of similar molecules. An electric current is passed through a medium containing the mixture, and each kind of molecule travels through the medium at a different rate, depending on its shape, size and electrical charge [22].

Organic chemicals and biochemicals are made of a range of functional groups with some being uncharged and others carrying charges of different magnitudes and polarities and these charged groups may be evenly distributed over the molecules giving a significant average charge, like phosphate groups in nucleic acids [22].

The net charge divided by the molecular mass of DNA, not the absolute value of the charge, is an important factor in electrophoretic separation. Charge to mass ratios are virtually constant for nucleic acids. The addition of one nucleotide increases both the

molecular weight and charge, so that the charge-to-weight ratio is independent of fragment length. This proportionality dramatically affects the procedures that have been used for their separation. The strong negative charge of nucleic acid at neutral pH values ensures that they will all migrate towards the anode; however, because of their constant charge to mass ratios in open-pored system (a system with no sieving effect) they tend to move together. Therefore, the separation has to rely on sieving effects acting on the differently sized molecules and the wide range of molecular sizes requires the availability of a wide range of gel pore sizes [22].

The surface charge of molecules being separated electrophoretically can vary depending on the chemical environment. In a pure solution, a simple molecule will have a certain charge dependent on the nature of its ionizable groups. In electrolyte solutions (i.e. electrophoresis buffers) the molecules attract an ion cloud which changes the effective surface charge. Most organic charged groups are rather weak, consequently they are frequently only partially ionized. pH value can influence the extent of ionization with molecules becoming more positively charged as pH falls and vice versa. Small changes in pH are important in changing molecular charge and of course pH extremes can cause serious, irreversible changes in molecular structure [22].

1.2.3 Comparison of Different Fluidic Flows

One of the advantages of electrokinetic flow is that electroosmotic flow produces a nearly uniform plug profile, which results in reduced sample species dispersion as compared to the velocity gradients associated with pressure-driven flows [24]. However, sample dispersion in the form of band broadening is still a concern for electroosmotic pumping. Another advantage to electrokinetic flow is that it is straightforward to couple other applications on the chip. However, electrokinetic flow often requires very high voltages, making it a difficult technology to miniaturize without off-chip power supplies [24].

It is important to note that electroosmosis results in a net mass transfer of the aqueous solution; whereas, electrophoresis causes movement of charged particles or molecules

through a stationary solution. In capillary electrophoresis, the ionic double layer at the capillary-wall surface is typically immobilized to suppress electroosmotic flow. Suppression of electroosmosis enables the DNA to migrate from the cathode toward the anode without the influence of bulk fluid flow [24].

1.3 Microchip Capillary Electrophoresis (CE)

Slab-gel electrophoresis is still a common technique used for the separation of proteins and nucleic acids. Running the gel can be very slow because of the low electric field applied in gel electrophoresis. In principle, capillary electrophoresis has several advantages over slab gel electrophoresis. The small diameter of the capillaries minimizes the heat dissipation and therefore the band broadening due to Joule heating. The band broadening phenomenon, which reduces the band resolution of the separation during gel electrophoresis, limits the separation capability in sequencing runs. One possible explanation of this phenomenon is that the distribution of the mobilities arises mainly from the conformational distributions. Other sources of band broadening can be listed as pH, temperature gradients and gel/DNA interactions [25,26]. Strong electric fields (up to 400 V/cm and more) can be used, therefore the run time and diffusion are reduced. Capillaries are available in a variety of diameters (about 10-300 μm) and their length can be chosen in a wide range.

The sensitivity of capillary electrophoresis is very high and minute amounts of sample can be analyzed. Because of the narrower peaks, capillary electrophoresis has potentially a very high separation efficiency and it is expected to have a better performance compared to slab gel systems. In contrast to slab gels, only one sample can be loaded at a time; however, capillary arrays and capillary microchannels have been proposed to circumvent the problem [27–29]. Backhouse *et al.* also presented 50 cm long microchannels in a monolithic device for high resolution and long read-length DNA sequencing [30]. In summary, capillary electrophoresis offers the possibility of rapid and automated analysis with high reproducibility and improved quantification [31].

Developments in microfluidics and microinstrumentation during the last several years have opened the possibility of fabricating devices with increased functionality and complexity for chemical and biochemical applications. Various electrically driven separation techniques for liquid-phase analysis such as capillary electrophoresis (CE) have been successfully adapted to a microchip format [32–37].

Perhaps the most compelling reason to build micro-chip devices is the potential to inte-

grate sample handling, analysis, and the ability to obtain precise optical positioning across an array of channels, (i.e. Micro total analysis system (μ-TAS)). There are some interesting reports on the integration of PCR amplification and CE. Recently, a successful method was presented in [38] for the integration of PCR-CE using PDMS instead of a glass micro-chip. Since the microfabrication procedure is based on photolithography, high-density arrays, for high throughput applications, can readily be obtained.

The separation performance of a micro-chip system was compared with conventional capillaries in [30, 39]. Backhouse *et al.* demonstrated that the microchannel geometry or glass composition did not contribute significantly to band broadening compared to cylindrical fused-silica capillaries. They also concluded that the advantage of microchips for DNA sequencing may lie in ease of manufacturing of large numbers of high density arrays and the future integration of sample preparation with these devices [30]. Rodrigues *et al.* believed that the main disadvantage of the microchip system is the lower sensitivity obtained. They also expected that the detection sensitivity could be enhanced by using higher concentration of the sample, controlling the injection channel potentials during separation to eliminate leakage, or by using better optics, a brighter source and a more sensitive photon detector [39].

1.3.1 Separation Methods

In traditional gel electrophoresis, the gel has two main functions: it is used as an anti-convective medium as well as a sieving matrix for separation [40]. Convection is rather low in capillary electrophoresis and micro-chips due to small dimensions of the capillaries. This might increase the possibility of gel-free separation. However, as discussed in section 1.2.2, biopolymers such as DNA and RNA have constant charge to mass ratio and no separation would occur in free solution. There are some possible approaches for separating biopolymers electrophoretically. DNA or RNA can be modified so that the charge to mass ratio is not constant (Free Solution Electrophoresis). A separation matrix as in traditional electrophoresis can also be used. Recently, Han *et al.* proposed the "microfabricated en-

tropic trap array" in [41]. A nanofluidic channel device, consisting of many entropic traps, causes electrophoretic mobility differences. A brief description of these three methods is given in the following subsections.

1.3.1.1 Free Solution Electrophoresis

The idea of modifying biopolymers in order to obtain electrophoretic separation in free solution was proposed in the early 1990's by two groups, [42] and [43]. It is based on the fact that by attaching the same molecule to one or both ends of all biopolymer molecules to be separated, the charge to mass ratio would not be constant any more. Therefore, it is called "end-labeled free-solution electrophoresis" or ELFSE. The attached molecule should have a different charge to mass ratio than DNA but has to be exactly the same for all DNA molecules. The ELSFE mobility of a DNA fragment is given by [43]:

$$\mu/\mu_0 = 1/(1+\alpha/M) \tag{1.5}$$

where μ_0 is the free solution mobility of a bare DNA fragment, M is the length of the DNA (bp), and α is the friction coefficient of the label relative to that of one DNA base pair.

1.3.1.2 Matrix Based Separation

Electrophoretic separation was adapted from slab format to capillary format by using the same matrices (e.g. cross-linked polyacrylamide or agarose). The gels can be prepared in the same manner as slab gels, however, gel-filled capillaries have limited life times. The small dimensions of the capillary with low convection and strong capillary forces made it possible to use polymer solutions instead of cross-linked polymers. For separating DNA in capillary electrophoresis, a number of different polymers have been reviewed [44,45].

1.3.1.3 Microfabricated Entropic Trap Array

Large DNA fragments (longer than 5000 bp) can be separated by an entropic trap array. The basic design of the entropic trap array consists of alternating thin and thick regions in a microfabricated channel. The channel depth of the thin region is smaller than the radius of gyration of the DNA molecules being separated, and thus it works as a molecular sieve [41]. The radius of gyration can be thought of as the effective radius of the mass distribution with respect to its inertial response to rotation ('gyration') about the chosen axis.

1.3.2 Separation Regimes

The exact transport mechanism of DNA in capillary electrophoresis is generally thought to be a complex function of the electric field strength and the size of the gel pores relative to the effective DNA size. Mechanisms proposed for DNA electrophoresis through gels include simple Ogston sieving (for small DNA) [46], simple biased reptation, reptation with fluctuations, reptation with stretching and others (reviewed in [47, 48]).

The first mechanism proposed for the description of gel electrophoresis, the Ogston model [46], assumes that the mobility of a particle is proportional to the fraction of the volume available to it in the gel. The low-field electrophoresis of small analytes in a gel of concentration C is often interpreted using the Ogston model [49]. Using purely geometric arguments, Ogston derived an expression for the mobility of a globular particle in a random array of fibres [50]:

$$\mu = \mu_0 exp(-K_R C) \tag{1.6}$$

where μ_0 is the mobility in pure solvent, K_R is the retardation coefficient (proportional to R^2, the particle radius) and C is the gel concentration.

The Ogston model does not account correctly for the mobility of large DNA molecules, so that a number of models based on the so-called reptation concept were developed. The biased reptation model predicts that the electrophoretic mobility in DNA electrophoresis is approximately related to the DNA molecular size and the electric field. In the biased

reptation model (BRM), the DNA chain is assumed to thread its way, without changing its length, through a "tube" defined by the fibres (for a rigid mesh) or the "blobs" (for a flexible network) surrounding it [50]. As the chain migrates through the gel, it creates new tube sections of length, a, the mean gel pore size. These chain sections are oriented by the electric forces in order to minimize their potential energy. Another model is the "biased reptation with fluctuations" (BRF) [51], a generalization of the earlier biased reptation model. The biased reptation with fluctuation model allows for reptation tube length fluctuations during the migration [49].

1.3.3 Detection Methods

The micro-chip technology has matured very rapidly, however, the development and availability of effective detectors has lagged behind. New detection protocols are highly desirable to meet the growing needs of microfluidic systems and for integrating the analytical micro-chip and the control instrumentation [52].

UV absorption measurement, the most widely used detection method in High Performance Liquid Chromatography (HPLC) and conventional CE, is not very sensitive among the detection methods used. Laser-Induced Fluorescence (LIF) or Mass Spectrometry (MS) are two common detection methods for microchip electrophoresis, however, the high cost and large size of the instrumental set-up for these techniques are incompatible with the concept of low cost μ-TAS. Alternative detectors that can be micro-fabricated on a chip can reduce both cost and size [53].

1.3.3.1 Laser-Induced Fluorescence (LIF)

Lower amounts of sample are used in capillary electrophoresis because of the smaller size of the capillary reservoirs, so sensitive detection methods are needed in capillary electrophoresis. Among the several detection methods, laser induced fluorescence (LIF) is the most widely used for detection of micro-chip separation, despite its limitations. The main disadvantage of the LIF method is that it is only applicable for fluorescent samples or

samples capable of fluorescent labeling. Nevertheless, LIF has now become the standard detection method for micro-chip separation.

In laser induced fluorescence (LIF), a fluorescent molecule absorbs radiation from a laser and some of its molecules are excited to higher energy levels. Fluorescence is emitted at wavelengths longer than the exciting radiation. Fluorescence detection is more sensitive than absorption measurements since the emitted wavelength is different from the exciting wavelength. Single atoms and molecules have also been detected in a capillary by LIF [54]. Usage of intercalating dyes followed by LIF detection is a common labeling method in micro-chip electrophoresis.

1.3.3.2 Mass Spectrometry (MS)

Mass Spectrometry (MS) is a method for identifying molecules based on the detection of the mass-to-charge ratio of ions generated by vaporization and electron bombardment. Due to the increased interest in proteomics and the analysis of biological samples present at very low concentrations, demands for this sensitive and highly valuable analysis system have increased [53]. Capillary Electrophoresis Mass Spectrometry (CE–MS) detection on micro-chip has been studied extensively by [55, 56].

1.3.3.3 ElectroChemical Detection (ECD)

Electrochemical detection has attracted great interest in recent years for various reasons: its easy operation, low cost, selectivity, and high sensitivity without the need for additional systems. Unlike LIF, there is no need for labeling in electrochemical detection [53].

Electrochemical detection can work on different principles. The most common way is to control the potential of the working electrode at a fixed value and monitor the current as a function of time. Such controlled-potential detectors are ideally suited for monitoring analytes that are easily oxidizable or reducible compounds. Additional compounds may be detected in connection to proper derivatization reactions. The proper use of Capillary Electrophoresis Electrochemical detection (CE-EC) in micro-chips requires knowledge of

the redox reactions of the target analytes and their dependence upon the composition of the running buffer and the working-electrode material [52]. The suitability of electrochemical detection for micro-chip electrophoretic systems has been demonstrated in connection to fixed-potential amperometric measurements in [57–59].

1.4 Micro-chip Based Mutation Detection

With the completion of the Human Genome Project, genetic characterization has become very important in the detection and treatment of human disease. Screening for mutations in DNA samples is essential for a variety of applications such as molecular diagnosis of complex inherited disorders, population screening for genetic diseases, studies of the genetic basis of variable drug response (pharmacogenetics) as well as the discovery and investigation of new drug targets (pharmacogenomics) [60].

DNA sequencing is still considered as the gold standard for mutation detection and is typically used to establish the identity of the specific nucleotide variation(s) resulting in genetic disease. Sequencing technology has improved dramatically over the past decade, however, it is still too laborious and costly for screening large numbers of samples. Thus, a substantial amount of effort has been spent in the development of alternative mutation detection strategies [1].

Mutation detection strategies may be divided into two types: those that identify specific, known sequence variations, and those that detect unknown sequence variations. These strategies are termed specific and scanning methods, respectively. Examples of mutation specific detection technology are primer extension, allele-specific amplification, allele-specific oligonucleotide hybridization, and oligonucleotide ligation assay. Mutation scanning technology includes methods such as single-stranded conformation polymorphism (SSCP), heteroduplex analysis (HA), denaturing gradient gel electrophoresis (DGGE), temperature gradient gel electrophoresis (TGGE), and methods utilizing either DNA repair enzymes or resolvases (a group of enzymes that mediate site-specific recombination in prokaryotes) for the detection of mismatches [1].

The Human Gene Mutation Database [61] reports that over 90 % of disease-causing mutations in human are caused by micro-lesions (single-base transitions, transversions, small deletions and/or inversions), as opposed to gross lesions (repeat expansions, complex gene rearrangements, gross insertions, deletions or duplications). Therefore the issue of sensitivity (the percentage of mutations that are successfully detected) in both the specific

and scanning methods is significantly important.

SSCP and HA are both widely used mutation scanning methods because of their relative sensitivity and technical simplicity. The next sections discuss these methods in more detail.

1.4.1 Heteroduplex Analysis (HA)

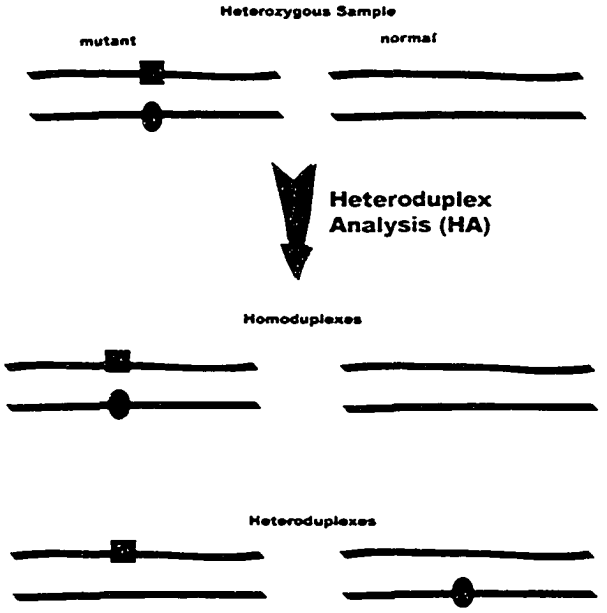

Figure 1.3: Schematic illustrating the principle of heteroduplex analysis. The heteroduplex containing the mismatched bases usually tends to have lower electrophoretic mobility.

The principle of heteroduplex analysis (HA) is simple and it depends on the conformation of duplex DNA, which consists of complementary strands or strands that have a sequence mismatch [1]. DNA is normally double stranded but in many procedures such as

genetic amplification methods, the DNA is separated into single strands. Under the right conditions (often simply a lower temperature), in a process of self-assembly, these single strands will have the chance to recombine. In doing so, they each may recombine with a perfectly complementary sequence (forming a homoduplex) or a nearly complementary sequence (forming a heteroduplex, e.g. a mutant sequence paired with a wild-type sequence). The imperfect fit in a heteroduplex creates a bulge or bubble and this affects the shape of the assembled molecule, typically lowering its mobility during electrophoretic movement [1]. A heterozygous sample will generate four different duplexes, two homoduplexes and two heteroduplexes, as it is shown in Figure 1.3, and since the heteroduplexes typically migrate more slowly than the homoduplexes, heterozygous sample can be distinguished from homozygous sample. Unfortunately, the molecules often co-migrate such that separate peaks are not resolved [62].

1.4.2 Single-Strand Conformation Polymorphism (SSCP)

Orita *et al.* developed SSCP more than 10 years ago for polyacrylamide gel electrophoresis [63]. The process of SSCP involves the PCR amplification of the fragment of interest, denaturation of the double-stranded PCR product with heat and/or formamide, and electrophoresis on a nondenaturing matrix. During electrophoresis, single-stranded DNA fragments fold into a three-dimensional shape according to their primary sequence. The electrophoretic mobility of separation then becomes a function of the shape of the folded, single-stranded molecules. If the wild-type sequence differs from that of the fragment being tested, even by only a single nucleotide, it is possible that at least one of the strands, if not both, will adopt different three-dimensional conformations and exhibit a unique electrophoretic mobility [1]. Figure 1.4 shows a simplified illustration of SSCP.

The advantages of SSCP analysis are: (i) simplicity of usage; (ii) no special equipment necessary; (iii) mutant bands separated from wild-type can be isolated for analysis; (iv) non-radioactive labeling available. The disadvantages of SSCP analysis are: (i) the size of fragment analyzed is limited; (ii) absence of predictive theory; (iii) multiple conditions to

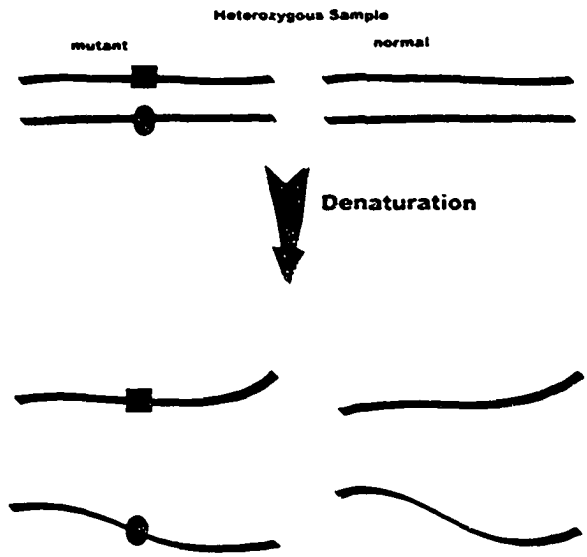

Figure 1.4: Schematic illustrating the principle of SSCP analysis during electrophoresis in a nondenaturing medium [1].

detect all mutations; (iv) gels sometimes are difficult to interpret; and (v) less applicable to DNA with unknown sequence [1].

The HA method involves the use of electrophoretic conditions that enhance velocity differences between the duplexes so that the process of duplex self-assembly can be used to determine the presence of a heterozygous state. Similarly, in SSCP, by altering the kinetics of the self-assembly process so that each strand of ssDNA does not encounter its complementary strand, portions of each strand may find near-complementary sequences on the same strand, with the result that the strand folds upon itself in a sequence dependent manner forming new conformations. This is an overly simplified description since both

ssDNA without self-similar sequences, and dsDNA without mismatches, may already have complex structures [62].

1.4.3 Combined SSCP and HA

Although HA achieves a sensitivity of about 80 %, and SSCP about 95 %, Kozlowski and Krzyzosiak [64] achieved 100 % sensitivities by combining two methods. This achievement was based on a method in which the pre-labelled dsDNA and ssDNA were prepared separately in a procedure that involved thermal processing and extensive dilution (40 to 160 times) before recombining. Similarly, Kourkine *et al.* [65] used both SSCP and HA to achieve detection sensitivities of 100 % by combining these two methods. Their success was also based on a method of snap-cooling pre-labelled samples in a manner that produced both dsDNA and ssDNA, and they prevented the renaturation of the ssDNA by diluting the sample considerably (by 10 to 40 times). The drawback to such approaches is that they require significant preparation that does not lend itself to on-chip integration. Moreover, microchip-based methods may have difficulty in analyzing dilute samples without significant degradation in the signal-to-noise ratio. It is worthwhile to note that neither of the above reports ([64] and [65]) was microchip-based. Although these works have demonstrated a very powerful capillary-based combination of electrophoretic approaches to mutation analysis (SSCP and HA), a more general application to micro-chips will require further improvements in terms of sample preparation, signal intensity, labeling and in developing separation conditions that are compatible with both SSCP and HA [62].

1.5 Intercalating Dyes

The term intercalator was first used by Lerman [66] in the 1960s to define a molecule containing a planar aromatic structure that inserts itself between two base pairs (bp) of dsDNA. In this process, the compound inserts between two stacked base pairs of DNA by positioning itself within the center of the DNA double helix. Hydrophobic stacking interactions with adjacent base pairs stabilizes the intercalated molecule. The binding of an intercalating molecule results in a lengthening of the DNA helix, since two adjacent base pairs must physically separate to accommodate the intercalated molecule. In addition, intercalation results in the unwinding of dsDNA by relaxing negative supercoils [3].

Intercalating dyes, chemicals that are weakly fluorescent and become strongly fluorescent upon forming complexes, are excellent for CE-LIF because of their low backgrounds. Common intercalating dyes include ethidium homo-dimer (EthD), benzoxazolium-4-pyridinium dimer (POPO-3), benzoxazolium-4-quinolinium dimer (YOYO-1), benzothiazolium-4-quinolinium dimer (TOTO-1), and ethidium bromide (EtBr) which all have planar aromatic or heteroaromatic rings that can be inserted between adjacent base pairs of dsDNA.

Yan *et al.* evaluated different nucleic acid stains for sensitive dsDNA analysis with CE separation. Among the five tested nucleic acid stains, the Sytox Orange stain was shown to have the best sensitivity for dsDNA detection by CE [67]. Ren *et al.* showed labelling of dsDNA and ssDNA with an inverse-flow labelling technique using thiazol orange [68]. Dimeric cyanine nucleic acid dyes developed by Molecular Probes have been reported to offer the best detection limits of any of the fluorescent probes available for nucleic acid staining [69]. In addition to their high affinity for nucleic acids, these probes are essentially nonfluorescent in the absence of nucleic acids and exhibit 100- to 1000-fold fluorescence enhancements upon binding to DNA [70]. Gibson *et al.* examined some of the cyanine intercalation dyes, especially POPO-3, for rapid and sensitive detection of DNA fragments by capillary electrophoresis [69]. A rapid on-column DNA labeling technique was used [71] to detect viral restriction DNA fragments by capillary electrophoresis with laser-induced fluorescence (LIF) detection using intercalating dye POPO-3. Figeys *et al.* reported separation

of dsDNA fragments by labelling them with the intercalating dyes POPO-3, YOYO-3 and YOYO-1 [72]. Staining the DNA on chip gives significant advantages in providing strong signals and in being able to deal with PCR products from reactions with unlabeled primers. It is also a significant step toward higher levels of integration. The on-chip labeling could be used to analyze DNA without the need for amplification by means of PCR.

Chapter 2

Integrated Method for Mutation Detection Using On-Chip Sample Preparation by SSCP and HA

2.1 Introduction

A rapid microfluidic technique that can produce single stranded DNA (ssDNA) and heteroduplexes of renatured double-stranded DNA (dsDNA) from a sample of dsDNA is presented in this chapter. The technique also involves the application of two complementary methods of mutation detection. The mutation analysis of ssDNA is by means of single-stranded conformation polymorphism analysis (SSCP) and the mutation analysis of dsDNA is by means of the method of heteroduplex analysis (HA). As part of this process it is also possible to fluorescently label the ds and ssDNA. The denaturation, renaturation, labelling and both methods of mutation detection are performed upon a microfluidic chip without the need for reloading the chip. This combination of several procedures on a single chip represents a significant step in the development of higher levels of integration upon microfluidic devices.

As discussed in the previous chapter, with the completion of the sequencing of the hu-

man genome, genetic characterization has become increasingly important in the detection and treatment of human disease. Much of this genetic characterization centers around the detection of changes in genetic sequence such as the detection of inserted or deleted bases, or substitutions of one base for another (i.e. single nucleotide polymorphisms or SNPs). Perhaps the most important characteristics of the methods used to detect mutations are the cost and the sensitivity. Both SSCP and HA are mutation detection methods that are based on the self-assembly of DNA and are far less costly than sequencing, although the sensitivity of each method is significantly lower (ca. 90 %). By combining these two techniques (e.g. as in the capillary-based work of [65]) it has been reported that sensitivities of 100 % can be achieved. A microchip integration of SSCP and HA is presented in this chapter. This chapter is based upon the recently published journal paper by Vahedi *et al.* [62].

2.2 Materials and Methods

2.2.1 General

DNA was extracted from the lymphocytes of volunteers (prepared with informed consent) and was then purified using phenol-chloroform-isoamyl alcohol extractions [73] or with the QIAmp DNA Blood kit (QIAGEN, Mississauga, ON). After purification, the DNA was solubilized in TE buffer (pH 8.0) that consisted of tris(hydroxymethyl)aminomethane (Tris) and ethylenediaminetetraacetic acid tetrasodium salt (EDTA) and stored at 4°C. Genotypes were confirmed by sequencing on an ABI Prism 377 Slab Gel Sequencer (Applied Biosystems, Streetsville, ON), using an ABI Prism BigDye Terminator v3.0 Ready Reaction Cycle sequencing Kit with AmpliTaq DNA Polymerase (Applied Biosystems). For showing this integration of HA and SSCP, we amplified regions of two different genes: Exon 20 of the gene BRCA1 (associated with cancer predisposition) and Exon 2 of the gene HFE (associated with haemochromatosis).

2.2.2 PCR

HFE Exon 2 (234 bp) was PCR-amplified for a test panel of clinically relevant DNA templates. The genomic DNA obtained from the individuals wild-type (denoted -/-), heterozygous (denoted +/-) and homozygous (denoted +/+) for for the H63D and S65C mutations in HFE Exon 2. PCR was performed in 25 μL reactions, with thermal cycling as follows: 94°C for 2 min, 37 cycles of (94°C for 30 s, 55°C for 30 s, and 72°C for 30 s), and finally 72°C for 10 min. For all samples, the PCRs were performed with 6 ng of genomic template DNA, 200 μM of dNTPs, 1.5 mM of $MgCl_2$, 1x reaction buffer, 2.5 units of Platinum Taq DNA Polymerase and with the primers as detailed in Table 2.1.

BRCA1 Exon 20 (234 bp) was PCR-amplified from a test panel of clinically relevant DNA templates. The samples contained wild-type (denoted -/-) as well as heterozygous (denoted +/-) for the 5396+1G>A and 5382insC mutations. PCR was performed in 50 μL reactions, with thermal cycling as follows: 95°C for 3 min, 35 cycles of (95°C for 45 s,

60°C for 30 s, and 72°C for 30 s), and finally 72°C for 10 min. For these samples, the PCRs were performed with 12 ng of genomic template DNA, 200 μM of dNTPs, 1.5 mM of $MgCl_2$, 1x reaction buffer, 2.5 units of Platinum Taq DNA Polymerase and with the primers (with the final concentration of 0.4uM) as detailed in Table 2.1.

Table 2.1: Unlabelled Primers Used for PCR

Amplicon-Primer	Sequence	Final Conc.
HFE Exon 2-forward	5'-TCA GAG CAG GAC CTT GGT CTT TCC-3'	0.4uM
HFE Exon 2-reverse	5'-CAT ACC CTT GCT GTG GTT GTG ATT-3'	0.4uM
BRCA1 Exon 20-forward	5'-GAA GGA AGC TTC TCT TTC TCT TA-3'	0.4uM
BRCA1 Exon 20-reverse	5'-AGT CTT ACA AAA TGA AGC GG-3'	0.4uM

PCR reagents (buffers, primers and polymerase) were purchased from Invitrogen (Burlington, ON). The 10x reaction buffer for PCR, the stock solution, contains 200 mM Tris-HCl (pH 8.4) and 500 mM KCl. Following PCR, the samples were stored frozen at -20°C. More details about this PCR protocol could be found in [74] and [75] . The primers were not fluorescently labeled and were not designed specially for this application but were chosen simply to bracket the desired mutation, , not to amplify homologues. The present micro-chip based HA/SSCP method requires no off-chip preparation of the DNA sample in terms of labelling and denaturation, and needs only that the DNA sample be on the order of 200-300 bp in length, the size range generally used in HA and SSCP work.

2.2.3 Microchip Equipment

The micro-chips used here were manufactured by Micralyne (Edmonton, AB). These chips had a simple cross design consisting of 4 wells (each containing ca. 3 μL) in 2.2mm thick borofloat glass. These wells are linked by two micro-channels that are nominally 50 μm wide and 20 μm deep. One of the channels provides a separation channel approximately

80 mm in length (Figure 2.1). As described previously by [76], the Microfluidic Tool Kit (μTK, Micralyne, Edmonton, AB) provided high voltages power supplies and a laser induced fluorescence (LIF) system with excitation at a wavelength of 532 nm and detection at 578 nm. The application of high voltages to the micro-chip is fully controlled by the μTK and the interface to the μTK is provided by a compiled Labview program (supplied by Micralyne) running on a PC connected to the μTK by a serial link. The μTK acquired the LIF signal at 200 Hz and the data were recorded by the PC. The fluorescence signal is recorded in Volts and is graphed as relative fluorescence units (RFU) versus time.

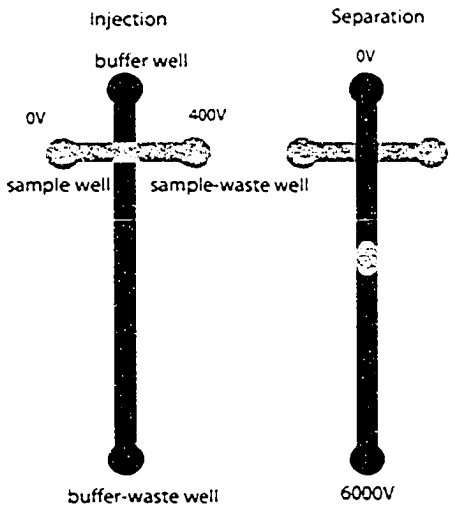

Figure 2.1: Diagram of the simple cross microchip made of glass. The circles represent reservoirs 2 mm in diameter and 1.1 mm deep, each holding ca. 3 μL. The lines forming the cross represent microchannels nominally 50 μm wide, 20 μm deep and having an approximately semi-circular cross section. a) The microchip in the injection phase b) The microchip in the separation phase.

2.2.4 Microchip Electrophoresis

All operations upon the μTK were automated through the use of a LabVIEW interface. These operations consisted of sample injection and sample separations. In sample injection, by applying a potential of 400 V for 60 s at the sample waste well and 0 V at the sample well (corresponding to an electric field of 500 V/cm) (the buffer and buffer waste wells are electrically disconnected automatically) the negatively charged DNA is moved from the sample well through the injection channel and into the sample waste well. This is depicted in Figure 2.1a.

In sample separations, by applying a potential of 6000 V for 180 s at the buffer waste well and 0 V at the buffer well (corresponding to applying an electric field of 740 V/cm) (with the sample and sample waste wells electrically disconnected automatically) the DNA within the intersection of the channels is moved down the separation channel toward the buffer waste well. This is depicted in Figure 2.1b.

The laser-induced fluorescence was detected at a point located 76 mm from the intersection (indicated by an x in Figure 2.1). After the first two runs (each consists of 60 s injection and 180 s separation), additional runs were performed by using 5 s injections each followed by 180 s separations. Each sample was analyzed with four runs and the arrival times of the DNA during the separation varied by less than ca. 1 %. As will be discussed later (section 2.2.6), no formamide was present in the first run of each load in order to validate the on-chip denaturation.

2.2.5 Reagents

A Tris Borate with EDTA buffer (TBE) was made with Tris Base and Boric Acid from Fisher Scientific (NJ, USA) and EDTA from Merck (Darmstadt, Germany). GeneScan polymer from PE Applied Biosystems (Foster City, CA) was mixed with glycerol from Sigma (Saint Louis, MO) and TBE buffer so that the final concentration of Genescan was 5 % (w/w) and the final concentration of glycerol was 10 % (w/w). This dilution, referred to as 5GS10G, was used as the sieving medium for electrophoresis. The running

buffer, referred to as 1xTBE10G, was made from glycerol and TBE buffer so that the final concentration of glycerol was 10 % (w/w). A dilution of this solution to 1 part in 10 in de-ionised water is used for sample preparation and is referred to as 0.1xTBE1G. Deionized formamide (minimum 99.5 %) was purchased from Sigma (Saint Louis, MO).

Sytox Orange, an intercalating dye suitable for labelling dsDNA, was obtained as a 5 mM stock solution in DMSO (Dimethylsulfoxide) from Molecular Probes (Eugene, OR). A second DNA stain, POPO-3, was also purchased as a 1 mM stock solution in DMF (Dimethylformamide) from Molecular Probes. Sytox Orange and POPO-3 solutions were diluted to 0.2 μM and 0.5 μM in 1xTBE respectively.

2.2.6 Chip Preparation

The channels of a micro-chip, either a new or rinsed (see below) one, were first filled by a mixture of 5GS10G with 0.2 μM Sytox Orange (the final concentration) using a 1 mL syringe. After 1 minute the mixture was flushed out of the channels, the wells were rinsed with de-ionised water for 30 s, and the wells and channels were dried by forcing air through the channels with a 1mL syringe. To remove excess Sytox Orange, the channels were filled with 1 M sulphuric acid for 2 minutes and then the channels and wells were each rinsed with de-ionised water for 30 s. The wells and channels were then again air-dried. We observed artifacts (discussed later) indicative of excessive dye labelling (heavy labelling) without this sulphuric acid treatment. After drying the chip and the wells, the channels were filled with the sieving matrix, 5GS10G. The sample well of the micro-chip was loaded with 2.7 μL of diluted running buffer, 0.1xTBE1G, and 0.3 μL of unlabeled PCR product. The buffer well and sample-waste well were loaded with 3 μL of running buffer, 1xTBE10G. In order to label dsDNA and ssDNA on the chip, following the inverse-flow method, the buffer-waste well was loaded with 3 μL of the mixture of 1xTBE10G with 0.5 μM POPO-3 (the final concentration). Following the above loading procedure we performed four runs, each consisting of a sample-injection stage and a separation stage. The first run consists of a run with a 60 second injection and a 180 second separation

and it shows only dsDNA. Following this first run, 2 μL of the mixture in the sample well was replaced with formamide (in order to denature the DNA within the sample well). After the addition of the formamide a second run with a 60 second injection, and 180 second separation was performed. In the second separation stage both ds and ssDNA were present. Two subsequent runs were made for verifying reproducibility, each with a 5 second injection and 180 second separation (data not shown) that gave results similar to those of the second run.

The process for pre-treating the micro-chip requires several minutes but once it is prepared the chip is capable of being used for three samples (a total of 12 runs). After the third sample loading, the intensities of peaks are too low for reliable use, with peaks that are less than 0.1 V (data not shown), this is the time that the chip should be cleaned and re-treated with Sytox Orange. This cleaning step consists of loading the micro-chip with 1 M sulphuric acid for 20 minutes. We verified that this 20-minute sulphuric acid treatment removes any residual Sytox Orange from the micro-chip by analyzing a sample of BRCA1 Exon 20 5382insC and verifying that no signal was present i.e. the DNA sample was unlabeled (data not shown).

2.2.7 Data Analysis

A C++ program performed the analysis of the fluorescence data by removing the spurious, isolated spikes due to electrical noise (i.e. peaks consisting of a single point). The data were recorded at 200 Hz, much faster than the signals from DNA passage, and so this processing did not affect the peaks due to the passage of DNA. In successive runs with the same sample the peaks from DNA were consistently present. The analysis program then wrote postscript files for all of the analyzed data. More details can be found in [76].

2.3 Results and Discussion

The integrated method of SSCP and HA that is demonstrated in this chapter is rapid, easily performed, and is compatible with higher levels of micro-chip integration. The ability to stain the DNA on-chip gives significant advantages in providing strong signals. Following this on-chip labeling method, it is possible to deal with PCR products from reactions with unlabelled primers. This method could also be used for analyzing DNA from sources other than PCR amplification. Signal strength given by such stains has led to demonstrations of single-molecule detection (e.g. [77]).

Methods have been developed for performing accurate and high-resolution capillary electrophoresis separations of dsDNA using dimeric intercalation dyes as noncovalent labelling reagents. Although the use of intercalators such as POPO-3 (e.g. [71]) and Sytox Orange (e.g. [67] has been widely reported with pre-labelled DNA or with the intercalator present in sieving matrix, we have found that such methods are very sensitive to subtle variations in preparation and concentrations (especially of salts). Marino *et al.* also reported that when the DNA was complexed with dimeric dyes and injected in the column, poor results were obtained evidenced by low signal and loss of resolution, mainly due to peak broadening [66].

In particular, these dyes are often in a dynamic equilibrium with their environment such that pre-labelled DNA (i.e. that contains the intercalator) is, in our experience, often not fluorescent by the time it reaches the LIF detection point. Using glass chips, we have attributed this to the uptake of the intercalator by the channel walls since channel walls are deprotonated (i.e. they are negatively charged) and intercalating dyes are positively charged. These effects appear especially strong with POPO-3 (and may also be exacerbated by our use of conditions that enhance conformation effects). Clark *et al.* investigated the ionic effects on the stability and electrophoretic mobility of DNA-dye complexes (i.e. pre-labelled DNA with intercalating dyes) in [78]. Backhouse *et al.* have used Sytox Orange successfully in the past [79] and the method appears relatively stable against such effects but unfortunately Sytox Orange does not stain ssDNA [80].

Figure 2.2 shows the fluorescence versus time of the HFE Exon 2 wildtype sample. As can be seen there is no signal for the first 60 s of injection and it is followed by a slightly higher baseline once the laser is turned on. The laser would be slightly more stable if left on for a long period before the analysis, however, turning it on at the beginning of the separation step provides a convenient marker and prevents the possible photobleaching of the fluorescence within the separation channel by means of undesired waveguiding effects in the microchannel.

As the unlabeled DNA travels through the micro-chip, dye molecules, that also travel through the micro-chip but in the opposite direction, intercalate in both the single-stranded (POPO-3) and double-stranded (Sytox Orange) forms. At about 140 s weak signals were detected from the arrival of the primers; the dsDNA at about 168 s and the four ssDNA peaks at about 185 s arrived after the primers. After adding formamide, in the injection step, the neutral formamide is left behind as the ssDNA enters the microchannel. Once in the microchannels the ssDNA may then self-assemble. Figure 2.2b shows the period 165 s to 205 s with higher resolution. In the same figure, there are four peaks related to ssDNA in the electropherogram of the wild-type sample, i.e. more than one peak per sequence of ssDNA. This could be due to multiple secondary structure of the ssDNA or it may be due to primer-ssDNA constructs that were formed during denaturation [65, 81]. Kourkine *et al.* demonstrated this primer-ssDNA mechanism with an experiment in which removal of the primers led to the disappearance of primer-ssDNA constructs, and the re-addition of the primers resulted in the re-appearance of the construct peaks [81]. Whatever the source of the peaks, the basis of the SSCP method is that the electropherograms of the wildtype and mutant samples need only differ.

In the present work, we found it effective to passivate the microchannels with Sytox Orange. We applied the inverse-flow method by adding POPO-3, an intercalating dye (section 2.2.5), to the buffer waste well [68] (after passivating the channels) to label both ssDNA and dsDNA. The whole idea of the inverse-flow method is that the negatively charged DNA fragments migrate from the negative polarity to the positive polarity, while the positively charged dye ions migrate in the opposite direction. When DNA fragments meet with dye

ions. DNA-dye complexes are formed and the complexes continue migrating to the positive end, due to their net negative charge. We also tried the same experiment, i.e. inverse flow method for labelling, without Sytox Orange pre-treatment and obtained no fluorescence (data not shown). We found out that without the Sytox Orange pre-treatment, the DNA would not be fluorescent at the detection point since dye ions (POPO-3) would stick to the negatively charged walls (no DNA-dye complex would form).

As discussed in section 2.2.6, there is a stage of sulphuric acid treatment after Sytox Orange passivation (to make inactive or less reactive the surface by chemical treatment) to prevent the accumulation of excessive amounts of Sytox Orange. Without the 2 minute filling of the channels with 1 M sulphuric acid we observed that the peaks were broadened to the extent that there was insufficient resolution for HA/SSCP. Under these circumstances the peaks may arrive significantly later than expected, also as reported [68, 82]. The late arrival is probably due to the positive charge of the dye decreasing the overall charge-to-mass ratio of the DNA-dye complexes.

The 2-minute sulphuric acid treatment provides a high enough resolution for HA/SSCP and reliable arrival times. Sulphuric acid probably removes the extra dye molecules stuck to the channels. Unless otherwise specified all runs utilized a 2-minute sulphuric acid treatment in the chip procedure. The use of DNA stains in this manner provides strong signals; however, the 2-minute sulphuric acid treatment decreased the intensity. The peaks for on-chip labeled samples in the present work are still stronger than primer-labeled samples. Figures 2.3 and 2.4 show examples of heavy labelling and normal labelling for BRCA1 samples i.e. heterozygous sample of 5382insC and 5396+1G>A respectively. In Figure 2.3a (with a 2-minute sulphuric acid treatment) the dsDNA and ssDNA are labelled normally with the dsDNA peaks showing the multiple peaks characteristic of when heteroduplexes are present, and the ssDNA peaks all being clefted as is often characteristic of a heterozygous sample. In Figure 2.3b (without a 2-minute sulphuric acid treatment) there is evidence of heavy labelling i.e. very strong peaks and low resolution to the extent that the ssDNA clefts have been lost and the dsDNA multiple peaks smeared considerably. The same could be said for Figure 2.4a and Figure 2.4b for 5396+1G>A sample.

To demonstrate that the formamide is denaturing the DNA within the chip we show the results before and after the addition of formamide. Figure 2.5 shows the runs for the mixture of wildtype of HFE Exon 2 with the homozygous mutant S65C before and after adding formamide to the sample well. The first analysis, done without the addition of formamide, shows as a single dsDNA peak –as expected from a non-denatured sample of homoduplexes 2.5a(2.6a). As shown in Figure 2.5b, only after the addition of formamide are the ssDNA peaks evident, verifying that the formamide denatured the sample DNA. In addition, the dsDNA profile is now indistinguishable from that presented by a HA analysis of a heterozygous sample (data not shown). This indicates that the dsDNA peaks are from DNA that was reassembled on-chip. Figure 2.6a and Figure 2.6b also corresponded to two runs before and after the addition of formamide for the mixture of wildtype of HFE Exon 2 with the homozygous H63D.

As described above, we found the effective use of formamide to denature the dsDNA in the sample well. The act of injection leaves the formamide behind in the sample well since it is uncharged. Depending upon the amount of time given the ssDNA once it is in the microchannel, the degree of recombination can be controlled to the extent that mainly ssDNA or mainly dsDNA can be produced. Perhaps most importantly, this gives us the ability to compare two sources of DNA on-chip by denaturing and then performing HA and/or SSCP. A more detailed investigation of the control of DNA self-assembly in this manner will be presented elsewhere [83].

As discussed in 1.1.2.2 and equation 1.3, formamide reduces the melting temperature of DNA duplexes in a linear fashion (by $0.72^{\circ}C$ for each percent of formamide). Calculating T_m for our samples from equation 1.3, having %(G+C)= 51 for HFE Exon 2 (234 bp) and 47 for BRCA1 Exon 20 (234 bp), %formamide= 66 and M= 1.78 mM (consisting of Na+ ions from EDTA in TBE buffer and K+ ions in PCR buffer), we found T_m of ca. $9.2^{\circ}C$ and $7.6^{\circ}C$ for HFE Exon 2 and BRCA1 Exon 20 samples respectively. This calculation shows that on-chip denaturation/re-hybridization in room temperature presented in this work is theoretically feasible. The presence of ssDNA in Figure 2.5b(2.6b) indicates successful on-chip denaturation.

Figure 2.7 shows the results of HA and SSCP for the BRCA1 Exon 20 wildtype and heterozygous samples after adding formamide to the sample well. Figure 2.7a shows the results for a wildtype sample of BRCA1 Exon 20. The reassembled wildtype dsDNA contains sequences that are exactly complementary (i.e. a homoduplex). As expected then, one peak is seen in the electropherogram of the dsDNA (Figure 2.7a). The wildtype sample provides DNA that contains two sequences of ssDNA once denatured by the action of the formamide in the sample well. Three peaks are seen in the electropherogram of the ssDNA (Figure 2.7a).

The heterozygous sample of BRCA1 Exon 20 5396+1G>A produces both homoduplexes and heteroduplexes and, given the subtlety of the mutation (a SNP) the change in the dsDNA profile is relatively subtle. The electropherogram of the dsDNA of this sample, (Figure 2.7b) shows two closely spaced peaks, likely the homoduplexes (first peak) followed by the heteroduplexes. The electropherogram of the ssDNA of this sample shows three peaks, the last two each having two clefts. The heterozygous sample of BRCA1 5382insC produces both homoduplexes and heteroduplexes and, given the less subtle nature of the mutation (1 base insertion) we can now distinguish more resolved duplexes. Figure 2.7c shows the analysis of a heterozygous sample of 5382insC. The electropherogram of the dsDNA of this sample (Figure 2.7c) shows three peaks while that of the ssDNA shows another 3 peaks, each clefted. Comparing Figures 2.7b and 2.7c with 2.7a, both heterozygous 5382insC and 5396+1G>A mutations can be detected by this combined HA/SSCP method.

Figure 2.8 also shows the results of HA and SSCP for the HFE Exon 2 wildtype and homozygous samples after adding formamide to the sample well. Figure 2.8a shows the results for a wildtype sample of HFE Exon 2. The reassembled wildtype dsDNA contains sequences that are exactly complementary (i.e. a homoduplex). As expected then, one peak is seen in the electropherogram of the dsDNA (Figure 2.8a).

The homozygous sample of HFE Exon 2 S65C plus wildtype produces both homoduplexes and heteroduplexes. The electropherogram of the dsDNA of this sample, (Figure 2.8b) shows two closely spaced peaks, likely the homoduplexes (first peak) followed by

the heteroduplexes. The electropherogram of the ssDNA of this sample shows three peaks, the last two each having two clefts. The homozygous sample of HFE H63D plus wildtype produces both homoduplexes and heteroduplexes. Figure 2.8c shows the analysis of a homozygous sample of HFE H63D plus wildtype. The electropherogram of the dsDNA of this sample (Figure 2.8c) shows a clefted peak while that of the ssDNA shows another 4 peaks, each clefted. Comparing Figures 2.7b and 2.7c with 2.7a, both homozygous H63D and homozygous S65C mutations can be detected by this combined HA/SSCP method.

2.4 Conclusion

An effective integration of a method for on-chip denaturing and re-hybridizing of DNA, for the on-chip labelling of the resulting ss and dsDNA, and for performing SSCP and HA has been demonstrated in this chapter. We analyzed three different PCR products for each type of sample i.e. BRCA1 Exon 20 (wildtype, heterozygous 5396+1G>A and heterozygous 5382insC) and HFE Exon 2 (wildtype and homozygous H63D, wildtype and homozygous S65C) and we had reproducible results from run to run for each PCR product. The present HA/SSCP method has shown readily interpreted electropherograms that show a clear distinction between wildtype and mutant samples. Although Tian *et al.*, [84] demonstrated SSCP on a micro-chip, in the present work we use unlabelled samples and can perform all processing of the sample on chip (rather than requiring, e.g. off-chip thermal treatments).

Taking several minutes for the preparation of the micro-chip before each set of runs, our micro-chip HA/SSCP method is only slightly more complex than the very direct and rapid method Backhouse *et al.* previously presented (for HA alone) [75]. The HA method in [75] used fluorescently labelled primers in PCR reactions to produce end-labelled dsDNA, obviating the need for the use of intercalating dyes. Although our present method achieved similar electropherograms, in comparison, two features stand out– the present work has significantly stronger signal–to–noise ratios (i.e. the effects of noise were quite apparent in the previous method) and the mutation sensitivity of the present method is higher (i.e. the electropherograms of mutations have more structure).

With the significant research towards integrating multiplexed PCR and electrophoretic analysis arrays it has been suggested that microfluidic systems may provide throughputs that are as much as 100 times higher than presently attainable [85]. This integrated mutation detection device is a significant step towards that goal.

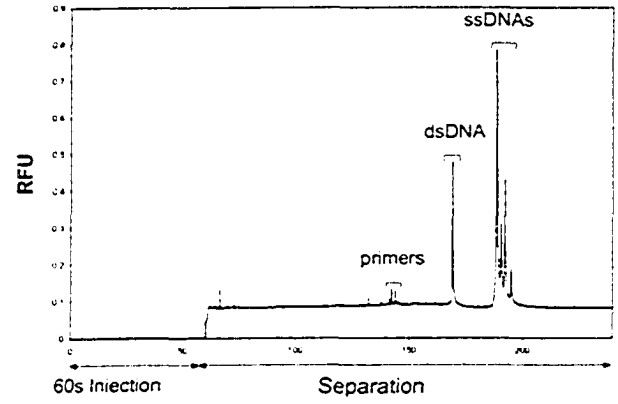

(a)

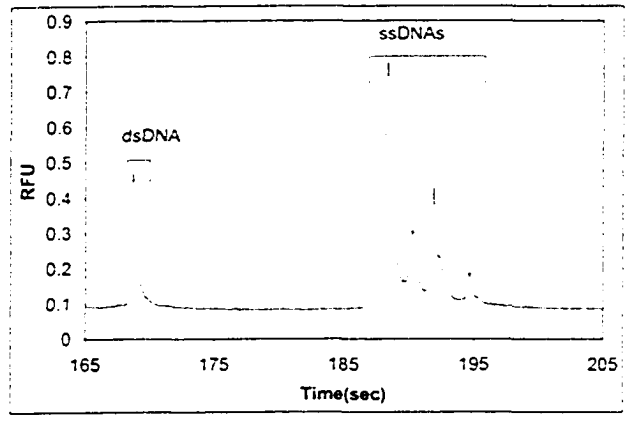

(b)

Figure 2.2: a) The electropherogram of a wildtype sample of HFE Exon 2 with the x-axis representing time and the y-axis the fluorescence intensity in relative fluorescence units (RFU). An injection was performed for 60s followed by a separation of 180s. Primers, dsDNA and ssDNA peaks are seen at approximately 140s, 168s and 185s respectively. Analysis done immediately after the addition of formamide. b) The inset shows the dsDNA and ssDNA peaks of a) in higher resolution.42

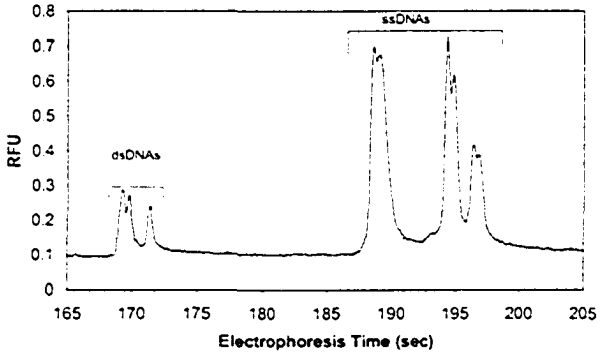

(a)

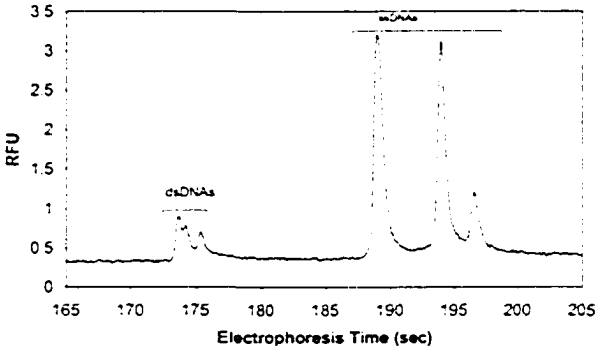

(b)

Figure 2.3: Examples of heavy and normal labelling for BRCA1 Exon20, heterozygous 5382insC. Analysis done immediately after the addition of formamide. a) normal labelling b) heavy labelling

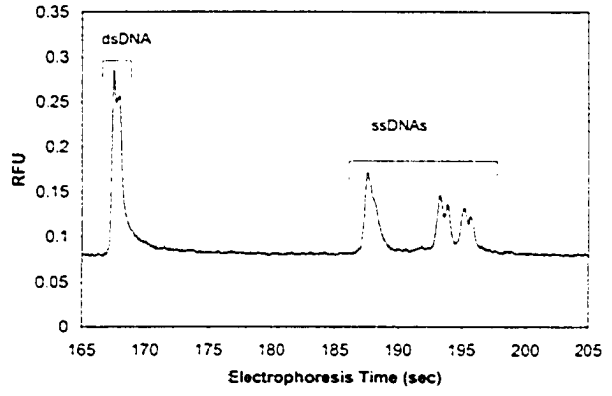

(a)

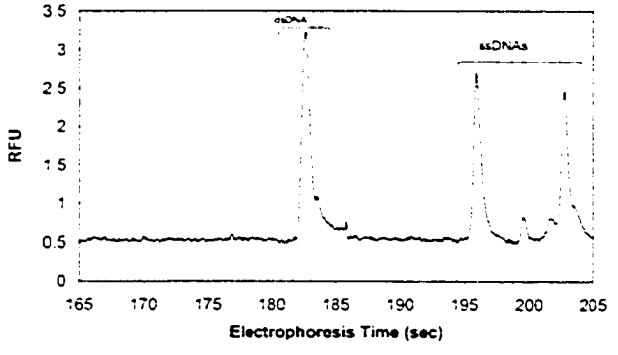

(b)

Figure 2.4: Examples of heavy and normal labelling for BRCA1 Exon20, heterozygous 5396+1G>A. Analysis done immediately after the addition of formamide. a) normal labelling b) heavy labelling

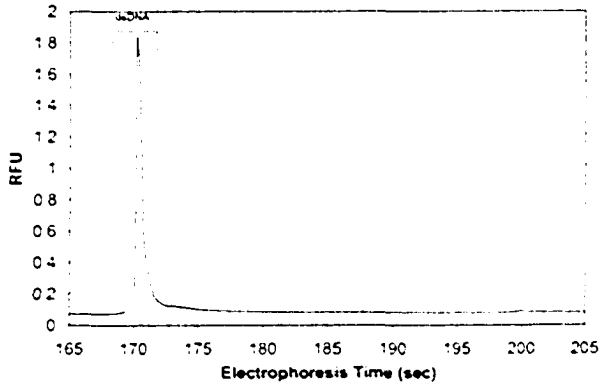

(a)

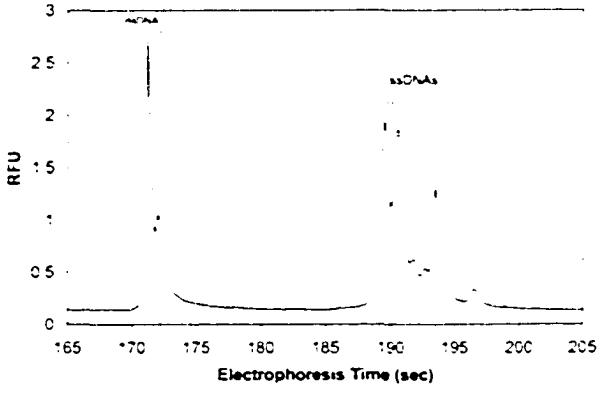

(b)

Figure 2.5: Mutation analyses of HFE Exon 2 DNA samples by HA/SSCP before and after adding formamide for the mixture of wildtype and S65C (homozygous) in the sample well. a) dsDNA for HFE Exon 2 (S65C homozygous + WT) before adding formamide b) dsDNA and ssDNA for HFE Exon 2 (S65C homozygous + WT). Analysis done immediately after the addition of formamide.

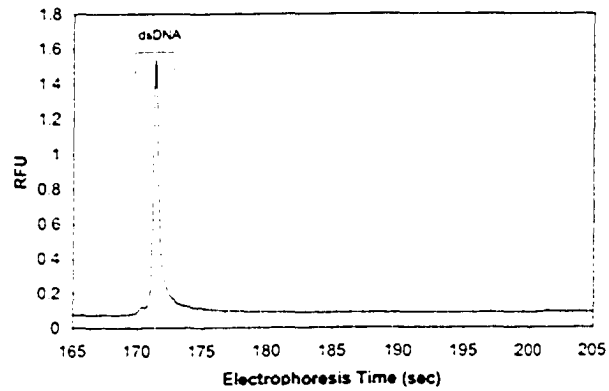

(a)

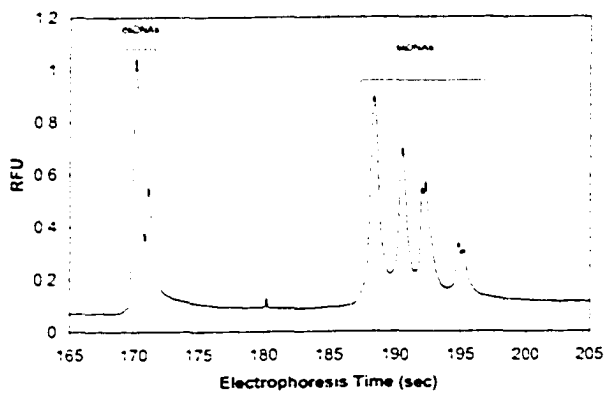

(b)

Figure 2.6: Mutation analyses of HFE Exon 2 DNA samples by HA/SSCP before and after adding formamide for the mixture of wildtype and H63D (homozygous) in the sample well. a) dsDNA for HFE Exon 2 (H63D homozygous + WT) before adding formamide b) dsDNA and ssDNA for HFE Exon 2 (H63D homozygous + WT). Analysis done immediately after the addition of formamide.

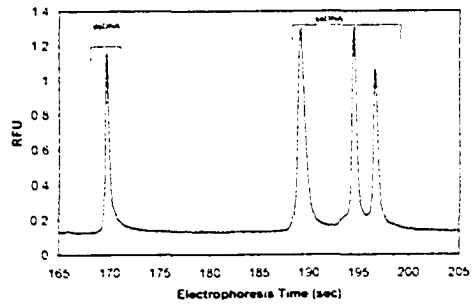

(a)

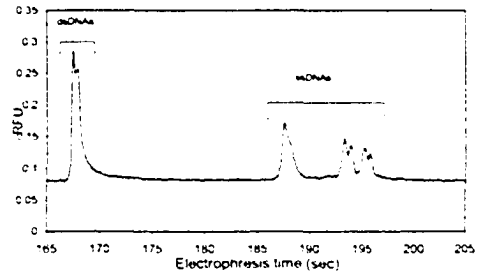

(b)

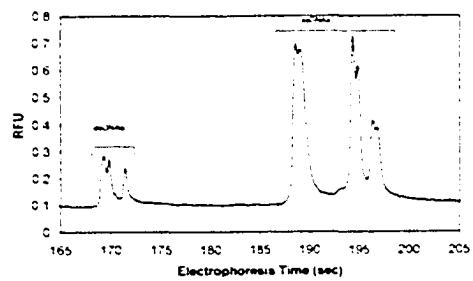

(c)

Figure 2.7: Mutational analyses of BRCA1 Exon 20 DNA samples by HA/SSCP for wild-type, heterozygous 5396+1G> and heterozygous 5382insC after addition of formamide. a) dsDNA and ssDNA for BRCA1 Exon 20 WT b) dsDNA and ssDNA for BRCA1 Exon 20 heterozygous 5396+1G>A c) dsDNA and ssDNA for BRCA1 Exon 20 heterozygous 5382insC

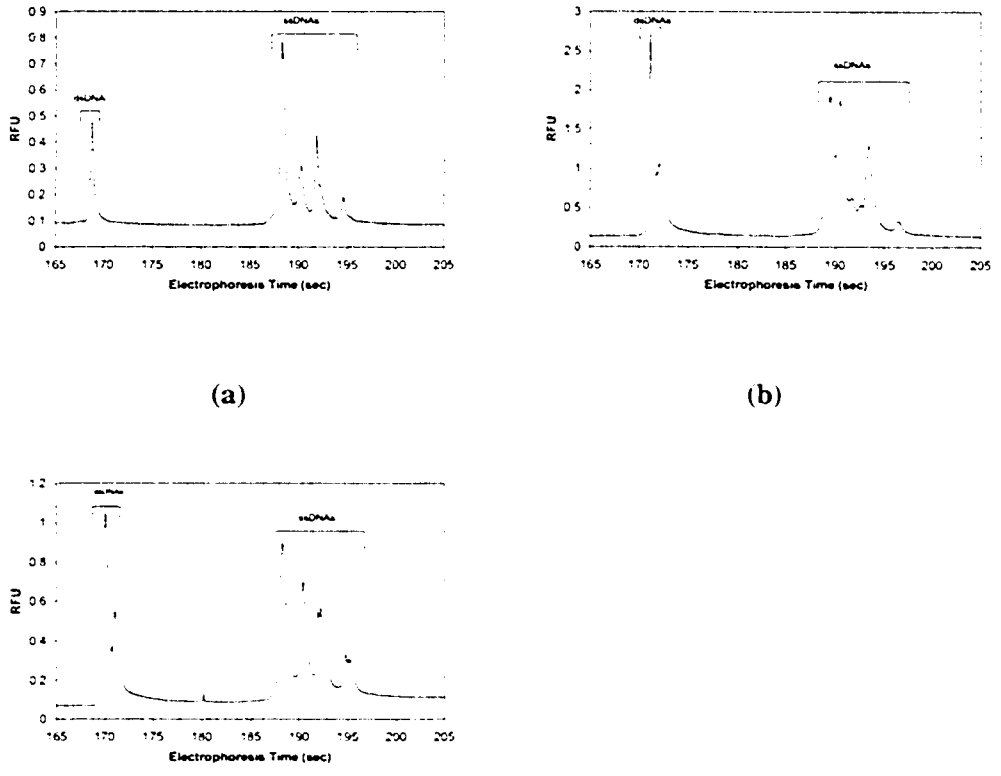

Figure 2.8: Mutational analyses of HFE Exon 2 DNA samples by HA/SSCP for wildtype, homozygous H63D and homozygous S65C after addition of formamide. a) dsDNA and ssDNA for BRCA1 Exon 2 WT b) dsDNA and ssDNA for BRCA1 Exon 2 homozygous plus WT S65C c) dsDNA and ssDNA for BRCA1 Exon 2 homozygous plus WT H63D

Chapter 3

Preliminary Work Towards Enhanced Resolution in Separations Using Intercalators

3.1 Introduction

The ability to do on-chip labeling using intercalating dyes gives significant advantages by providing low cost and sensitive detection techniques. The signal strength given by such stains has led to the demonstration of single-molecule detection (e.g., [77]) and the on-chip labeling could be used to analyze DNA without the need for amplification by means of PCR. However, the use of intercalating dyes typically results in reduced electrophoretic resolution due to the statistical distribution of dye molecules.

Intercalating dyes can also cause slight unraveling and elongation of the duplex DNA [86]. This may change the conformation of DNA and consequently can affect the sensitivity (the percentage of mutations that are successfully detected) of mutation detection techniques like heteroduplex analysis (HA). HA is an easy and inexpensive mutation detection method although it does not have a detection sensitivity that is as good as DNA sequencing [1]. The optimum conditions of different parameters in HA like sample preparation,

labeling, assay temperature, sieving matrix and buffer composition should be investigated in order to increase the sensitivity of this mutation detection technique.

A method was proposed in this chapter in order to detect bright DNA sample without losing the resolution of separation using intercalating dyes. In this method, dye molecules label the dsDNA at the end of the channels just prior to detection and this will ensure minimal disruption of the mobility of dsDNA molecules, enabling high resolution analyses. This idea may also serve to increase the mutation detection sensitivity of HA by introducing minimal change in the conformation of heteroduplexes.

3.1.1 Intercalating Dyes Usage in CE-LIF

Micro-chip capillary electrophoresis in conjunction with laser-induced fluorescence (LIF) provides remarkable speed, sensitivity and resolving power [87], however, this technology requires the fluorescent labeling of target nucleic acids. There are a number of fluorescent reagents that are commercially available for labeling DNA and proteins.

The covalent labeling of DNA with highly fluorescent and stable non-intercalating dyes, such as Lissamine rhodamine-B sulfonyl chloride (Lissamine 20), tetramethyl-rhodamine isothiocyanate (TRITC), sulfoindocyanine succinimidyl ester (Cy5) is common for DNA analysis by CE-LIF [87].

The addition of dye dilutions to the DNA sample prior to separation, usually involved with different periods of incubation time, is called pre-column labelling. When working in pre-column mode, the main advantages of covalent dyes include: (1) conditions for derivatization and separation can be independently chosen for optimum sensitivity and separation efficiency; (2) the separation system is relatively simple and flexible. However, attention must be paid to overcome problems associated with poor labeling efficiency and multiple labeling of the analytes [87]. Most covalent labeling reactions rely on reagents that attack primary amines. These reagents do not distinguish efficiently between the different amine groups in the sample and the ones associated with lysine residues, and as a result, the labeling reaction produces a complex mixture of products [88].

Intercalating dyes, chemicals that are normally weakly fluorescent and become strongly fluorescent upon forming complexes, are a simpler alternative to covalently attached dyes for labeling DNA fragments [89]. The intercalating dyes lend themselves to higher levels of integration in micro-chip analysis since they can be used for the on-column labeling of DNA. A potential drawback of the use of this kind of dye in micro-chips is the exchange of intercalating dyes between DNA, running buffer, and in our experience, the glass walls of the micro-channels.

Complicated band splitting patterns or band-broadening have been reported in cases where DNA fragments were pre-stained prior to sample loading [90–92]. Carlsson *et al.* showed the gel electrophoresis of the dsDNA (38 kbp) and YOYO (the intercalator) complexes at various dye concentrations (Figure 2a of [90]). Below the dye/bp ratio of 0.10 two zones could be observed (band-splitting) where the faster component continues the trend of increasing velocity as the amount of dye added decreases [90]. Zhu *et al.* also showed the bands in the preformed DNA-TOTO complex separation were broad and overlapping, and this result persisted under a wide variety of conditions (Figure 3 of [92]). Tan *et al.* [71] explained these observations as follows: when the DNA-dye complexes migrate toward the detection end, they traverse a dye-depleted zone as the unbound dye molecules migrate toward the injection end. The complexation equilibrium will favor the formation of free dye and DNA in this dye-depleted region. The loss of dye results in a heterogeneous distribution in the number of dye molecules complexed with the DNA strands, which leads to peak broadening [71] (as shown in Figure 3.1). This can greatly reduce the resolution of separations in capillary electrophoresis.

3.1.2 Intercalating Dyes and Heteroduplex Analysis

Heteroduplex analysis (HA) is one of the most widely used methods for screening unknown mutations [1]. HA relies on the fact that, under native conditions, homoduplexes and heteroduplexes with a mismatched base pair(s) (formed during PCR amplification) usually have different electrophoretic mobilities [1]. Providing proper conditions so that

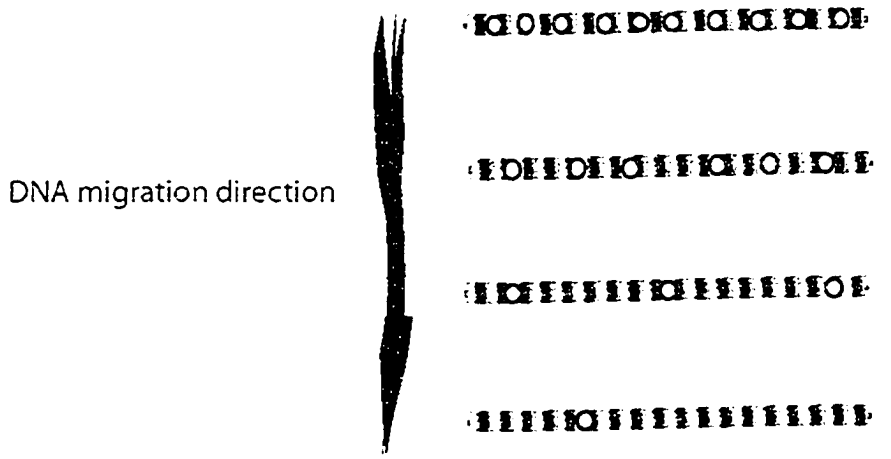

Figure 3.1: Schematic presentation of the heterogeneous distribution of dye molecules (circles) on DNA strands.

the mobility difference is high enough to be detected through heteroduplex analysis can be a challenge for subtle mutations, especially if the resolution is degraded. Much work has been done in applying HA for mutation detection (more in section 1.4). Rossetti *et al.* developed a sensitive heteroduplex analysis technique by staining the dsDNA with ethidium bromide [93]. Tian *et al.* explored the potential of capillary and microchip electrophoresis for HA-based mutation detection in [84, 94, 95]

Kaji *et al.* [96] showed that YO-PRO-1, an intercalating dye, stacks between the base pairs and extends the contour length (the maximum end-to-end distance of a polymer chain) of the DNA and also changes the electric charge of the DNA. Habbersett *et al.* recently developed an analytical system based on a compact flow cytometer for DNA fragment sizing and single-molecule detection [97]. They believe that the intercalation extends the DNA polymer by doubling the interbase-pair distance from 3.4 to 6.8 Å [98], and unwinds the helix by 18° for each intercalated dye molecule [99].

In order to achieve higher sensitivity, conditions for mutation detection techniques like HA and SSCP should be optimized when microchip capillary electrophoresis is used. Rodrigues *et al.* expected that the detection sensitivity could be enhanced by using higher concentration of the sample, controlling the injection channel potentials during separation to eliminate leakage, or by using better optics, a brighter source and a more sensitive photon detector [39]. Andersen *et al.* reviewed different parameters, like sample preparation, assay temperature, sieving matrix and buffer composition, that can affect the mutation detection sensitivity of SSCP in [100]. From the above references, the intercalating dyes are able to change the inter-base-pair distance, net charge and conformation of DNA. In this work, we investigated the effect of labeling method on the conformation of heteroduplexes in HA.

3.2 Materials and Methods

3.2.1 General

BRCA1 Exon 20 (234 bp) was PCR-amplified from a test panel of clinically relevant DNA templates. The samples were wild-type (denoted -/-) or heterozygous (denoted +/-) for the 5382insC mutations. The samples were PCR-amplified following the same protocol presented in section 2.2.1. GeneScan-500 (PE Biosystems, Foster City, CA), a size standard, containing 16 fragments (35-500bp), was used in the chip calibration protocol.

3.2.2 Inverted Microscope

A microscope (Axiovert 200) for transmitted light and epifluorescence was purchased from Zeiss (Gottingenn, Germany). The Axiovert 200 is an inverted microscope and is mainly used for the examination of cell and tissue cultures and of sediments in culture flasks in transmitted and reflected light.

3.2.3 Microchip Equipment

The micro-chips used here were manufactured by Micralyne (Edmonton, AB). Since the experimental platform in chapter 2 and this chapter is the same, details are provided here only when they differ from those in section 2.2.3.

3.2.4 Microchip Electrophoresis

More information can be found in section 2.2.4. No formamide was added to the well for this experiment since there was not any denaturation.

3.2.5 Reagents

A Tris Borate with EDTA buffer (TBE) was made with Tris Base and Boric Acid from Fisher Scientific (NJ, USA) and EDTA from Merck (Darmstadt, Germany). GeneScan polymer from PE Applied Biosystems (Foster City, CA) was mixed with glycerol from Sigma (Saint Louis, MO) and TBE buffer so that the final concentration of Genescan was 5 % (w/w) and the final concentration of glycerol was 10 % (w/w). This dilution, referred to as 5GS10G, was used as the sieving medium for electrophoresis. The running buffer, referred to as 1xTBE10G, was made from glycerol and TBE buffer so that the final concentration of glycerol was 10 % (w/w). A dilution of this solution to 1 part in 10 in de-ionised water is used for sample preparation and is referred to as 0.1xTBE1G. Sytox Orange, an intercalating dye suitable for labelling dsDNA, was obtained as a 5 mM stock solution in DMSO (Dimethylsulfoxide) from Molecular Probes (Eugene, OR). Sytox Orange solution was diluted to 0.2 μM in 1xTBE10G.

3.2.6 Chip Calibration Protocol

The calibration protocol was developed in the Backhouse lab (University of Alberta, Edmonton) and it has been used for measuring the performance of microfluidic chips. The channels of a cleaned microchip (section 2.2.6) were filled with 5GS10G. The sample well

was loaded with 2.7 μL of diluted running buffer (0.1xTBE1G) and 0.3 μL of Genescan-500 (PE Biosystems, Foster City, CA). The buffer well, the sample-waste well and the buffer-waste well were loaded with 3 μL of running buffer, 1xTBE10G. Placing the laser at 76 mm from the intersection, the first run of the calibration load consisted of a 60 s injection followed by a 180 s separation. The second run consisted of a 10 s injection followed by a 180 s separation, and it checked the reproducibility of the first run.

The full-width-half-max (FWHM) of three peaks in Genescan-500 size standard, i.e. 200, 250 and 300 bp, were calculated by a C++ program performing the analysis of the fluorescence data. For a chip with good performance, we expect the FWHM to be less than 0.3 s.

Another procedure called the flow check was started after the second injection-separation. In the flow check run, the laser point was located 125 μm from the channel intersection toward the sample well. The electric voltages and timings of the μTK for this test are listed in Table 3.1. The flow check run included three re-injection stages. In each stage, a separation voltage was applied for 5s to remove the sample plug from the channel intersection and move it towards the LIF detection point (steps 2, 5 and 9 in Table 3.1). An extra 40s injection was added before the 5 seconds separation in the 1st stage (step 1 in Table 3.1). The sample in the injection channel was then pulled back toward the sample well and the sample waste well respectively (steps 3, 6, and 10 in Table 3.1). In the next steps, the separation voltage was applied between the buffer well and the buffer waste well for various durations (0s, 30s and 60s for each stage respectively). After each such separation, the sample was again moved toward the intersection (step 4, 8 and 12 in Table 3.1). Each of these re-injection stages tests the time that takes for the DNA sample to return to the detection point after different separation intervals.

The returning time of the sample in each flow check stage (named t_1, t_2, t_3 for each stage respectively) was calculated based on the derived data of electropherograms of the flow check. First, the average and standard deviation of the returning times are calculated for the LIF data in the last part of the preceding pullback step (when no DNA is present). The time when the signal is equal to the average plus 100 times the standard deviation is

Table 3.1: Voltage and Electric Polarity Settings for The Flow Check Procedure

Step	Time	Sample-waste well	Buffer-waste well	Sample well	Buffer Well
1	40s	0.40 kV	Float	Ground	Float
2	5s	Float	6.00 kV	Float	Ground
3	15s	0.20 kV	Float	0.20 kV	Ground
4	10s	0.40 kV	Float	Ground	Float
5	5s	Float	6.00 kV	Float	Ground
6	15s	0.20 kV	Float	0.20 kV	Ground
7	30s	Float	6.00 kV	Float	Ground
8	10s	0.40 kV	Float	Ground	Float
9	5s	Float	6.00 kV	Float	Ground
10	15s	0.20 kV	Float	0.20 kV	Ground
11	60s	Float	6.00 kV	Float	Ground
12	10s	0.40 kV	Float	Ground	Float

defined as the sample returning time. The difference between the 2nd re-injection and the 1st re-injection is defined as $d_1 = t_2 - t_1$ and the difference between the 3rd re-injection and the 1st re-injection was defined as $d_2 = t_3 - t_2$. The chips with good resolution have d_1 and d_2 smaller than 0.5s. More detail about the flow check in microchips can be found in [101].

3.2.7 Chip Preparation

In this chapter, in order to label the dsDNA on the chip, a micro-chip was passivated by one of two methods. In the first method, the channels of a micro-chip, either a new or cleaned (see below) one, were first filled by 0.2 μM Sytox Orange diluted in 1xTBE10G without using a syringe. In this method, the buffer-waste well was loaded with 3 μL of 0.2 μM Sytox Orange diluted in 1xTBE10G. Without the aid of a syringe, the channels were filled with this mixture by the capillary forces. Three minutes after the channels were

filled properly, the mixture was flushed out of the channels, the wells were rinsed with de-ionised water for 30 s, and the wells and channels were dried by forcing air through the channels with a 1 mL syringe. Finally, the channels were filled with the sieving matrix, 5GS10G. The sample well of the micro-chip was loaded with 2.7 μL of diluted running buffer, 0.1xTBE1G, and 0.3 μL of unlabeled PCR product, either heterozygous BRCA1 Exon20 5382insC or homozygous BRCA1 Exon20 wild-type. The buffer well, sample-waste well and the buffer-waste well were loaded with 3 μL of running buffer, 1xTBE10G. This method has been called the "slow-labeling method" for the rest of the chapter since the dye mixture fills the microchannels slowly (it took approximately 10 s).

The second method is the same as the first one except in the dye mixture loading step. In this method, the channels of a micro-chip, either a new or cleaned (see below) one, were first filled by 0.2 μM Sytox Orange diluted in 1xTBE10G using a 1 mL syringe. All other steps were the same as the first method. This method has been called the "fast-labeling method" for the rest of the chapter since the dye mixture fills the microchannels quickly compared to the previous method (it took approximately 1 s).

Following the above loading procedure, for each passivation method, we performed three runs, each consisting of a sample-injection stage and a separation stage. The first run consisted of a run with a 60 second injection and a 180 second separation. Following this first run, two subsequent runs were made for verifying reproducibility, each with a 10 second injection and 180 second separation (data not shown) that gave results similar to those of the first run.

In order to remove the residual effects of Sytox Orange, the chip should be cleaned after each load by filling the channels with 1 M sulphuric acid for 20 minutes. As discussed in section 2.2.6, we verified that this 20-minute sulphuric acid treatment removes any residual Sytox Orange from the micro-chip by analyzing a sample of BRCA1 Exon 20 5382insC and verifying that no signal was present i.e. the DNA sample was unlabeled (data not shown).

3.2.8 Data Analysis

As discussed in 2.2.7, more details can be found in [76].

3.3 Results and Discussion

3.3.1 Calibration of the Microfluidic Chip

Calibration is an important issue in microchips because of aging phenomena that can introduce artifacts in electrophoretic analyses [101]. Since the resolution of different methods was investigated in this work, the chip used was calibrated each day before starting experiments.

At the Backhouse lab (University of Alberta, Edmonton), a calibration protocol (section 3.2.6) is used to measure the performance of microchips (more detail could be found in the previous work [101]). The criterion for a well-performing microchip, in terms of resolution, is to have an FWHM of less than 0.3 s for the 200, 250 and 300 bp fragments in the Genescan-500 size standard (more detail provided in section 3.2.6).

Figure 3.2 shows an electropherogram for the size standard separation, Genescan-500 (end-labeled PCR products), when the chip is cleaned. The FWHM of the 200, 250 and 300bp fragments in Figure 3.2 were measured to be around 0.24 s, an indication of good performance.

Figure 3.3 shows the separation of Genescan-500 on the same chip when it had Sytox Orange residues (the separation of GS-500 was done following a load presented in section 3.3.3). In this figure, the baseline has some additional features, there are more peaks than expected and some of the peaks are clefted. An explanation for the extra peaks would be the existence of unlabeled fragments in Genescan-500. The FWHM of the 200, 250 and 300bp fragments were measured to be around 0.4 s, and it shows that the intercalation has slightly decreased the resolution of the Genescan-500 separation. Defining Rs to be:

$$Rs = |P_1 - P_2| \div FWHM \tag{3.1}$$

where P_1 and P_2 are the peak arrival times during separation, FWHM is the full-widths at half maximum of the desired peak. We defined the resolution as the product of the difference in the fragment length between a given peak and the next peak (in this case 50bp, the difference between 250bp and 300bp) divided by Rs. The addition of intercalating dyes to an end-labeled DNA decreased the resolution of the separation from 3 bp (Figure 3.2) to 5 bp (Figure 3.3). This peak broadening is explained in the next section.

3.3.2 Poisson Distribution of Intercalating Dyes

The statistical distribution of dye molecules into DNA molecules can be assumed to be Poisson ([102]). If μ is the average number of dye molecules, then the standard deviation (the square root of the variance, used as a measure of the variations in a distribution) in Poisson distribution is $\sqrt{\mu}$. With this assumption, the number of dye molecules intercalated into a DNA molecule will be in the range of $\mu \pm \sqrt{\mu}$. Since intercalators are positively charged molecules, they can change the net charge of DNA samples upon the formation of DNA-dye complexes. A distribution of charge of DNA fragments is the consequence of the distribution of intercalating dyes. Since DNA fragments (of the same length) with different charges migrate with different velocities, a broad peak would be detected after the separation.

A bigger value for μ (and hence for $\sqrt{\mu}$) will generate a broader peak (bigger deviation of charge distribution). If μ is small enough, then almost all DNA molecules will have either no dye molecule μ=0 (undetected) or a dye molecule μ =1. This gives a sharp profile (high resolution), however, it requires similarly sensitive (and expensive) equipment to that needed in work with end-labeled DNA.

3.3.3 Increasing the Resolution of On-Chip Labeling

An ideal goal for on-chip labeling is to detect a bright DNA sample without losing the resolution of separation. The idea of our method was that if dye molecules label the dsDNA only at the end of the channels just prior to detection, the band-broadening should be sup-

pressed because the DNA fragments with the same length but different charges do not have the time to separate.

We initially believed that in the slow-labeling method (section 3.2.7), dye molecules move slowly enough that they are adsorbed at the end of the channel, while in the fast-labeling method, the fast entry of the mixture distributes the dye molecules more evenly through the channel. We also observed the fluorescent intensities of the channels following two methods by looking at the chips under the fluorescent microscope. These observations showed that the end of the channels were fluorescent in the slow-labeling approach while more distribution of dye molecules was present in fast-labeling method (visual observation). However, we were not able to record those images when we ran the experiments (recording software was not available at that time).

Figure 3.4 shows the dsDNA profile of homozygous sample of BRCA1 Exon20 wildtype following the slow-labeling method presented in section 3.2.7 with the measured FWHM being 0.66 s. While Figure 3.5 shows the dsDNA profile of the same sample following the fast-labeling method in section 3.2.7 with the measured FWHM being 0.57 s. We observed similar profiles for homozygous sample of BRCA1 Exon20 wildtype following the two represented labeling methods. The arrival timing, peak intensity and the resolution of slow-labeling method, i.e. using no syringe for the passivation stage, do not show a significant difference over the arrival timing, peak intensity and the resolution of the fast-labeling method, i.e. using a syringe for passivation stage. This observation suggests that the slow labeling and fast labeling method may have had similar a distribution of dyes along the channels, not as expected. We also applied the same methods to label heteroduplex samples and investigated if any difference in the heteroduplex conformation can be obtained following these two methods. Figure 3.6 shows the heteroduplex analysis of heterozygous sample of BRCA1 Exon20 5382insC following the slow-labeling method presented in section 3.2.7 while Figure 3.7 shows the dsDNA profile of the same sample following the fast-labeling method in the same section. Unlike the wildtype sample, we observed different profiles for the heterozygous sample of BRCA1 Exon20 5382insC following the two represented labeling methods.

Labeling heteroduplexes by intercalating dyes may cause unwindings of the double helix (Gao *et al.* [99]). A possible explanation for the different profiles in Figure 3.6 and Figure 3.7 can be as follows: in the fast-labeling method, the DNA-dye complex forms early in the channel and this might affect the heteroduplex conformation since the intercalators have more time to unwind the helix and consequently change the conformation of the heteroduplexes. On the other hand, in the slow-labeling method, DNA is labeled at the end of the channel just before being detected and the conformational change of heteroduplexes is minimal. Given the preliminary nature of these experiments, it is likely that the dye distributions are not reproducible and further investigation is needed.

There were only two loads for each sample following each method (each load contained three runs) in our database. The reproducibility of these results was not tested because of the shortage of time.

3.3.4 Fluorescence Images

Recently we were provided with a camera that could record the fluorescent images and the images of the fluorescent molecules at the glass surfaces, Figure 3.8, were recorded following each of the two chip preparation methods. Figure 3.8a and Figure 3.8b are related to the passivation of a chip following the slow-labeling method and the fast-labeling method, respectively. Both images were taken after loading the chip with the dye mixture (and before loading the sieving matrix). The patterns for two methods recorded by the microscope were reproducibly seen for three loads of the chip.

Figure 3.9a and Figure 3.9b showed the fluorescent intensity versus distance (pixel number from the loading well) for Figure 3.8a and Figure 3.8b, respectively. As can be seen in Figure 3.9a and Figure 3.9b, the slow labeling and fast labeling method have a similar distribution of dye along the channels thereby explaining the similar resolution in Figure 3.4 and Figure 3.5.

Figure 3.8 shows approximately 40 mm of the channel, and only 1/4 of this part of the channel showed different fluorescent intensities (from pixel number 439 to pixel number

239 in Figure 3.9) suggesting that the DNA-dye complex may form around 1cm earlier in Figure 3.9b than Figure 3.9b.

Since the images (Figure 3.8) were taken two months after the experiments in Figure 3.4, Figure 3.5, Figure 3.5 and Figure 3.7 they might not be representative of the dye distribution at the time of initial experiments.

3.4 Conclusion

Intercalating dyes are used for on-chip labeling of a wide variety of DNA samples, however, they are capable of inducing peak-broadening in microchip electrophoresis. The peak broadening (lower resolution) can be explained by Poisson distribution of dye molecules. DNA fragments with the same size but different charges would migrate with different velocities and they will be detected at different timings (the peak-broadening phenomenon). An idea for eliminating the peak-broadening is to intercalate at the end of the channel so that the DNA-dye complexes could form just prior to the detection point. We initially believed that our slow-labeling method (section 3.2.7) had most of the dye molecules just at the end of the channels while the fast-labeling method (section 3.2.7) distributed the dye molecules along the entire channel (from our observations under the fluorescent microscope by eye). However, our fluorescent images (Figure 3.8 and Figure 3.9) and our electropherograms of WT samples (Figure 3.4 and Figure Figure 3.5) showed that the two labeling methods have almost the same distribution of dye molecules.

Another set of experiments showed that the profiles of heterozygous samples (Figure 3.6 and Figure 3.7) were different following two methods. Since the fluorescent images might not be representative of the dye distribution at the time of initial experiments, further loads are needed on the heterozygous sample to see if the resutls are repeatable. A less probable explanation was also based on the earlier formation of DNA-dye complex in fast-labeling method versus slow-labeling method. The difference between the timing of DNA-dye formation in two methods might have been enough to generate different conformations of the heteroduplexes in (Figure 3.6 and Figure 3.7).

There were two experiments (each experiment contained three runs) for each sample following each method and the fluorescent images were taken two months after the experiments. The results presented in this work should be reproduced for a conclusive result and images should be taken at the time of the experiments.

Although our proposed labeling protocols did not show what we expected, the principle is valid and we need to develop a more effective method of controlling the dye distribution. The effect of intercalating dyes like Sytox Orange on DNA may be useful in manipulating the conformation of DNA in heteroduplex analysis methods. This may be able to increase to the mutation detection sensitivity.

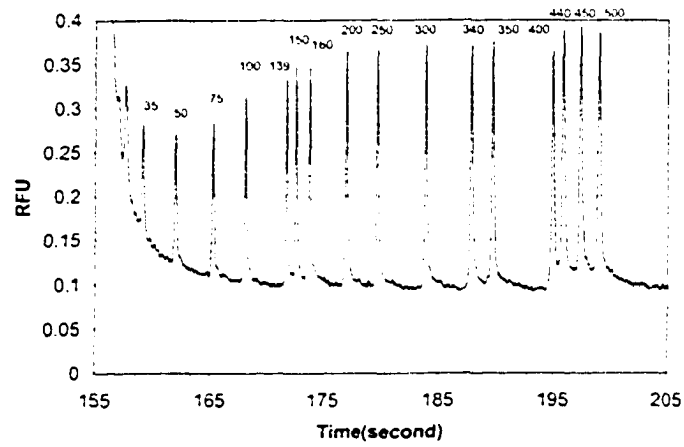

(a)

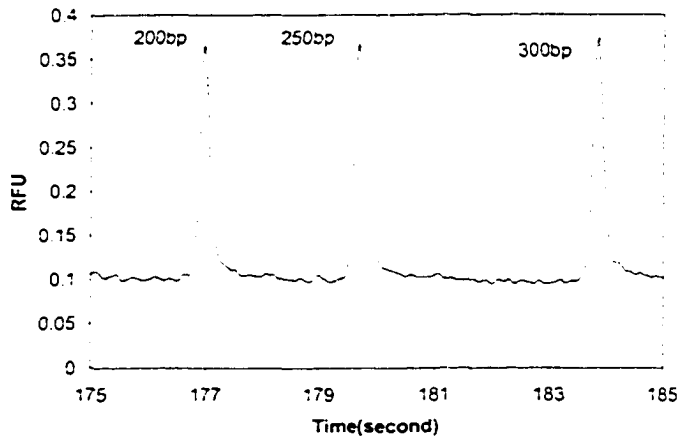

(b)

Figure 3.2: Calibration Electropherogram: GeneScan-500 Separation, freshly-cleaned channels a) zoomed electropherogram, b) The inset shows 200,250 and 300bp

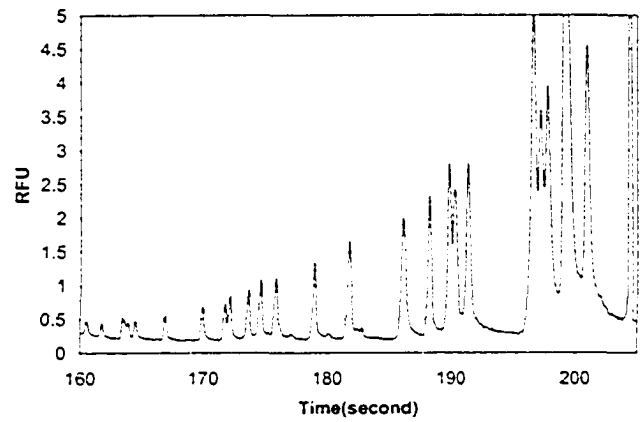

(a)

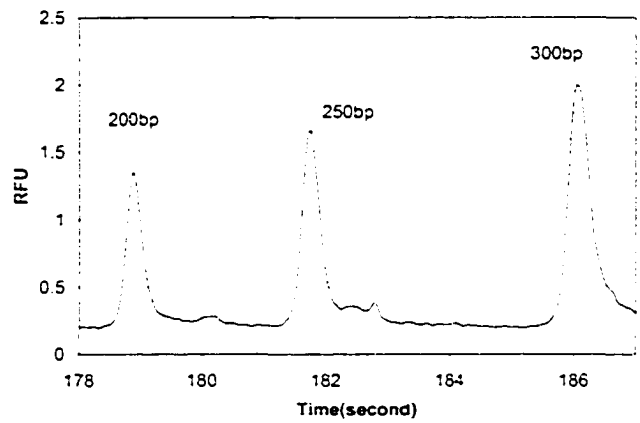

(b)

Figure 3.3: Calibration Electropherogram: GeneScan-500 load following a load presented in section 3.3.3 (with no cleaning of the chip with sulfuric acid) a) zoomed electropherogram, b) The inset shows 200, 250 and 300bp

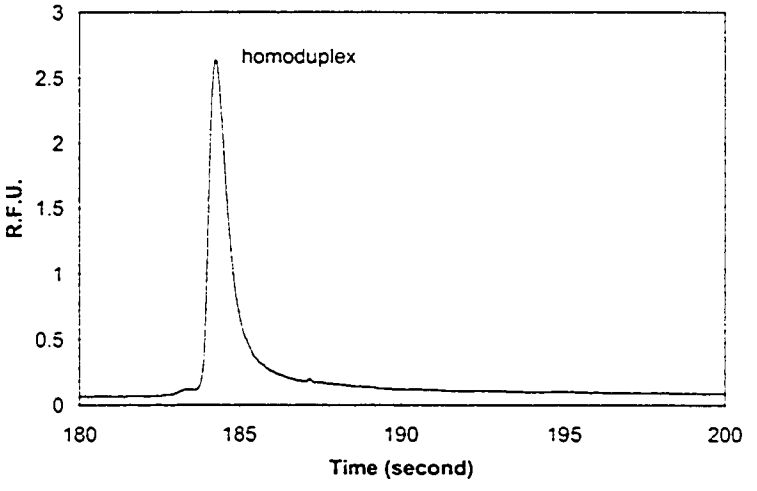

Figure 3.4: The electropherogram of a wildtype sample of BRCA1 Exon 20, the chip was passivated with Sytox Orange using the slow-labeling method represented in section 3.2.7. Measured FWHM=0.66 s

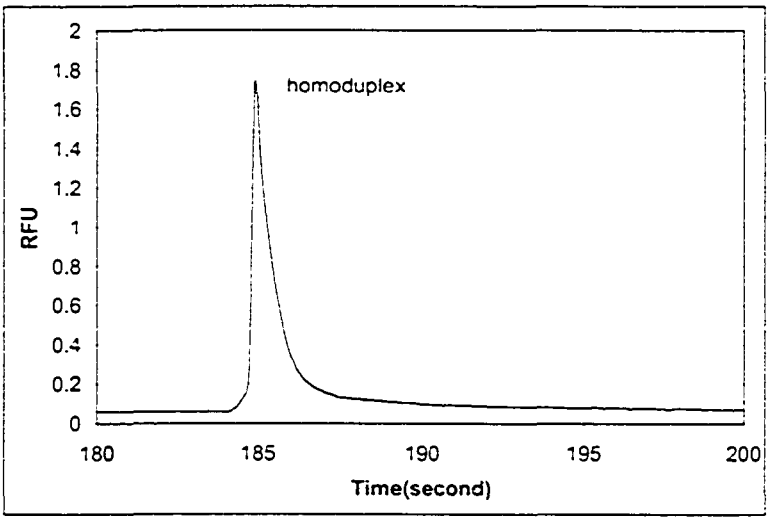

Figure 3.5: The electropherogram of a wildtype sample of BRCA1 Exon 20, the chip was passivated with Sytox Orange using the fast-labeling method represented in section 3.2.7. Measured FWHM=0.57 s

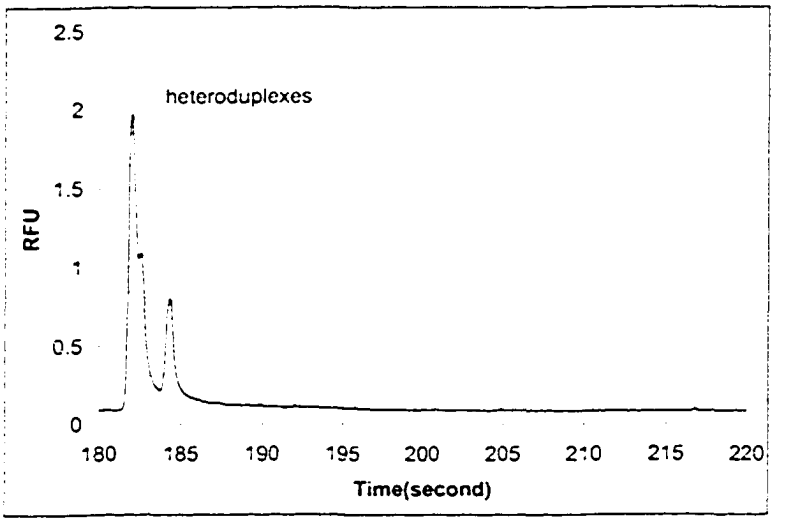

Figure 3.6: Heteroduplex analysis of a heterozygous sample of BRCA1 Exon 20, 5382insC, the chip was passivated with Sytox Orange using the slow-labeling method represented in section 3.2.7

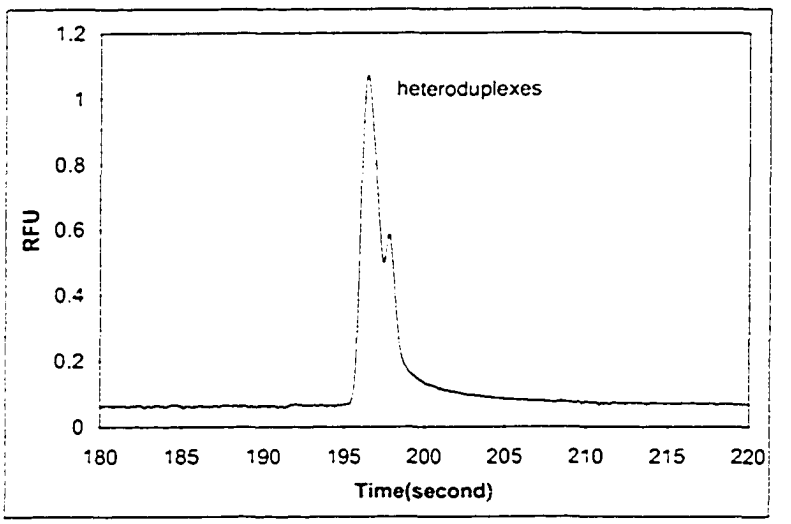

Figure 3.7: Heteroduplex analysis of a heterozygous sample of BRCA1 Exon 20, 5382insC, the chip was passivated with Sytox Orange the fast-labeling method represented in section 3.2.7

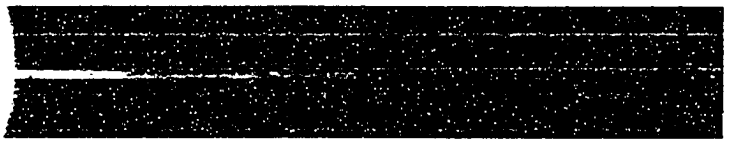

(a)

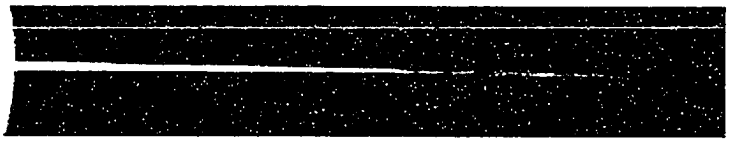

(b)

Figure 3.8: Fluorescent Images of the chip after the two presented labeling methods. Each images took 40 mm of a microchip from the loading well (buffer-waste well). The laser was located 4mm from this well (76mm from the intersection). a) Image of the chip after the passivation following the slow-labeling method b) Image of the chip after the passivation following the fast-labeling method

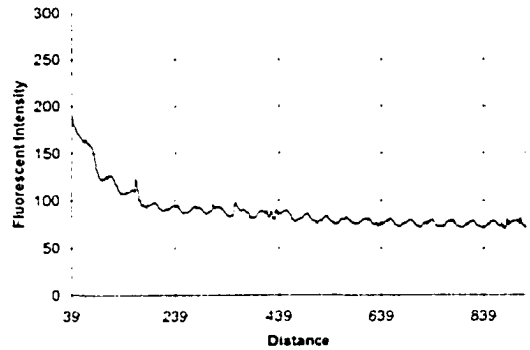

(a)

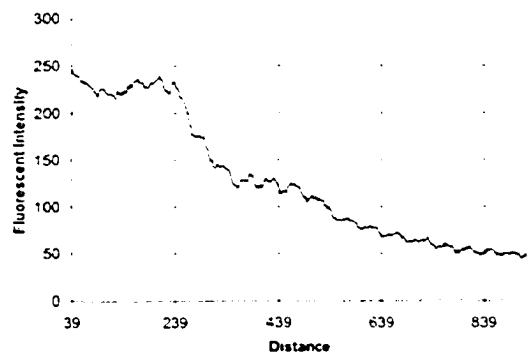

(b)

Figure 3.9: Fluorescent intensity versus distance (x axis represent pixel number)(made by a C program called "Image slice intensity", written by Guijun Dai in the Backhouse lab) that calculates the average pixel value for each column of a slice and output the result to a data file. Whole distance corresponds to around 40 mm of a microchip from the loading well (buffer-waste well). The laser was located 4mm from this well (76mm from the intersection). a) Fluorescent intensity versus distance corresponds to Figure 3.8a, b) Fluorescent intensity versus distance corresponds to Figure 3.8b

Chapter 4

Preliminary Work Towards the Rapid Genetic Analysis of Mitochondrial DNA Using Microfluidic Devices

4.1 Introduction

The major goal of this chapter is to develop a reliable sizing protocol on microchips that would allow us to detect the large mtDNA deletions characteristic of Kearns-Sayre Syndrome (KSS) and other mitochondrial myopathies. Mutations in mitochondrial DNA (mtDNA) may play a role in a variety of diseases like cancer, Alzheimer's and Parkinson's. The preparation of mtDNA is one of the most critical issues in mtDNA mutation detection techniques because it is labor intensive and very small amounts of mtDNA could be obtained from large amounts of tissue. In this preliminary work, we may have purified mtDNA from nuclear DNA and if this statement is proven to be correct, then this is the first report for the on-chip mtDNA purification from nuclear DNA contaminants. A successful on-chip sample purification followed by on-chip mutation detection could revolutionize mtDNA research. This is a preliminary report toward that goal and further work is needed.

We believe that the DNA used as a template in PCR amplification (prepared by phenol-

chloroform-isoamyl alcohol extractions [73]) typically contains both nuclear DNA and mtDNA. Upon applying an injection voltage between the sample well and the sample-waste well, the nuclear DNA (3.2 billion base pairs) may stay behind and it may not enter the porous medium (the sieving matrix) in the microchannels because of its size whereas the mtDNA (16.5 kbp) may enter the microchannels. We also examined a sample that lacks mtDNA to establish a reference experiment to be compared with template DNA.

4.1.1 Mitochondria and Mitochondrial Diseases

Mitochondria are organelles responsible for generating energy in cellular processes [103]. Over the past twenty years, mitochondrial defects have been implicated in a wide variety of degenerative diseases, aging, and cancer [104]. Human mitochondrial DNA is a double-stranded, circular molecule that encodes 13 protein subunits of 4 enzyme complexes and 24 RNAs (2 ribosomal RNAs [rRNAs] and 22 transfer RNAs [tRNAs]) that are required for the intra-mitochondrial translation of the protein-coding units [105]. Mitochondria, which probably evolved from independent organisms that became part of the cell, are able to replicate, transcribe, and translate their DNA independently of nuclear DNA, however, cellular function and mitochondrial function are interdependent [106].

The mitochondrial DNA is reported to be in supercoiled form [107,108], however, there are also topoisomerase (enzymes that control and modify the topological states of DNA in cells) activities in mitochondria. Mansouri *et al.* believed that supercoiled mtDNA might be converted to circular DNA because of the activation of topoisomerases [109]. Mitochondrial DNA is maternally inherited and is not thought to recombine; therefore, mutations accumulate sequentially through maternal lineages [103]. Normal and mutant mitochondrial DNA can coexist within the same cell and this condition is known as heteroplasmy while homoplasmy is the presence of a single population of either completely normal or completely mutant mitochondrial DNA [103].

The first pathogenic mitochondrial DNA (mtDNA) mutations were described in 1988 [103]. Kearns-Sayre Syndrome (KSS) exhibiting progressive external ophthalmoplegia,

pigmentary degeneration of the retina, myopathy and cardiac conduction defects was found to be associated with large mtDNA deletions encompassing several structural and tRNA genes [110]. Wallace *et al.* demonstrated a point mutation in the ND4 gene (G11778A) in Leber's Hereditary Optic Neuropathy (LHON) was a major cause of maternally inherited blindness [111]. Shortly thereafter, two further maternally inherited disorders, myoclonic epilepsy with ragged-red fibers (MERRF) [112, 113], and mitochondrial encephalopathy lactic acidosis and stroke-like episodes (MELAS) [114] were linked to mtDNA point mutations. Since then, a vast number of point mutations and large-scale mtDNA rearrangements associated with a diversity of clinical phenotypes have been reported [115].

4.1.2 Genetic Analysis of Mitochondrial DNA

The advances in understanding the molecular genetic basis of mitochondrial diseases have already had a significant effect on their detection and evaluation. A set of sensitive and specific molecular genetic analysis methods has been developed for a number of mitochondrial mutations [115–119]. The unambiguous diagnosis of a mitochondrial disease by such methods is obviously the first step in appropriate genetic counselling and treatment [103]. The other step would be the investigation of the correlation between nutrition deficiencies, environmental factors and mitochondrial condition.

Capillary electrophoresis (CE) with laser-induced fluorescence (LIF) detection has been used to detect known point mutations in mtDNA. Piggee *et al.* detected three different point mutations in human mitochondrial DNA associated with Leber's Hereditary Optic Neuropathy (LHON) by annealing a primer immediately 5' to the mutation on the template and extending the primer by one fluorescently labeled dideoxy terminator complementary to the mutation [120]. PCR-based analysis by capillary electrophoresis (CE) had been used to discriminate the highly polymorphic mitochondrial DNA (mtDNA) D-loop region (the non-coding highly variable region of human mtDNA) [121]. Application of CE-LIF for analysis of PCR-amplified DNA fragments from three different genetic loci including mitochondrial DNA was presented [122].

High-performance hereditary haemochromatosis and short tandem repeat genotyping assays were demonstrated on microfluidic devices along with rapid mitochondrial DNA sequence polymorphism analysis [85]. Guttman *et al.* also used agarose to analyze mitochondrial DNA heteroplasmy in diabetes [118]. They did the PCR-amplification of the desired region of mtDNA containing a point mutation prior to chip loading. The PCR products of mtDNA were then separated using a 18cmx7.5cmx190μm float glass microchip cassette (essentially a very thin slab-gel) [123]. They suggested that a PCR-RFLP based diagnostic test in conjunction with their reported gel micro-chip electrophoresis [123] could facilitate the analysis of specific point mutations in mtDNA.

4.1.3 Supercoiled DNA Separation

Ding *et al.* [124] developed a Lab-on-a-chip plasmid assay that runs on the Agilent 2100 Bioanalyzer. They also used PDMA as the sieving matrix and Taps as the separation buffer. The assay determines the sizes of the multiple forms of plasmid samples. For each purified plasmid sample, the major topological isoforms were separated. The migration order for all plasmids tested showed that the supercoiled closed-circular molecules appeared first, followed by the linearized plasmid, and then the open circle form (defined in section 1.1.3).

In order to obtain high resolution for the separation of supercoiled DNA ladder optimum conditions should be investigated. The effect of $MgCl_2$ on electrophoretic separation of supercoiled DNA was described previously in [125] and was attributed to the increased writhe of plasmids (section 1.1.3) in solutions containing Mg^{2+} ions or high concentrations of NaCl. Meisner *et al.* investigated the addition of cesium chloride to the sieving matrix [126]. Obtaining higher resolution by the addition of alkali metal cations was observed to increase with the size of the cation. Changes in DNA structure due to interactions with the cation as well as changes in the mobility were proposed to occur [127]. Furthermore, cations such as sodium or cesium are thought to interact with the present free binding sites on the coated capillary wall and, in this way, suppress any residual electroosmotic flow (EOF) [128].

DNA separations by capillary and microchip electrophoreses are accomplished mainly through the use of a sieving matrix (section 1.3.1). Polymers such as cellulose derivatives, linear poly(acrylamide) (LPA), poly(dimethylacrylamide) (PDMA), poly(ethylene oxide) (PEO), poly(vinylpyrrolidone) (PVP), poly(N-isopropylacrylamide)- g-poly(ethyleneoxide), and poly(dimethylacrylamide- co-allyl glycidyl ether) (PDMA-AGE) have been used by other researchers as the sieving matrices to separate DNA molecules. Several polymers, such as PDMA, PVP, HPMC (hydroxypropylmethylcellulose), PEO, and PDMA-AGE, have been used as a dynamic surface coating for DNA analysis in bare fused-silica capillaries and plastic microchips. The proposed mechanisms for the dynamic surface coating include the surface adsorption of the polymers via the hydrogen bonding of the polymer [129]. In this set of experiments, we synthesized PDMA in our laboratory following the procedure reported by Ding *et al.* [124].

Oana *et al.* [130] and Mao *et al.* [131] have provided good experimental descriptions of supercoiled plasmid migration in a diluted polymer. Mao *et al.* [131] reported a CE separation of pBR 322 in an HPMC-based buffer. Despite all this, a consistent model for the migration of DNA circular forms (supercoiled molecules, single topoisomers, and open-circular forms (section 1.1.3)) in diluted or semi-diluted polymers is not currently available.

4.1.4 Agarose Based Separation of Large Linear DNA and Circular DNA

Gurrieri *et al.* investigated the movement of megabase-pair DNA molecules [132] using 1% agarose gel in 0.5xTBE buffer and the field strength of 5 V/cm. They showed that large DNA molecules became trapped in agarose gel pores during electrophoresis if the electric field exceeded a few volts per cm [132].

Ohsugi *et al.* showed that large DNA remained at the origin of the gel and could not penetrate the agarose gel matrix [133]. DNA samples were separated in 0.8% agarose gel containing in TAE buffer (40mM Tris base, 20mM acetic acid and 1mM EDTA) and were

electrophoresed in this solution at 8 V/cm [133].

Singh *et al.* employed a method for assessing damages to mtDNA caused by radiation upon agarose gel electrophoresis, blotting (a technique for transferring nucleic acid from an electrophoresis gel matrix to a microporous membrane), and visualization by hybridization with mtDNA probes [134]. They used 0.7 % agarose gel in TBE, pH=8, containing $2\mu g$/ml of ethidium bromide. The samples were run at 100V for 2 hours. In order to purify the mtDNA (isolated from mouse liver), employing slab gel electrophoresis they believed that the nuclear DNA was retained on the top of the gel whereas the mtDNA entered the gel. However, there were some bands in agarose gel electrophoresis distinct from mtDNA as identified by mtDNA-hybridized blots. These bands were not likely to be circular duplex DNA molecules because they disappeared upon heat denaturation. They were not also related to RNA since they were not eliminated after the RNAse treatment. They believed that the lack of clear identification of mtDNA as fluorescent bands reflects the low concentration of these bands relative to contaminant nuclear DNA [134].

Guttman *et al.* also used agarose in microchip electrophoresis to analyze PCR-amplified mitochondrial DNA fragments [118]. They also employed 2 % agarose in TBE buffer in their float glass microchip cassette (section 4.1.1) [123] applying 500 V separation voltage.

4.1.5 Highly Integrated mtDNA Purification Using Microfluidic Chips

Very small quantities of mtDNA can be extracted following labor intensive preparation protocols, consequently, the process of mtDNA isolation is very costly. There has not been any work so far, to our knowledge, on microchip electrophoresis mutation detection using the circular mtDNA without PCR-amplification.

In this work, we tried to develop an on-chip mtDNA purification protocol following the proposed method by Singh *et al.* [134]. The template DNA (normally used in PCR-amplification) which is expected to contain both nuclear DNA and mtDNA was tested to see if the nuclear DNA is able to enter the porous medium in the channels upon applying an injection voltage. We also examined a sample that lacks mtDNA, to establish a reference

experiment to be compared with that of template DNA.

Three sieving matrices, i.e. PDMA diluted in Taps (section 4.2.1), agarose (diluted in TBE) and Genescan (diluted in TBE) were used in this work for the separation of the circular DNA. PDMA was chosen since we tried to repeat the Ding *et al.* work [124]. Agarose was tried because of the previous report of the separation of nuclear DNA from mtDNA [134]. Genescan was also used as a polymer because of its dynamic coating and its common usage in the Backhouse lab.

Kearns-Sayre syndrome (KSS) is a sporadic disorder characterized by mitochondrial DNA (mtDNA) with a 4.977-bp common deletion in the mtDNA of muscle and other tissues [135]. A continuously updated summary of the human mtDNA deletions in KSS may be found in the MITOMAP at [136]. We have developed a method to size supercoiled DNA ladder (2-16kbp). Since the mtDNA is typically in supercoiled form ([107,108]), it is likely that the ability to effectively size a supercoiled DNA size standard will enable us to size mtDNA. This may ultimately allow us to detect the large mtDNA deletions characteristic of Kearns-Sayre Syndrome (KSS).

4.2 Materials and Methods

4.2.1 Reagents

A Tris Borate with EDTA buffer (TBE) was made with Tris Base and Boric Acid from Fisher Scientific (NJ, USA) and EDTA from Merck (Darmstadt, Germany). GeneScan polymer from PE Applied Biosystems (Foster City, CA) was mixed with glycerol from Sigma (Saint Louis, MO), TB buffer and $MgCl_2$ so that the final concentration of Genescan was 0.2 % (w/w), the final concentration of glycerol was 10 % (w/w) and the final concentration of $MgCl_2$ was 3 mM. This dilution, referred to as 0.2GS10G, was used as the sieving medium for electrophoresis in one set of our experiments.

The running buffer, referred to as 1xTBE10G, was made from glycerol and TBE buffer so that the final concentration of glycerol was 10 % (w/w). A dilution of this solution

to 1 part in 10 in de-ionised water is used for sample preparation and is referred to as 0.1xTBE1G. Another running buffer, referred to as 1xTB10G, was made from glycerol, TB buffer and $MgCl_2$ so that the final concentration of glycerol was 10 % (w/w) and the final concentration of $MgCl_2$ was 2 mM. A dilution of this solution to 1 part in 10 in de-ionised water is used for sample preparation and is referred to as 0.1xTB1G. Since 0.2GS10G and 1xTB10G were made in TB buffer, they do not contain EDTA.

Taps (N-tris[hydroxymethyl]methyl-3-aminopropanesulfonic acid), pH 8.0, was from Sigma-Aldrich. A dilution of 200 mM Taps plus 5 mM $MgCl_2$ was used as the separation buffer. PDMA, polydimethylacrylamide, was made in our laboratory based on [124] at 0.2 % concentration in the running buffer (200 mM Taps, 5 mM $MgCl_2$, pH 8.0). This solution was used as sieving matrix for one set of our experiments. Agarose gel powder (Gibco BRL) was added into 1x TBE buffer so that the final concentration was one percent (w/w) and it was heated and stirred until a homogeneous liquid was formed. This solution was used as sieving matrix in some of the separations.

Sytox Orange, an intercalating dye, was obtained as a 5 mM stock solution in DMSO (Dimethylsulfoxide) from Molecular Probes (Eugene, OR). The Sytox Orange solution was diluted to 0.2 μM in 1xTBE10G. RNAse (DNAse free) (with the concentration of 10mg/mL) was purchased from Molecular BioProducts.

4.2.2 Supercoiled DNA Ladder

Supercoiled DNA ladder (catalog number 15622-012) was purchased from Invitrogen Corp. (Carlsbad, CA). The supercoiled DNA ladder contains eleven DNA plasmids for sizing supercoiled DNA from 2 to 16 kb. Agarose gel analysis, Figure 4.1, shows that all eleven bands are distinguishable. The concentration of the sample was 250ng/μL.

4.2.3 Template DNA Preparation

Template DNA was extracted in the Molecular Diagnostics Laboratory (MDL) (University of Alberta, Edmonton) from the lymphocytes of volunteers (prepared with informed con-

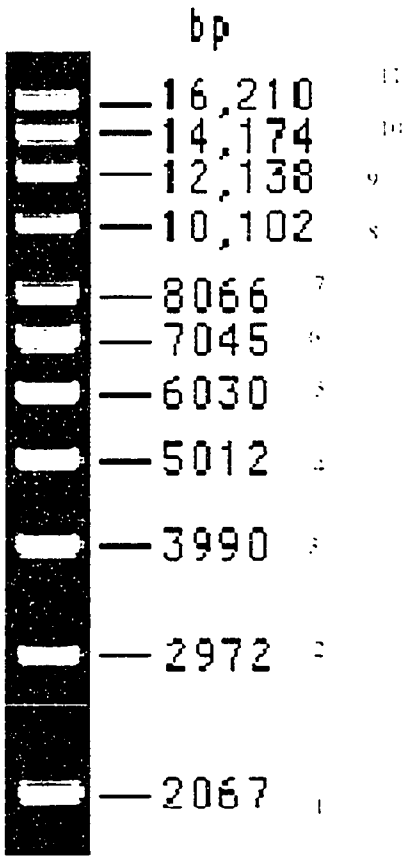

Figure 4.1: Supercoiled DNA Ladder. Extracted from "Supercoiled DNA Ladder Manual", (Copyright 2004 Invitrogen Corporation. All Rights Reserved.) Used With Permission. The number at the right of each band corresponds to the length of the plasmid DNA. We also numbered the bands (1-11) for our reference.

sent) and was then purified using phenol-chloroform-isoamyl alcohol extractions [73] or with the QIAmp DNA Blood kit (QIAGEN, Mississauga, ON) (section 2.2.1). The concentration of the aliquoted samples was 15ng/μL.

4.2.4 rho0 DNA Preparation

This part was extracted from the thesis of Karmon Helmle (Glerum Lab, University of Alberta, Edmonton) [137]: " Primary fibroblast cell lines were cultured in T25, T75, or T150 vented tissue culture flasks (Corning) with Dulbecco Modified Eagle Medium which contained 10 % Fetal Bovine Serum, 100 μ/mL Pen/Strep, 50 μ/mL uridine and 100 μ/mL sodium pyruvate (Gibco) at 37°C. Once fibroblast cells were confluent, cells were washed two or three times with sterile 1X Phosphate Buffered Saline (PBS) (Gibco). Cells were then trypsinized with two to four mL of 2.5 % trypsin (Gibco), preheated to 37°C, and rocked gently for one to three minutes. Cells were released from the flask by a sharp tapping motion. Then, approximately 8 mL of the culture media was quickly added to halt the trypsin digestion, and the cells were redistributed to two or more new culture flasks."

Fibroblast cell lines lacking mtDNA (rho0) (Dr. Brian Robinson, Hospital for Sick Children, ON) were grown following the above manner in the Glerum lab and the culture media was supplemented with 20 % Fetal Bovine Serum. The concentration of DNA in the rho0 sample (aliquoted) was 15ng/μL.

Karmon Helmle (Glerum lab, University of Alberta, Edmonton) designed PCR primers specific to a sequence in the D-loop region of mtDNA (the non-coding highly variable region of human mtDNA, approximately 1150 bp long, and is used for the purpose of forensic genetics [138]). Primers were tested on a rho0 cell line to verify that the amplification of nuclear pseudogenes did not occur [139]. In other words, since the primer sequence was known to be unique to mtDNA, this was a test of the presence or absence of mtDNA in rho0 samples.

4.2.5 Mitochondrial DNA Preparation

Mitochondrial DNA was prepared by Dr. Ivette Sosova, in the Glerum lab (University of Alberta, Edmonton) as follows: After removing the medium of the confluent human skin fibroblasts, 1 mL of sucrose buffer (SB) (sucrose 0.25 M/Tris 20 mM/EDTA 1 mM, pH 7.4) was added and subsequently, it was removed from the mixture. Cells were scraped with a

rubber policeman (scraper) (glass with rubber sleeve; used to stir, assist in pouring liquids, and for removing precipitates from a container) after the addition of 1 mL of SB to the first plate. This mixture was then transferred to the next plate. It was scraped, transferred and so on until a thick suspension of scraped cells in SB formed. The suspension was homogenized in Glass/Glass Tight (Wheaton A) homogenizer with 30 passes. SB was added then to increase the volume to 6 mL. The mixture was then centrifuged at 3,000 rpm for 7 mins, followed by a 10, 000 rpm centrifugation for 10 mins. After the second centrifugation, the pellet was resuspended in 2 mL SB in Teflon homogenizer and homogenized (5 passes were enough for full resuspension and it was brought up to 5 ml). The final centrifugation would be at 3,000 rpm for 7 mins followed by a 10,000 rpm for 10 mins. The final pellet, pure mitochondria, was resuspended in a desired volume of 50-1000 μL SB.

Mitochondrial DNA (mtDNA) was extracted from highly purified mitochondria (above recipe). The mitochondrial pellet (573 μg) was resuspended in 500 μL 75mM NaCl and 50 mM EDTA (pH 7.6), and 62.5 μL of proteinase K (Sigma, 20 mg/ml stock) was added. After 30 min incubation at 50°C, SDS was added to a final concentration of 0.5% (w/v), and the incubation was extended for another 120 min. To purify mtDNA from proteins and lipids, phenol-chloroform-isoamyl alcohol (25:24:1) was added 1:1 (v/v) and mixed by several hand inversions. The sample was then centrifuged at 7,000 rpm for 10 min in a tabletop microcentrifuge at 4°C. After three successive phenol-chloroform-isoamyl alcohol extractions, the aqueous phase was transferred to a new 1.5 mL microcentrifugation tube, and 0.05V (volume) of 5M NaCl was added, followed by the addition of 3V (volume) of ice-cold (4°C) 100 % ethanol and incubation for 40 min at −80°C (V represents the volume, it means if the sample volume is 100 μL, the solution volume is 300 μL). Precipitated mtDNA was sedimented in a tabletop microcentrifugation at 12,000 rpm, at 4°C, for 30 min. The pellet was washed twice with 70% ethanol, vacuum-dried for 10 min (SpeedVac Plus SC110 A, Savant), and resuspended in 20 μL sterile TE buffer (10 mM Tris-HCl, 0.1 mM EDTA, pH 7.6). The concentration of purified mtDNA was determined in a UV-1601 PC spectrophotometer (Shimadzu Corp., Japan). In this technique, A_{260} and A_{280} are measured. The ratio will show the purity of the sample. More detail was provided in

section 1.1.2.1. The concentration of mtDNA in aliquoted samples was 300 ng/μL.

4.2.6 RNAse treatment of Mitochondrial DNA

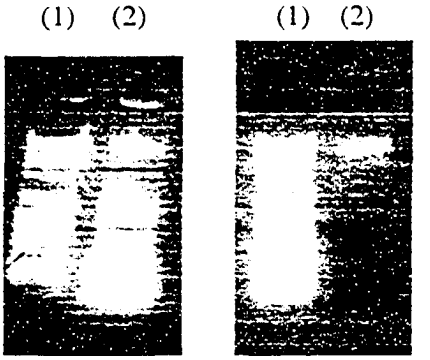

Figure 4.2: Gel Electrophoresis showing the RNAse treatment of mtDNA in the Glerum lab. a) Lane 1 shows the supercoiled DNA ladder and Lane 2 shows the untreated mtDNA b) Lane 1 shows the supercoiled DNA ladder and Lane 2 shows the RNAse treated mtDNA

Dr. Ivette Sosova (Glerum lab, University of Alberta, Edmonton) showed that there is RNA contamination in the isolated mtDNA presented in previous section. Figure 4.2a shows the gel electrophoresis of mtDNA prior to RNAse treatment (an enzyme that catalyzes the hydrolysis of RNA). Lane 1 corresponds to plasmid DNA ladder and Lane 2 corresponds to untreated mtDNA. In Figure 4.2b the RNAse treatment of mtDNA following the below procedure shows one band (Lane 2) for mtDNA separation corresponded to a 16kbp plasmid in supercoiled DNA ladder (Lane 1).

In order to make template DNA plus RNAse (and rho0 DNA plus RNAse) mixtures, 1 μL of DNA, 9 μL of TE buffer (Taps buffer in the PDMA based experiments) and 0.2 μL of RNAse were mixed and heated to 37$^{\circ}C$ for half an hour using the thermo-cycler prior to the chip loading. Since the concentration of the template or rho0 DNA was 15 ng/μL, by preparing the mixture following the above procedure, the DNA concentration would be

1.5ng/μL (the final concentration of the DNA in the mixture). The addition of 2 μL of this mixture to the sample well provided 3 ng of DNA in each load. The RNAse treatment in the PDMA-based method was not successful since the high concentration of Taps had not been considered. More detail is given in section 4.3.1.

In order to do RNAse treatment for mtDNA, 1 μL of mtDNA, 9 μL of TE buffer (Taps buffer in the PDMA based experiments) and 0.2 μL of RNAse were mixed and heated to 37°C for half an hour using the thermo-cycler prior to the chip loading. Since the concentration of the mtDNA (section 4.2.5) was 300 ng/μL, 1 μL of this mixture provided 30 ng of mtDNA in the sample well in each load. The mixture was stored frozen at -20°C.

4.2.7 Mitochondrial DNA Purification Using Gel Filtration

RNAse-free purification of plasmid DNA has been reported in [140, 141]. Duval *et al.* proposed a filtration method that takes advantage of the significant size difference between RNA and plasmid DNA to remove RNA in an RNase-free plasmid purification process [141]. Enzmann *et al.* believed that digestion with RNAse eliminated the RNA contamination of their samples however the supercoiled mtDNA was transformed into the relaxed form by the RNAse treatment [142].

Other methods have also been reported for the purification of plasmid DNA from chromosomal DNA and RNA. Levy *et al.* showed the use of nitrocellulose membranes to decrease chromosomal DNA contamination in plasmid DNA [143]. They believed that the chromosomal DNA was selectively retained by the nitrocellulose membrane while most supercoiled plasmid DNA was recovered in the filtrate. They also showed that under specific condition a fraction of contaminant RNA was also retained by the membrane filter [143]. Wang *et al.* used multi-compartment electrolyser separated by ultrafilter membranes to remove the contamination of RNA, genomic DNA and protein from plasmid DNA [144]. A multi-compartment electrolyser with isoelectric membranes has the character of electroseparation and membrane separation to purify biological materials [144].

Our presented purification was used as an alternative for the RNAse method since the

usage of RNAse might change the conformation of the mtDNA [142]. The procedure described in this section depends on gel filtration chromatography [145], which separates molecules based on their relative size. If a molecule can enter and exit the pores of the gel matrix, its rate of movement is determined by the flow of the buffer and the diffusion properties of the molecule. Smaller molecules enter and leave many pores of the matrix, thus traversing the length of the column relatively slowly. Larger molecules do not enter the gel pores and therefore elute rapidly from the column [146]. Uchiyama *et al.* reported the separation of low molecular RNA from high molecular RNA species employing a high-speed gel filtration method [147].

In order to remove the RNA present in mtDNA, some of the mtDNA was purified by gel filtration using Sephacryl S1000 (a sorbent) (Amersham Biosciences) by Alexey Atrazhev (Cross Cancer Institute, Edmonton). A 1 mL plastic pipette was plugged with glass wool and used as a column. It was filled with Sephacryl S1000, the sorbent, and equilibrated with 4 mL of Taps buffer by attaching a funnel to the pipette and it was left overnight. Ten μL of mtDNA mixed with a dye was loaded into the pipette. The column was then washed once the dye reached half of the column with 50 μL of Taps buffer and the purified mtDNA was collected in an eppendorf tube. This process was repeated eight times and the mtDNA fractions were collected in eight tubes. The idea is that dye molecules travel more slowly in the sorbent than mtDNA since they are smaller molecules and they are a rough estimate for the arrival of mtDNA to the bottom of the column. Aliquots of 4 μL of each tube were analysed on 1 % agarose gel in TBE/ethidium bromide and the tubes containing mtDNA were mixed in one tube. One band was observed on agarose gel by Alexey Atrazhev and the size corresponded to mtDNA size. Starting from the mtDNA concentration of 300 ng/μL, the concentration of the purified sample was measured to be 20 ng/μL (O.D.=0.38) (section 1.1.2.1). However, as mentioned in section 1.1.2.1, this value might correspond to the presence of both DNA and RNA.

4.2.8 Microchip Equipment

The micro-chips used here were manufactured by Micralyne (Edmonton, AB). Since the experimental platforms for the experiments in chapter 2 and this chapter are the same, details were provided here only when they differ from those in section 2.2.3.

4.2.9 Microchip Electrophoresis

The details of the experiments are as follows: in the PDMA-based method: detection point=10mm, injection time=60s, separation voltage=3000V; in the agarose-based method: detection point=10mm, injection time=200s, injection voltage=100 V, separation voltage=400V; in the GeneScan-based method: detection point=22mm, injection time=45s, separation voltage=3000V.

The sample well of the micro-chip was loaded with DNA samples as follows: mtDNA 40ng and supercoiled DNA ladder 75ng. The amount of DNA used in rho0 or template DNA experiments varied from 10ng to 30ng. We are able to detect lower amounts of DNA (1 ng) on our microchips, however, the above values were chosen for the developing protocols to ensure ready detection.

4.2.10 Chip Preparation

Passivation (to make inactive or less reactive the surface by chemical treatment) was used in all three methods for labelling the plasmid DNA: the channels of a micro-chip, either a new or rinsed one (see section 2.2.6), were first filled by a mixture of 1xTBE10G with 0.2 μM Sytox Orange (the final concentration) using a 1 mL syringe. After 3 minutes, the mixture was flushed out of the channels, the wells were rinsed with de-ionised water for 30 s, and the wells and channels were dried by forcing air through the channels with a 1 mL syringe.

In the first method, called PDMA-based chip loading, the channels were filled with the sieving matrix, 0.2 % PDMA plus 5 mM $MgCl_2$, using a 1 mL syringe. The amount of DNA in the sample well was in the range of 5-75 ng (more detail in section 4.2.9).

The buffer well and sample-waste well were loaded with 3 μL of the running buffer, i.e. (200 mM Taps, 5 mM $MgCl_2$). The final concentration of running buffer in the sample well, in all three methods, should be one tenth of the other wells in order to produce the sample stacking effect ([148]), otherwise with higher amounts of ions in the sample well, the negative DNA has a lower chance to enter the intersection because of the competition between buffer ions and DNA molecules [148].

In the second method, called agarose-based chip loading, the channels were filled with the sieving matrix, 1 % agarose in 1xTBE. In order to facilitate loading with agarose, the chip should be slightly heated on the hot plate (still touchable). The agarose was carefully introduced into the microchannel through the buffer waste well using a 1 mL syringe and matured for 5 min at room temperature. The microchannels should be totally filled with the introduced gel and in order to prevent gel contraction, there should be some extra pressure with the syringe to partially fill the wells (10 more seconds of pressure with the plunger when the channels have been filled). The amount of DNA in the sample well was in the range of 5-75 ng (more detail in section 4.2.9). The buffer well and sample-waste well were loaded with 3 μL of the running buffer, 1xTBE10G.

In the third method, called GeneScan-based chip loading, the channels were filled with the sieving matrix, 0.2GS10G plus 3 mM $MgCl_2$, using a 1 mL syringe. The amount of DNA in the sample well was in the range of 5-75 ng (more detail in section 4.2.9). The buffer well and sample-waste well were loaded with 3 μL of the running buffer, 1xTB10G plus 2 mM $MgCl_2$. The data related to the GeneScan-based experiments were collected by Ekua Yorke, the summer student of the Backhouse lab.

4.2.11 Data Analysis

As discussed in 2.2.7, more details can be found in [76].

4.3 Results

Three sieving matrices, i.e. PDMA diluted in Taps (section 4.2.1), agarose (diluted in TBE) and Genescan (diluted in TBE) were used in this work for the separation of the circular DNA. DNA samples were labeled in three methods by the passivation method (section 4.2.10). In the PDMA based method, the peaks corresponding to very small amount of DNA had a higher intensity when the detection point was closer to the intersection. This can be explained by the absorbance of dye molecules by the walls when very small amount of DNA has been used. In order to have consistent results, all the experiments in the PDMA based method were detected at 10 mm from the intersection. Very low voltage was used in agarose based method and the detection was done early after the intersection i.e. 10 mm. The detection point chosen for the Genescan method was 22 mm since the DNA samples could be detected at this point.

4.3.1 PDMA Based Supercoiled DNA Separation

In this work, we modified Ding's work [124] using our microchips. We employed 0.2% PDMA (in 200 mM Taps) as the sieving matrix and Taps as the separation buffer to separate the supercoiled DNA ladder (section 4.2.2). Figure 4.3 and Figure 4.4 show the profiles of the supercoiled DNA ladder at two detection points, i.e. 30 mm and 10 mm from the microchannel intersection. Each peak, numbered from 1 to 11, corresponds to a plasmid DNA (and a band numbered from 1 to 11) shown in Figure 4.1.

As expected, the peak spacing at 30 mm (Figure 4.3) is more than that at 10 mm (Figure 4.4). We observed that the peaks corresponded to very small amount of DNA had a higher intensity when the detection point was closer to the intersection as explained earlier.

Although the patterns of separation were very similar without the addition of $MgCl_2$ (data not shown), PDMA in 5 mM $MgCl_2$ showed a better resolution for supercoiled DNA ladder separation. Figure 4.5(a and b) and Figure 4.6 show the profiles of the template DNA and rho0 DNA, respectively, in 0.2% PDMA (detail in section 4.2.9). The peaks in Figure 4.5(a and b) are broader and have higher intensity than the peak in Figure 4.6. The

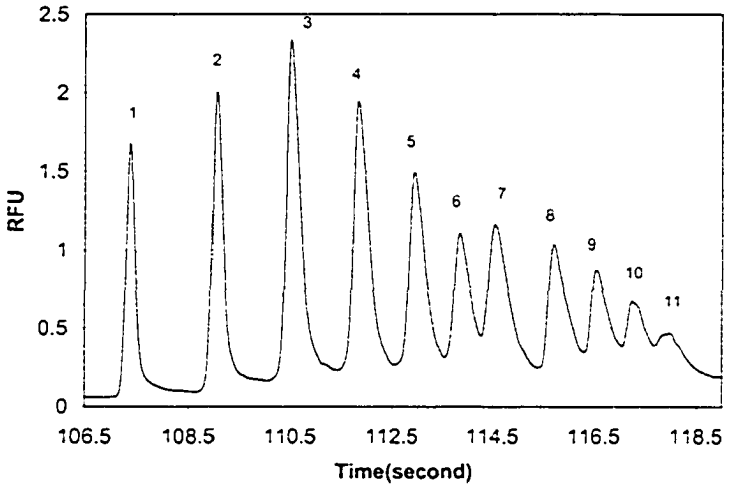

Figure 4.3: PDMA Based Supercoiled DNA Ladder Separation, detection at 30mm, injection time 60s, separation voltage 3000V.

timing and the peak profile for these two tests were reproducible (around 2% variation) (6 runs for rho0 DNA and 3 runs for template DNA at this detection point). There were some spikes present in Figure 4.5a and Figure 4.5b (two runs of one load). The spikes were also repeated in two more runs (of the same load, data not shown). However, the timing of the spikes are not reproducible (more detail for the spikes in section 4.3.4 and 4.4.4).

RNAse should be added to each template DNA and rho0 DNA to explore the presence of RNA. Initial attempts to do so were not successful in the PDMA based method. No sample was successfully injected after the RNAse treatment with the recipe in section 4.2.6 because of the inappropriate mixture of the sample and the Taps buffer with RNAse. The Taps concentration in the sample well was 0.6 of the other wells (as described before, in order to have sample stacking [148] it should be 0.1). For both rho0 DNA and template DNA, the amount of DNA in the sample well was very small (3 ng, section 4.2.6). There

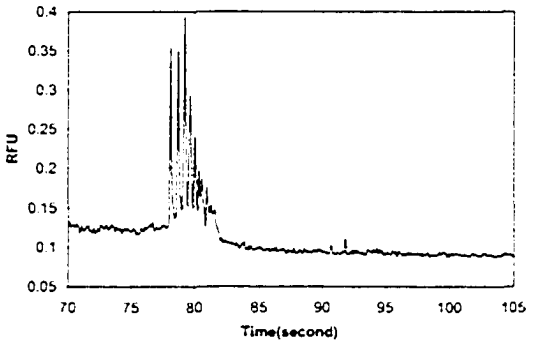

(a)

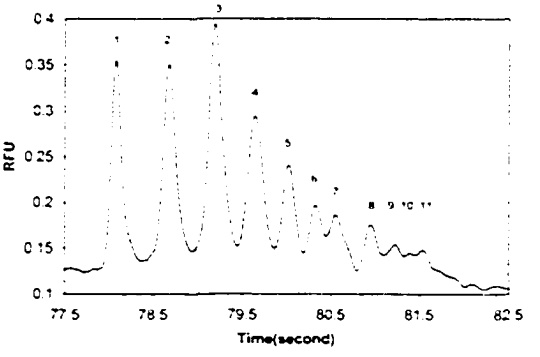

(b)

Figure 4.4: PDMA Based Supercoiled DNA Ladder Separation, detection at 10mm, injection time 60s, separation voltage 3000V. a) zoomed electropherogram b) the inset shows a) in higher resolution 77 s to 82 s

were higher amounts of ions in the sample well and the small amounts of negative DNA had lower chance to enter the channel because of the inappropriate concentration of the buffer.

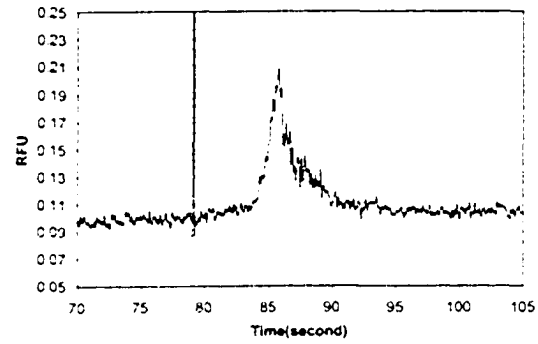

(a)

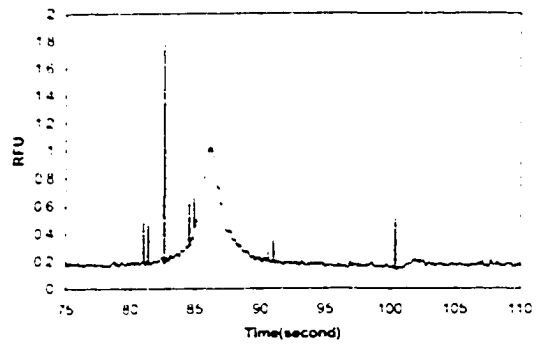

(b)

Figure 4.5: PDMA Based Template DNA Separation, detection at 10mm, injection time 60s, separation voltage 3000V, a and b are the profiles of two runs in one load

Figure 4.7 and Figure 4.8 show the profiles of the mitochondrial DNA (section 4.2.5) before and after the RNAse treatment, respectively. There are three peaks in Figure 4.7 which may correspond to mtDNA and RNA left from the preparation process as expected from the previous test on slab-gel (Figure 4.2, section 4.2.6).

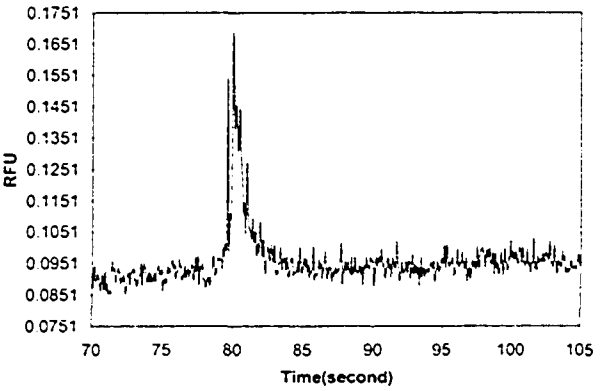

Figure 4.6: PDMA Based rho0 DNA Separation, detection at 10mm, injection time 60s, separation voltage 3000V

In Figure 4.2a (Lane 2) the bands which came earlier in the gel disappeared after the RNAse treatment and only one band remained in Figure 4.2b (Lane 2). This result might be similar to the RNAse treatment on the chip (Figure 4.8). The peaks in Figure 4.7 from 75 s to 81 s might be related to RNA and the remaining peak in Figure 4.8 might be from mtDNA. However, the only peak in Figure 4.8 does not exactly correspond to the 11th peak of supercoiled ladder or the peak in Figure 4.7 at 83 s, and it is slightly shifted.

It should be noted that since the amount of mtDNA in the sample well after the RNAse treatment was 30ng (10 times more than the rho0 DNA and template DNA), a peak was present after the RNAse treatment, however, as can be seen in Figure 4.8 the peak is very weak.

We also tried to purify the mtDNA sample from RNA, Figure 4.9, following an alternative method to avoid using RNAse (section 4.2.7). Figure 4.9 shows two profiles of the mtDNA purified by the method presented in section 4.2.7. In Figure 4.9a, the remaining peak is broad and a spike is also present at 85 s, and in Figure 4.9b, there is another peak

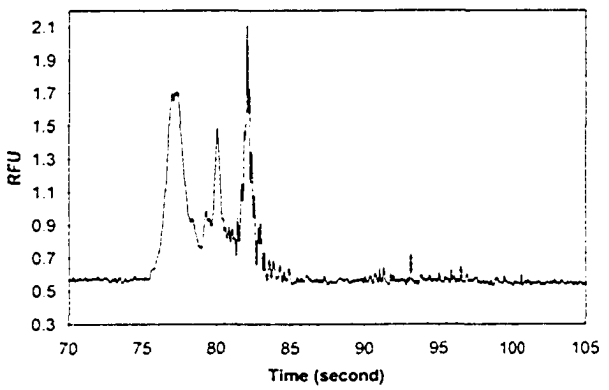

Figure 4.7: PDMA Based Mitochondrial DNA Separation, detection at 10mm, injection time 60s, separation voltage 3000V

present after the broad peak and the spike (at 84 s) (the spikes in Figure 4.9a and Figure 4.9b had the same timing and intensity). There are two broad peaks in Figure 4.9b (one from 82s to 85,and the other from 85s to 87s) which might be related to RNA, and similarly there are two broad peaks in Figure 4.7 (one from 78s to 80s and the other from 83s to 85s). The profiles in Figure 4.9b and Figure 4.7 suggests that the purification was not properly done.

4.3.2 Agarose Based Supercoiled DNA Separation

Figure 4.10 and Figure 4.11 show the profiles of the template DNA and rho0 DNA, respectively, in 1 % agarose in TBE (detail in section 4.2.9). A very low separation voltage, i.e. 400V (the separation current for 400 V was around 0.5μA), was applied to be representative of the standard slab-gel protocol. This test might be possible to run at higher voltages but the resolution may be lost. The profiles in Figure 4.10 and Figure 4.11 seem to be similar to those of Figure 4.5 and Figure 4.6. In Figure 4.10 and Figure 4.5, there is a

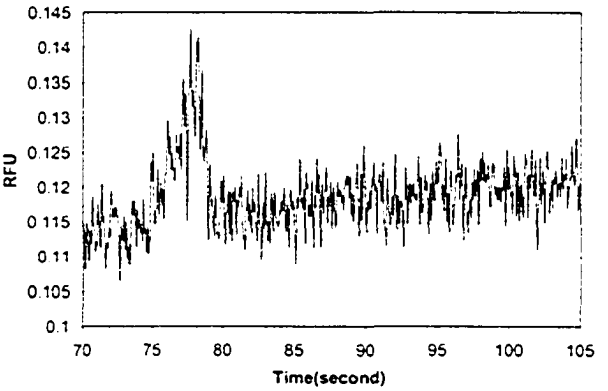

Figure 4.8: PDMA Based Mitochondrial DNA plus RNAse Separation (section 4.2.6), detection at 10mm, injection time 60s, separation voltage 3000V

broad peak which comes later than the narrow peak in Figure 4.11 and Figure 4.6. Usage of very low separation voltages can explain the huge difference between the timings of the peaks in Figure 4.10 and Figure 4.11. Lower voltages would result in higher arrival timing difference which can be explained as follows: assume two samples are being tested with mobilities μ_1 and μ_2. In system #1 using the voltage V_1, the peak for sample #1 comes at t_1 and the peak for sample #2 comes at t_2. In the same manner, in system #2 using voltage V_1' the peak for sample #1 comes at t_1' and the peak for sample #2 comes at t_2'. For each sample in each system we can assume:

$$v = \mu \times V/D \tag{4.1}$$

where v is the velocity and μ is the mobility of DNA, V is the separation voltage and D is the distance that the voltage was applied. The velocity is:

$$v = d/t \tag{4.2}$$

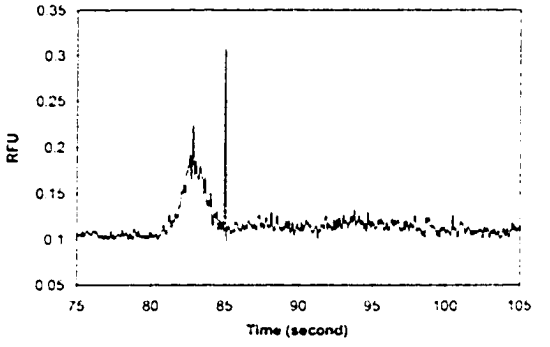

(a)

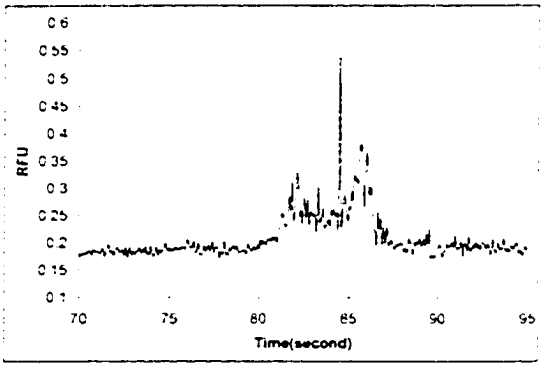

(b)

Figure 4.9: PDMA Based mtDNA Purified by Gel Filtration Sorbent, section 4.2.7, detection at 10 mm, injection time 60s, separation voltage 3000V
a and b are profiles of the same sample from two runs of different loads of the sample prepared in section 4.2.7.

where d is the distance and t is the time. It can be said for each sample in each system:

$$\mu \times V \times t = constant \tag{4.3}$$

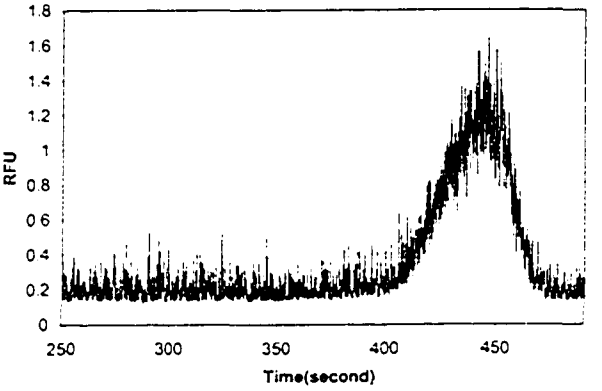

Figure 4.10: Agarose Based Template DNA Separation, detection at 10mm, injection time 200s, injection voltage=100V, separation voltage 400V

Assuming the mobility of each sample is constant in two systems, for sample #1:

$$V_1 \times t_1 = \acute{V}_1 \times \acute{t}_1 \tag{4.4}$$

For sample #2:

$$V_1 \times t_2 = \acute{V}_1 \times \acute{t}_2 \tag{4.5}$$

It can concluded that:

$$\acute{t}_1 - \acute{t}_2 = V_1/\acute{V}_1(t_2 - t_1) \tag{4.6}$$

In other words, the timing difference between the arrival timing of sample #1 and sample #2 in system #2 can be changed by the factor $(V_1/\acute{V}_1)$ comparing to the timing difference between the arrival timing of the same samples in system #1. If $\acute{V}_1$ is 10 times smaller than V1, the difference between the timings in two systems would be 9 times different.

As discussed in the previous section, the peak in the rho0 profile could be related to RNA left from the preparation procedure. To have a more conclusive result, RNAse should

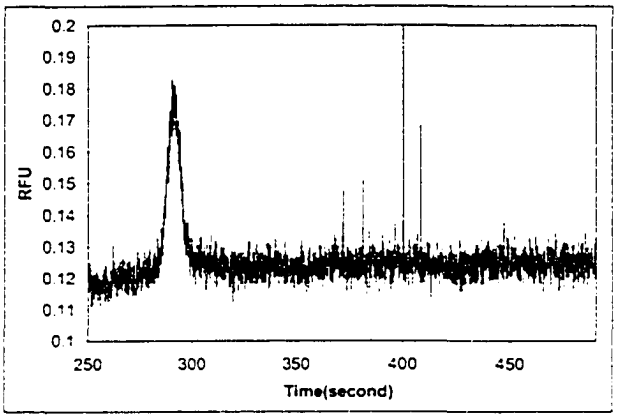

Figure 4.11: Agarose Based rho0 DNA Separation, detection at 10mm, injection time 200s, injection voltage=100V, separation voltage 400V

be added to each template DNA and rho0 DNA (following section). This test was not done in agarose-based method because of the shortage of time.

The DNA size standard was tested using higher voltages i.e. 1000V (no test was done at 400V due to the lack of time). Using 0.1 and 0.7 % agarose (at 1000V) as compared with 1% agarose did not show significant resolution improvement (data not shown, see the supplementary file for timestamps of the supercoiled DNA ladder separation) for the separation of size standards. For each sample, supercoiled DNA ladder and Genescan-500, a broad peak with a variable timing was obtained (data not shown). We related this huge timing variation (20 to 50 seconds from run to run) to the high separation voltage (1000V, $\sim 4\mu$A) which may melt the agarose. No test had been done for the supercoiled DNA ladder under the same conditions as Figure 4.10 and Figure 4.11 because of the shortage of time.

The injection voltage was 100 V for both experiments in Figure 4.10 and Figure 4.11. Assuming the same mobility for DNA over the range of 400V separation (47 V/cm) to

100V injection (125 V/cm), the appropriate value for the injection time based on the arrival timing of template DNA in Figure 4.10 is 500s (the template DNA arrival was 250 s after injection). Since the detection point is at 10mm, 500s is needed for the same sample to reach the intersection from the sample well i.e. around 5mm). However, in our experiment the results were repeatable (from first to later runs of same load) and this suggests that the sample did reach the intersection within 200s- possibly due to the mobility not being constant over the range of 400V separation (47 V/cm) to 100V injection (125 V/cm).

4.3.3 GeneScan Based Supercoiled DNA Separation

Similar experiments were done using GeneScan as the sieving matrix. Figure 4.12 shows the profile of the supercoiled DNA ladder separation in 0.2GS10G with the detection point 22 mm from the intersection of the microchannels. Figure 4.13(a-c) (three successive runs) and Figure 4.14(a-d) (four successive runs) show the profiles of the template DNA before and after the RNAse treatment.

The broad peak related to template DNA still exists after the RNAse treatment (Figure 4.14 after the RNAse treatment and Figure 4.13 before the RNAse treatment). There was also a spike present a few seconds before the broad peak, however, the timing for the spikes in Figure 4.14(a-d) is not repeatable and it does not corresponds to the spikes in Figure 4.13(a-c). The sporadic presence of the spikes in Figure 4.14(a-d) suggests that they are not related to RNA contamination. The broad peak and the spikes also came later after the RNAse treatment (Figure 4.14(a-d)) and one possible explanation for this observation is the slight change in DNA charge because of the RNAse treatment.

It should also be noted that the SYTO dyes, reported in Molecular Probes handbook [80], can stain both DNA and RNA. Although there has not been any report on the labeling effect of Sytox dyes on RNA, we believe that Sytox Orange is able to label double-stranded conformation of RNA which may exist in RNA solutions.

The profile of rho0 DNA is shown in Figure 4.15. The RNAse treatment to rho0 DNA did not show presence of any peak (i.e. flat baseline, Figure 4.16). It can be concluded that

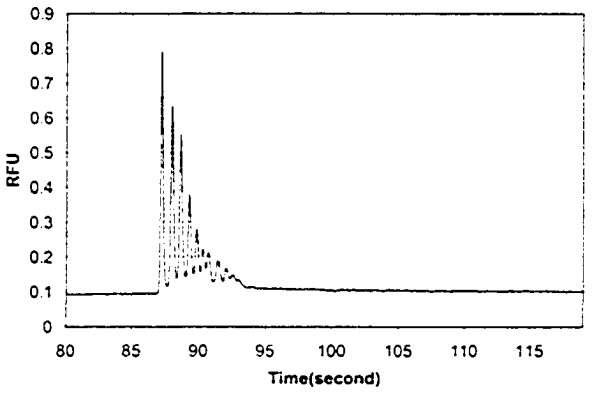

(a)

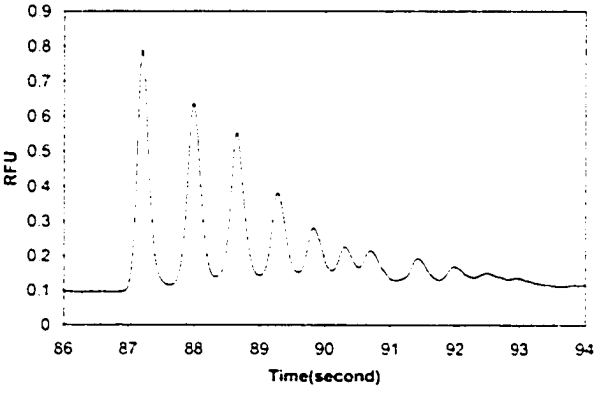

(b)

Figure 4.12: GeneScan Based Supercoiled DNA Ladder Separation, detection at 22 mm, injection time 45s, separation voltage 3000V, a) zoomed electropherogram b) the inset shows a) in higher resolution 86 s to 94 s

the peak in Figure 4.15 (or other rho0 profiles) is related to the presence of RNA. However, since this experiment was done only once (shortage of time) by the summer student, Ekua Yorke, the reproducibility of the result should be tested (more detail in section 4.3.4).

We also tried to separate the purified mtDNA sample in GeneScan, Figure 4.17 (section 4.2.7). The remaining peak is broad and in contrast to Figure 4.9, only one peak is present. There was only one experiment done (because of the shortage of time) by Ekua Yorke, the summer student, and further loads are needed to check the reproducibility of this result. This result can not be compared with the untreated mtDNA sample since there has not been any load of this sample at 22mm detection point at Ekua Yorke work (the shortage of the sample).

The spikes present in some of the presented experiments might come from the labelling procedure because of their random nature in time. Although we labelled all the samples in all the methods following the passivation procedure, there might have been some floating dye molecules dissolved from the walls in the sieving matrix or separation buffer. More detail for the spikes and the reproducibilities is given in next section.

4.3.4 Reproducibility of the Results

In order to develop a reliable technique for genetic analysis, the reproducibility of the results is an important issue. As discussed earlier in the introduction section, the procedure of mtDNA preparation is labor intensive and we also developed our protocols using limited amount of mtDNA. As discussed in section 4.3.1, the peaks corresponding to very small amount of DNA had a higher intensity when the detection point was closer to the intersection. The optimum detection point for both supercoiled DNA ladder and mtDNA was found after a set of trials. Hence, there are not many experiments for both supercoiled DNA ladder and other samples (mtDNA, template DNA and rho0 DNA) at this detection point, i.e. 10 mm for PDMA based and agarose based experiments and 22mm for Genescan based experiments, and further experiments are needed to test the reproducibility of the results.

In some cases, we were not able to repeat the results because of the shortage of the

sample. Ekua Yorke's work did not have the profile of untreated mtDNA at 22mm (the detection point she tried for other samples).

She also had only one experiment (because of the shortage of time) corresponding to the separation of template DNA after the RNAse treatment and she had 8 successive runs in this load with a reproducible peak similar to Figure 4.14(consistent timing and intensity for the broad peak, and also stable current). However, the spikes in Figure 4.14(a-d) were not repeated at the same time in these four profiles (a-d).

One experiment was only present in her work (because of the shortage of time) corresponding to the RNAse treatment of rho0 DNA. In this experiment, she could see flat baseline (with stable current) as in Figure 4.16 and it was repeatable in four successive runs. Although we relied on this single load in our reasoning, this experiment should be repeated in future to see the repeatability of the result.

The profile in Figure 4.8, corresponding to the RNAse treatment of mtDNA, was only present at this run (the first run of the experiment) and it is likely that it is due to the carry-over from the previous load since the peak was present in the profile of the previous load (the detection point was at 20mm and the arrival time was two times the arrival time of the peak in Figure 4.8).

The other profiles, related to supercoiled DNA ladder, rho0 DNA and template DNA were reproducible (consistent results in multiple runs for multiple loads), however, the timing variation made the sizing procedure very sensitive since the samples were separated only 10 mm (or 22mm) after the injection. For example, the timing difference for the separation of 2kbp and 11kbp supercoiled DNA was only 6 seconds (Figure 4.12). The arrival timing of the peaks in the supercoiled DNA ladder and mtDNA (untreated) had some variations (less than 3 s), however, this variations could not be ignored and further loads are needed to confirm the results.

Spikes were seen in some of the electropherograms of this work. As discussed before, the spikes in (Figures: 4.5, 4.13, 4.14, 4.15, 4.17) might come from the labelling procedure because of their random behavior. These spikes were not present in the PDMA based and agarose based experiments (Figure 4.10 and Figure 4.5) suggesting that they were only

related to the reagents used in the Genescan based method. However, the spike at 85 s in (Figure 4.9) was reproducible (the same timing and intensity were present in three runs from three experiments) and as discussed earlier it should not be ignored.

Three profiles of template DNA from three runs were shown in Figure 4.13. There is a spike in Figure 4.13a and Figure 4.13c at 85 s. The broad peak is very weak in Figure 4.13b however there is a spike at 83 s. These results were obtained from one experiment of Ekua Yorke and further work is needed to test the reproducibility of the results. The spike arrival times in Figure 4.14(a-d) were not repeatable in these four runs, however, this sporadic behavior may be related to the presence of supercoiled DNA and it should not be ignored. The statistical investigation of these spikes is given in section 4.4.4.

4.4 Discussion

In this set of experiments, we tried to differentiate the nuclear DNA, mtDNA and RNA contributions to electropherograms of DNA samples (template DNA, rho0 DNA, untreated mtDNA).

4.4.1 Was RNA Detected in Presented Methods?

In the GeneScan method, the treatment with RNAse (section 4.2.6) did not eliminate the major fluorescent peak in the template DNA (Figure 4.13 and Figure 4.14 before and after the RNAse treatment, respectively) although RNAse might have removed the overlapping RNA in Figure 4.13.

However, the addition of the RNAse to rho0 DNA resulted in a flat baseline (Figure 4.15 and Figure 4.16 before and after the addition of RNAs, respectively). With these two experiments, it can tentatively be concluded that the peak present in all rho0 DNA profiles is related to the presence of RNA in the sample. Since rho0 sample contains nuclear DNA, it can also be concluded that the nuclear DNA in rho0 DNA was not injected into microchannels. This also suggests that upon applying the injection voltage the nuclear

DNA in template DNA is retained in the sample well.

The RNAse treatment to rho0 DNA and template DNA were not tested in agarose-based and PDMA-based methods (because of the shortage of time and the lack of sample stacking (section 4.3.1), respectively). It is a part of future work to test the reproducibility of this result in all three methods.

4.4.2 Was Nuclear DNA Detected in Presented Methods?

Referring to the conclusion in the previous section that the peak in rho0 profile (Figure 4.15) may be related to RNA and the remaining peak in template DNA profile after the RNAse treatment (Figure 4.14) may show presence of no RNA, there are two possibilities for the source of the peak in the template DNA profile (Figure 4.14). This peak might be from either nuclear DNA or mtDNA. It is less probable that this peak corresponds to the nuclear DNA because if the nuclear DNA had a chance to enter the channels, there should have been one peak in the rho0 DNA profile after the RNAse treatment (Figure 4.16).

Nuclear DNA might be sheared into smaller fragments [149] and the profile of sheared nuclear DNA would contain random peaks because of the random shearing of the nuclear DNA. The broad peak in the template DNA profile (Figure 4.14 (a-d), Figure 4.10, Figure 4.5) is not likely to be related to the sheared nuclear DNA since it was reproducible with the same timing, width and intensity from run to run.

4.4.3 Was mtDNA Detected in Presented Methods?

The broad peak in template DNA profiles (Figure 4.14) does not correspond to either RNA or nuclear DNA (as described above) and it is probable that this peak is from the presence of mtDNA. In both the PDMA-based and Genescan-based methods the broad peak corresponding to template DNA (Figure 4.13 and 4.5) is still much broader than a single supercoiled plasmid DNA in the size standard. The broad peak in Figure 4.13a is 10 s wide (90 s to 100 s) while the supercoiled DNA ladder profile (2-16kbp) in Figure 4.12 is 6 s wide (starts at 87 s corresponds to 2kbp plasmid and ends at 93 s corresponds to 16kbp

plasmid). However, the spikes in Figure 4.13(a-c) and Figure 4.5 (a-b) might correspond to supercoiled mtDNA. The timing of these spikes were not repeatable although they appeared a few seconds before the broad peak.

We also tried to size mtDNA prepared by Dr. Ivette Sosova presented in section 4.2.5. We realized that the sample contains some RNA since two peaks disappeared in the electropherogram after the RNAse treatment (Figure 4.7 and Figure 4.8 before and after the RNAse treatment, respectively). The remaining peak after the RNAse treatment (Figure 4.8 around 78 second) does not correspond to the 11th peak of supercoiled DNA ladder (Figure 4.4 the peak at 82 second). This observation may suggest that the prepared mtDNA is not in supercoiled form. However, the reproducibility should be tested since we had only two runs showing this timing (shortage of mtDNA).

Since the mtDNA purified by Alexey Atrazhev (section 4.2.7) (Figure 4.9(a-b)) and the untreated mtDNA (Figure 4.7) showed similar profiles, we believe the mtDNA purification has not been done properly (more detail in section 4.3.4).

4.4.4 Statistical Investigation of the Peaks

In an effort to explain the occasional occurrence of the spikes with reproducible timing, we investigated whether they could be due to the occasional presence of a copy of chromosomal DNA or mtDNA. We first tried to calculate the number of chromosomes in template DNA (in each run) corresponding to the experiments in Figure 4.5 and Figure 4.13. Referring to Backhouse *et. al* [150], the plug separated in the separation stage typically carries 1/10,000 of the DNA in the well. Since 1 bp approximately corresponds to 650 amu (atomic mass unit=$1.67377\times10^{-24}g$), the nuclear DNA (3.2 billion basepairs) of a cell will weigh $1.67 \times 10^{-24} \times 650 \times 3.2 \times 10^{9} = 3.481 \times 10^{-12}g$. Since each cell contains 46 chromosomes, a chromosome will weigh $3.481 \times 10^{-12}/46 = 7.56 \times 10^{-14}g$. We used approximately 20ng in the sample well in each experiments corresponding to Figure 4.5 and Figure 4.13. Therefore, the number of nuclear DNA genomes in the well can be calculated as $20ng/3.481 \times 10^{-12} = 5745$. The number of chromosomes can also be cal-

culated as $20ng/7.56 \times 10^{-14} = 2.6 \times 10^5$. Separating 1/10,000 of this value as the plug, $2.6 \times 10^5/10,000 = 26.6$ chromosomes were roughly been able to be separated if they had a chance to leave the well. The same calculation for mtDNA in this sample can be done: there are $20ng/3.481 \times 10^{-12} = 5745$ nuclear DNA (from 5745 cells) in the sample well, and since there are roughly 1000 mtDNA loop in each cell [103], there are 5.745×10^6 mtDNA loop in the sample well and 1/10,000 of this value will be separated as the plug corresponding to rougly 574 mtDNA loops. This rough calculation shows that the ratio of the number of mtDNA loops to chromosomal DNA in the template DNA is 22.

The same calculation for mtDNA corresponding to Figure 4.9 (purified by gel filtration) can be done: each mtDNA loop (16.5kbp) approximately weighs $1.67377 \times 10^{-24} \times 650 \times 16.5 \times 10^3 = 7.071 \times 10^{-18} g$. Having approximately 20ng of mtDNA in the well, the number of mtDNA loops in the sample well would be $20ng/(7.071 \times 10^{-18} g)$ and 1/10,000 of this value will be separated as the plug: $20ng/(7.071 \times 10^{-18} g)/10.000 = 2.8 \times 10^5$. It means that 2.8×10^5 mtDNA loops (in section 4.2.7) could have been separated in each run.

It is also worthwhile to investigate the statistical behavior of the spikes. The spike present in the mtDNA purified by the RNAse-free method (section 4.2.7) appeared in 4 runs (out of 10 runs) of one load. The spike in Figure 4.9a appeared at 85s and the FWHM of the spike was 0.11s while the spike in Figure 4.9b appeared at 84.5s and the FWHM of the spike was 0.12s. The other two profiles of this sample were detected at another detection point (data not shown) with the FWHM of 0.115s and 0.110s.

The behavior of the spikes in the template DNA profile Figure 4.13 was also investigated. Since the baseline was spiky, in all the profiles there were many spikes with the FWHM of 0.11s or 0.115s (as described earlier might come from the labeling process) making it difficult to find any reproducible spike. There was a spike at 85s in Figure 4.13a with the FWHM of 0.15s and it was almost reproduced in Figure 4.13b at 86.5s with the FWHM of 0.165s and Figure 4.13c at 84.8s with the FWHM of 0.115s.

Because of the random behavior of the spikes in Figure 4.13, Figure 4.14 and Figure 4.9 (the FWHM was usually either 0.11 or 0.115, the same FWHM for the random spikes)

and the timing was not reproducible, we are not able to conclude that the spikes correspond to mtDNA loop at this stage and more experiments are needed.

4.5 Conclusion and Future Work

This work showed preliminary experiments toward the detection of the large mtDNA deletions characteristic of Kearns-Sayre Syndrome (KSS). Since mtDNA preparation is a costly and laborious process and only small quantities of mtDNA could be extracted, we proposed an on-chip mtDNA purification method. We used template DNA (used in PCR amplification) which typically contains both nuclear DNA and mtDNA and we tried to separate mtDNA from nuclear DNA relying on the fact that the nuclear DNA might not enter the microchannels and may remain in the sample well. We are not sure if mtDNA was separated from nuclear DNA in template DNA since the sizing of the remaining peak after the addition of the RNAse (to remove the RNA contamination)(Figure 4.14) did not correspond to the 16kbp supercoiled DNA in the size standard.

There are many more experiments that could be done for a conclusive result. In GeneScan based method, each of template DNA and rho0 DNA should be loaded with and without RNAse to see if the results are reproducible. It is also suggested to detect the DNA samples after longer separation times.

There is one probability that the broad peak in template DNA profile (Figure 4.14) is related to open-circular or linear conformation of mtDNA. Levy *et al.* [151] proposed a method to monitor the content of supercoiled form in DNA solutions. They employed 0.6-0.8% agarose gel in 1xTB buffer for the separation of the ambient and heated ($95^{\circ}C$)-cooled plasmid DNA. They took advantage of the reversible denaturation of supercoiled DNA [151] by relying on the fact that the complementary strands of supercoiled DNA can not be separated by heating.

A recommendation for the future experiments would be the addition of formamide to the template DNA in sample well and to the sieving matrix or the usage of a denaturant sieving matrix. The denatured DNA return to their native configuration when they are cooled

(or no denaturant is present) and show high fluorescence upon binding to Sytox Orange. In contrast, a portion of open-circular and linear form of circular DNA remain singe-stranded and show minimal fluorescence upon binding to Sytox Orange. If the broad peak in template DNA profile is related to the open-circular or linear conformation of mtDNA, it would not be detected by Sytox Orange upon denaturation. The sporadic behavior of the spikes (few seconds before the broad peak in Figure 4.13) in template DNA profile can also be explained if they remain in the electropherogram after the addition of formamide.

The final goal would be developing a reproducible and reliable sizing protocol on microfluidic chips. This would lead us to detect Kearns-Sayre Syndrome (KSS) which was found to be associated with large mtDNA deletions. Using another architecture of microchips can integrate the sample purification (our proposed method), enzymatic digestion of the desired region, and the novel HA/SSCP method in chapter 2 and this integration would allow us to detect other point mutations in mtDNA.

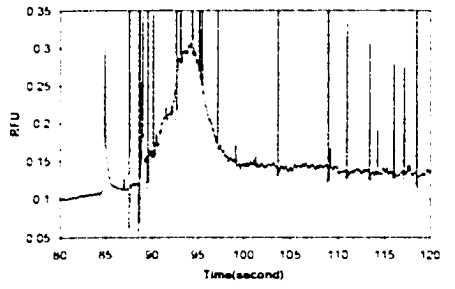

(a)

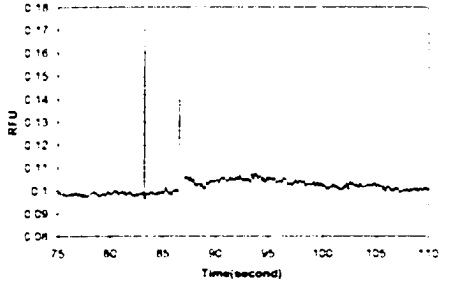

(b)

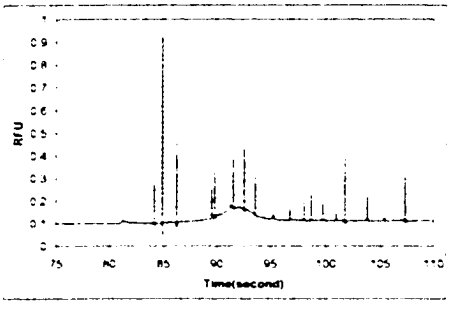

(c)

Figure 4.13: GeneScan Based Template DNA Separation, detection at 22 mm, injection time 45 s, separation voltage 3000V. a, b and c are three successive runs

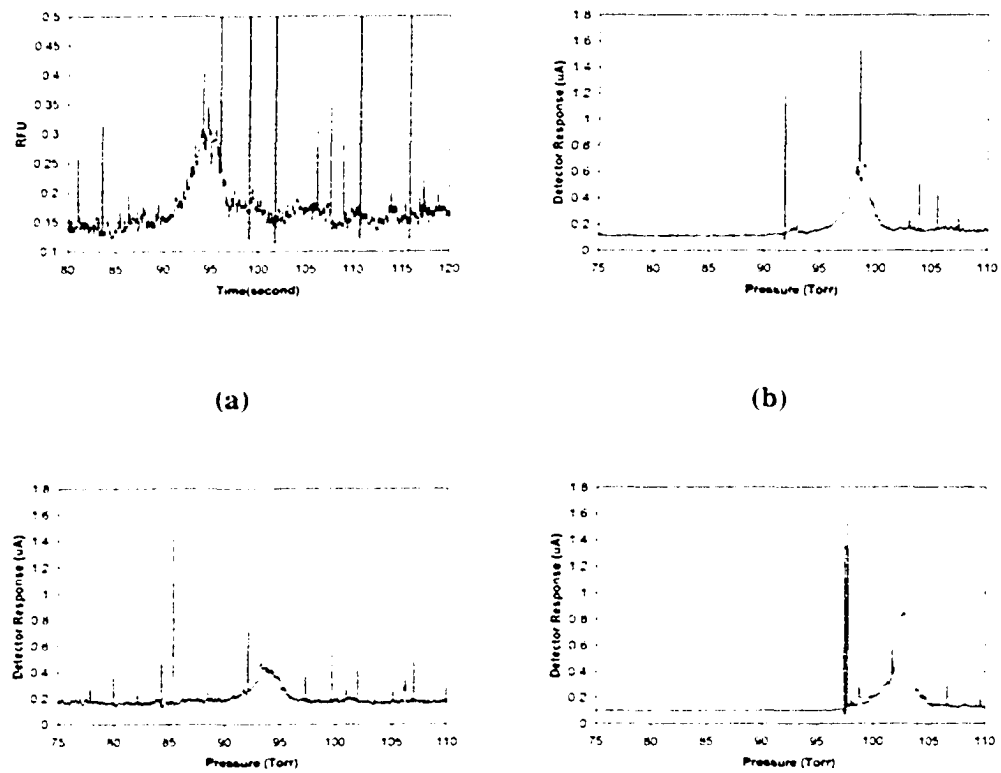

Figure 4.14: GeneScan Based Template DNA after the RNAse treatment (section 4.2.6) detection at 22 mm, injection time 45 s, separation voltage 3000V. a-d show successive runs

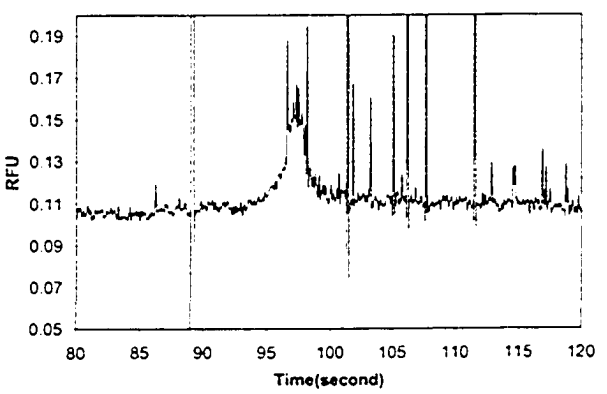

Figure 4.15: GeneScan Based rho0 DNA Separation, detection at 22 mm, injection time 45s, separation voltage 3000V

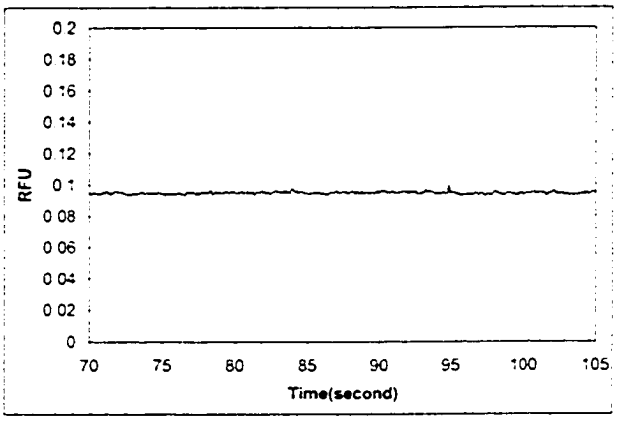

Figure 4.16: GeneScan Based rho0 DNA plus RNAse (section 4.2.6), detection at 22 mm, injection time 45s, separation voltage 3000V

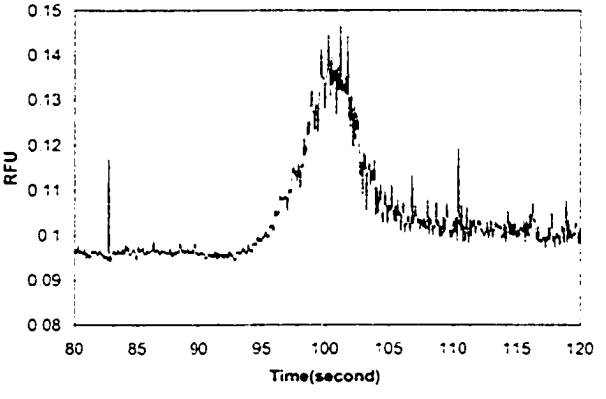

Figure 4.17: GeneScan Based mtDNA Purified by Gel Filtration Sorbent, section 4.2.7, detection at 22 mm, injection time 45s, separation voltage 3000V

Chapter 5

Conclusion

In these experiments, we developed different techniques that lend themselves to higher levels of integration in microchip capillary electrophoresis. The work done in chapter 2, can be used for single point mutation detection employing microfluidic devices. It eliminates the pre-labelling procedures for PCR-products and also off-chip denaturation. Combining HA/SSCP, 100 % sensitivity could be achieved and further experiments could be done by applying the same method and a variety of mutations could be detected.

In chapter 3 we showed that the intercalators can decrease the resolution of separation and by proper labeling of DNA sample on the chip higher resolution might be obtained. A labeling method was suggested to increase the resolution and it was also suggested that it is able to change the conformation of heteroduplexes. The desired results were not obtained following our methods, however, further work should be done in order to develop the proper labeling protocol.

As discussed in chapter 4, since mutations in mtDNA are recognized as important in diseases ranging from Parkinson's, Alzheimer's, heart disease, fatigue syndromes to numerous genetic conditions, it is essential to develop a rapid analysis tool for detection of mtDNA mutations. Using microfluidic chips, we tried to extract mtDNA from the mixture of nuclear DNA and mtDNA. We also tried to develop a sizing method for mtDNA so that it could be used for the diagnosis of Kearns-Syre Syndrome (KSS) which was found to be

associated with large mtDNA deletions. The successful results were brought in this chapter, however, there are more experiments to do for developing a more reliable diagnosis tool for mtDNA mutation detection. The list of future experiments are presented in section 4.5.

References

[1] A. J. Nataraj, I. Olivos-Glander, N. Kusukawa, and W. E. Highsmith, "Single-strand conformation polymorphism and heteroduplex analysis for gel-based mutation detection," *Electrophoresis*, vol. 20, no. 6, pp. 1177–1185, 1999.

[2] P. Raven and G. Johnson, *Biology*, 4th ed. St. Louis: Times Mirror/Mosby College Publishing, 1989.

[3] R. Sinden, *DNA Structure and Function*, 1st ed. Academic Press at San Diego, New York, Boston, London, Sydney, Tokyo, Toronto, 1994.

[4] M. Kiseleva, E. Zarochentseva, and N. Dodonova, "Absorption-spectra of nucleic-acids and their components in spectral region 120-280 nm," *Biofizika*, vol. 20, no. 4, pp. 561–565, 1975.

[5] M. J. Cavaluzzi and P. N. Borer, "Revised UV extinction coefficients for nucleoside-5'-monophosphates and unpaired DNA and RNA," *Nucleic Acids Research*, vol. 32, no. 1, 2004.

[6] P. Howley, M. Israel, M. Law, and M. Martin, "Rapid Method for Detecting and Mapping Homology between Heterologous DNAs - Evaluation of Polyomavirus Genomes," *Journal of Biological Chemistry*, vol. 254, pp. 4876–4883, 1979.

[7] G. Spiegelm, J. Haber, and H. Ho, "Kinetics of ribonucleic acid deoxyribonucleic acid membrane filter hybridization," *Biochemistry*, vol. 12, pp. 1234–1242, 1973.

[8] T. Cremer, P. Lichter, J. Borden, D. Ward, and L. Manuelidis, "Detection of chromosome-aberrations in metaphase and interphase tumor-cells by insitu hybridization using chromosome-specific library probes," *Human Genetics*, vol. 80, pp. 235–246, 1988.

[9] K. Cox, D. Deleon, L. Angerer, and R. Angerer, "Detection of Messenger-RNAs in Sea-Urchin Embryos by insitu Hybridization Using Asymmetric RNA Probes," *Developmental Biology*, vol. 101, pp. 485–502, 1984.

[10] J. Casey and N. Davidson, "Rates of Formation and Thermal Stabilities of RNA-DNA and DNA-DNA Duplexes at High-Concentrations of Formamide," *Nucleic Acids Research*, vol. 4, pp. 1539–1552, 1977.

[11] T. Schmidt, K. Friehs, M. Schleef, C. Voss, and E. Flaschel, "Quantitative analysis of plasmid forms by agarose and capillary gel electrophoresis," *Analytical Biochemistry*, vol. 274, no. 2, pp. 235–240, 1999.

[12] P. H. Johnson and L. I. Grossman, "Electrophoresis of DNA in Agarose Gels - Optimizing Separations of Conformational Isomers of Double-Stranded and Single-Stranded DNAs," *Biochemistry*, vol. 16, no. 19, pp. 4217–4225, 1977.

[13] H. V. Thorne, "Electrophoretic Characterization and Fractionation of Polyoma Virus DNA," *Journal of Molecular Biology*, vol. 24, no. 2, pp. 203, 1967.

[14] B. S. Shastry, "SNP alleles in human disease and evolution," *Journal of Human Genetics*, vol. 47, no. 11, pp. 561–566, 2002.

[15] M. Koch, A. Evans, and A. Brunnschweiler, *Microfluidic technology and applications*, Microtechnologies and microsystems series ; 1). Philadelphia, PA : Research Studies Press, c2000.

[16] D. J. Beebe, G. A. Mensing, and G. M. Walker, "Physics and applications of microfluidics in biology," *Annual Review of Biomedical Engineering*, vol. 4, pp. 261–286, 2002.

[17] G. Ramsay, "DNA chips: State-of-the-art," *Nature Biotechnology*, vol. 16, no. 1, pp. 40–44, 1998.

[18] A. van den Berg and T. S. J. Lammerink, "Micro total analysis systems: Microfluidic aspects, integration concept and applications," in *Microsystem Technology in Chemistry and Life Science*, vol. 194 of *Topics in Current Chemistry*, pp. 21–49, 1998.

[19] D. Qin, Y. N. Xia, J. A. Rogers, R. J. Jackman, X. M. Zhao, and G. M. Whitesides, "Microfabrication, microstructures and microsystems," in *Microsystem Technology in Chemistry and Life Science*, vol. 194 of *Topics in Current Chemistry*, pp. 1–20, 1998.

[20] C. S. Effenhauser, "Integrated chip-based microcolumn separation systems," in *Microsystem Technology in Chemistry and Life Science*, vol. 194 of *Topics in Current Chemistry*, pp. 51–82, 1998.

[21] A. Manz, N. Graber, and H. M. Widmer, "Miniaturized total chemical-analysis systems - a novel concept for chemical sensing," *Sensors and Actuators B-Chemical*, vol. 1, no. 1-6, pp. 244–248, 1990.

[22] D. Hawcroft, *Electrophoresis, the basics*, IRL Press at Oxford, New York, Tokyo, 1997.

[23] J. Molho, A. Herr, T. Kenny, M. Mungal, M. Garguilo, and P. Paul, "Fluid Transport Mechanisms in Microfluidic Devices," *Micro-Electro-Mechanical Systems (MEMS), ASME International Mechanical Engineering Congress and Exposition*, vol. DSC-Vol.66, 1998.

[24] S. Devasenathipathy and J. Santiago, *Micro- and Nano-Scale Diagnostic Techniques*. K.S. Breuer, Springer Verlag, New York, 2003, Chapter 3.

[25] G. W. Slater, "Theory of Band Broadening for DNA Gel-Electrophoresis and Sequencing," *Electrophoresis*, vol. 14, no. 1-2, pp. 1–7, 1993.

[26] B. Tinland, N. Pernodet, and A. Pluen, "Band broadening in gel electrophoresis: Scaling laws for the dispersion coefficient measured by FRAP," *Biopolymers*, vol. 46, no. 4, pp. 201–214, 1998.

[27] K. Ueno and E. S. Yeung, "Simultaneous Monitoring of DNA Fragments Separated by Electrophoresis in a Multiplexed Array of 100 Capillaries," *Analytical Chemistry*, vol. 66, no. 9, pp. 1424–1431, 1994.

[28] X. H. Huang and R. N. Zare, "Continuous sample collection in capillary zone electrophoresis by coupling the outlet of a capillary to a moving surface," *Journal of Chromatography*, vol. 516, no. 1, pp. 185–189, 1990.

[29] R. J. Zagursky and R. M. McCormick, "DNA Sequencing Report - DNA Sequencing Separations in Capillary Gels on a Modified Commercial DNA Sequencing Instrument," *Biotechniques*, vol. 9, no. 1, pp. 74–8, 1990.

[30] C. Backhouse, M. Caamano, F. Oaks, E. Nordman, A. Carrillo, B. Johnson, and S. Bay, "DNA sequencing in a monolithic microchannel device," *Electrophoresis*, vol. 21, no. 1, pp. 150–156, 2000.

[31] C. Heller, "Capillary electrophoresis of proteins and nucleic-acids in gels and entangled polymer-solutions," *Journal of Chromatography A*, vol. 698, no. 1-2, pp. 19–31, 1995.

[32] A. Manz, D. J. Harrison, E. M. J. Verpoorte, J. C. Fettinger, A. Paulus, H. Ludi, and H. M. Widmer, "Planar chips technology for miniaturization and integration of separation techniques into monitoring systems - capillary electrophoresis on a chip," *Journal of Chromatography*, vol. 593, no. 1-2, pp. 253–258, 1992.

[33] D. J. Harrison, A. Manz, Z. H. Fan, H. Ludi, and H. M. Widmer, "Capillary electrophoresis and sample injection systems integrated on a planar glass chip," *Analytical Chemistry*, vol. 64, no. 17, pp. 1926–1932, 1992.

[34] D. J. Harrison, K. Fluri, K. Seiler, Z. H. Fan, C. S. Effenhauser, and A. Manz, "Micromachining a miniaturized capillary electrophoresis-based chemical-analysis system on a chip," *Science*, vol. 261, no. 5123, pp. 895–897, 1993.

[35] S. C. Jacobson, R. Hergenroder, L. B. Koutny, R. J. Warmack, and J. M. Ramsey, "Effects of injection schemes and column geometry on the performance of microchip electrophoresis devices," *Analytical Chemistry*, vol. 66, no. 7, pp. 1107–1113, 1994.

[36] S. C. Jacobson, R. Hergenroder, L. B. Koutny, and J. M. Ramsey, "High-speed separations on a microchip," *Analytical Chemistry*, vol. 66, no. 7, pp. 1114–1118, 1994.

[37] K. Seiler, D. J. Harrison, and A. Manz, "Planar glass chips for capillary electrophoresis - repetitive sample injection, quantitation, and separation efficiency," *Analytical Chemistry*, vol. 65, no. 10, pp. 1481–1488, 1993.

[38] R. Prakash, S. Adamia, V. Sieben, and C. Backhouse, "Small Volume PCR in PDMS biochips with integrated fluid control and vapor barrier," *Submitted to the journal of Sensors and Actuators B Chemical*.

[39] I. Rodriguez, Y. Zhang, H. K. Lee, and S. F. Y. Li, "Conventional capillary electrophoresis in comparison with short-capillary capillary electrophoresis and microfabricated glass chip capillary electrophoresis for the analysis of fluorescein isothiocyanate anti-human immunoglobulin G," *Journal of Chromatography A*, vol. 781, no. 1-2, pp. 287–293, 1997.

[40] C. Heller, "Principles of DNA separation with capillary electrophoresis," *Electrophoresis*, vol. 22, no. 4, pp. 629–643, 2001.

[41] J. Han and H. G. Craighead, "Separation of long DNA molecules in a microfabricated entropic trap array," *Science*, vol. 288, no. 5468, pp. 1026–1029, 2000.

[42] J. Noolandi, "A New Concept for Sequencing DNA by Capillary Electrophoresis," *Electrophoresis*, vol. 13, no. 6, pp. 394–395, 1992.

[43] P. Mayer, G. W. Slater, and G. Drouin, "Theory of DNA-Sequencing Using Free-Solution Electrophoresis of Protein-DNA Complexes," *Analytical Chemistry*, vol. 66, no. 10, pp. 1777–1780, 1994.

[44] T. M. Sunada and H. W. Blanch, "Polymeric separation media for capillary electrophoresis of nucleic acids," *Electrophoresis*, vol. 18, no. 12-13, pp. 2243–2254, 1997.

[45] A. Guttman, "Gel and polymer-solution mediated separation of biopolymers by capillary electrophoresis," *Journal of Chromatographic Science*, vol. 41, no. 9, pp. 449–459, 2003.

[46] A. G. Ogston, "The spaces in a uniform random suspension of fibres," *Transactions of the Faraday Society*, vol. 54, no. 11, pp. 1754–1757, 1958.

[47] J. L. Viovy, "Electrophoresis of DNA and other polyelectrolytes: Physical mechanisms," *Reviews of Modern Physics*, vol. 72, no. 3, pp. 813–872, 2000.

[48] R. L. Rill, A. Beheshti, and D. H. Van Winkle, "DNA electrophoresis in agarose gels: Effects of field and gel concentration on the exponential dependence of reciprocal mobility on DNA length," *Electrophoresis*, vol. 23, no. 16, pp. 2710–2719, 2002.

[49] G. W. Slater, M. Kenward, L. C. McCormick, and M. G. Gauthier, "The theory of DNA separation by capillary electrophoresis," *Current Opinion in Biotechnology*, vol. 14, no. 1, pp. 58–64, 2003.

[50] L. Mitnik, L. Salome, J. L. Viovy, and C. Heller, "Systematic Study of Field and Concentration Effects in Capillary Electrophoresis of DNA in Polymer-Solutions," *Journal of Chromatography A*, vol. 710, no. 2, pp. 309–321, 1995.

[51] A. N. Semenov, T. A. J. Duke, and J. L. Viovy, "Gel-Electrophoresis of DNA in Moderate Fields - the Effect of Fluctuations," *Physical Review E*, vol. 51, no. 2, pp. 1520–1537, 1995.

[52] J. Wang, "Electrochemical detection for microscale analytical systems: a review," *Talanta*, vol. 56, no. 2, pp. 223–231, 2002.

[53] K. Uchiyama, H. Nakajima, and T. Hobo, "Detection method for microchip separations," *Analytical and Bioanalytical Chemistry*, vol. 379, no. 3, pp. 375–382, 2004.

[54] Y. H. Lee, R. G. Maus, B. W. Smith, and J. D. Winefordner, "Laser-induced fluorescence detection of a single-molecule in a capillary," *Analytical Chemistry*, vol. 66, no. 23, pp. 4142–4149, 1994.

[55] I. M. Lazar, R. S. Ramsey, S. Sundberg, and J. M. Ramsey, "Subattomole-sensitivity microchip nanoelectrospray source with time-of-flight mass spectrometry detection," *Analytical Chemistry*, vol. 71, no. 17, pp. 3627–3631, 1999.

[56] Q. F. Xue, Y. M. Dunayevskiy, F. Foret, and B. L. Karger, "Integrated multichannel microchip electrospray ionization mass spectrometry: Analysis of peptides from on-chip tryptic digestion of melittin," *Rapid Communications in Mass Spectrometry*, vol. 11, no. 12, pp. 1253–1256, 1997.

[57] A. T. Woolley, K. Q. Lao, A. N. Glazer, and R. A. Mathies, "Capillary electrophoresis chips with integrated electrochemical detection," *Analytical Chemistry*, vol. 70, no. 4, pp. 684–688, 1998.

[58] J. Wang, B. M. Tian, and E. Sahlin, "Micromachined electrophoresis chips with thick-film electrochemical detectors," *Analytical Chemistry*, vol. 71, no. 23, pp. 5436–5440, 1999.

[59] R. S. Martin, A. J. Gawron, S. M. Lunte, and C. S. Henry, "Dual-electrode electrochemical detection for poly(dimethylsiloxane)-fabricated capillary electrophoresis microchips," *Analytical Chemistry*, vol. 72, no. 14, pp. 3196–3202, 2000.

[60] L. A. Larsen, M. Christiansen, J. Vuust, and P. S. Andersen, "High throughput mutation screening by automated capillary electrophoresis," *Combinatorial Chemistry and High Throughput Screening*, vol. 3, no. 5, pp. 393–409, 2000.

[61] "http://www.hgmd.org/," 2004, Human Gene Mutation Database.

[62] G. Vahedi, C. Kaler, and C. J. Backhouse, "An integrated method for mutation detection using on-chip sample preparation, single-stranded conformation polymorphism, and heterduplex analysis," *Electrophoresis*, vol. 25, no. 14, pp. 2346–2356, 2004.

[63] M. Orita, Y. Suzuki, T. Sekiya, and K. Hayashi, "Rapid and Sensitive Detection of Point Mutations and DNA Polymorphisms Using the Polymerase Chain-Reaction," *Genomics*, vol. 5, no. 4, pp. 874–879, 1989.

[64] P. Kozlowski and W. J. Krzyzosiak, "Combined SSCP/duplex analysis by capillary electrophoresis for more efficient mutation detection," *Nucleic Acids Research*, vol. 29, no. 14, 2001.

[65] I. V. Kourkine, C. N. Hestekin, B. A. Buchholz, and A. E. Barron, "High-throughput, high-sensitivity genetic mutation detection by tandem single-strand conformation polymorphism/heteroduplex analysis capillary array electrophoresis," *Analytical Chemistry*, vol. 74, no. 11, pp. 2565–2572, 2002.

[66] M. A. Marino, J. M. Devaney, P. A. Davis, J. K. Smith, and J. E. Girard, "Spectral measurements of intercalated PCR-amplified short tandem repeat alleles," *Analytical Chemistry*, vol. 70, no. 21, pp. 4514–4519, 1998.

[67] X. M. Yan, W. Hang, V. Majidi, B. L. Marrone, and T. M. Yoshida, "Evaluation of different nucleic acid stains for sensitive double-stranded DNA analysis with capillary electrophoretic separation," *Journal of Chromatography A*, vol. 943, no. 2, pp. 275–285, 2002.

[68] J. C. Ren, N. H. Fang, and D. Wu, "Inverse-flow derivatization for capillary electrophoresis of DNA fragments with laser-induced fluorescence detection," *Analytica Chimica Acta*, vol. 470, no. 2, pp. 129–135, 2002.

[69] T. J. Gibson and M. J. Sepaniak, "Examination of cyanine intercalation dyes for rapid and sensitive detection of DNA fragments by capillary electrophoresis," *Journal of Capillary Electrophoresis*, vol. 5, no. 1-2, pp. 73–80, 1998.

[70] H. S. Rye, S. Yue, D. E. Wemmer, M. A. Quesada, R. P. Haugland, R. A. Mathies, and A. N. Glazer, "Stable Fluorescent Complexes of Double-Stranded DNA with Bis-Intercalating Asymmetric Cyanine Dyes - Properties and Applications," *Nucleic Acids Research*, vol. 20, no. 11, pp. 2803–2812, 1992.

[71] W. G. Tan, D. L. J. Tyrrell, and N. J. Dovichi, "Detection of duck hepatitis B virus DNA fragments using on-column intercalating dye labeling with capillary electrophoresis-laser-induced fluorescence," *Journal of Chromatography A*, vol. 853, no. 1-2, pp. 309–319, 1999.

[72] D. Figeys, E. Arriaga, A. Renborg, and N. J. Dovichi, "Use of the Fluorescent Intercalating Dyes POPO-3, YOYO-3 and YOYO-1 for Ultrasensitive Detection of Double-Stranded DNA Separated by Capillary Electrophoresis with Hydroxypropylmethyl Cellulose and Non-Cross-Linked Polyacrylamide," *Journal of Chromatography A*, vol. 669, no. 1-2, pp. 205–216, 1994.

[73] J. Sambrook and D. Russell, *Molecular cloning : a laboratory manual*, 3rd ed., vol. 3. N.Y., Cold Spring Harbor Laboratory Press., 2001.

[74] T. Footz, M. J. Somerville, R. Tomaszewski, B. Elyas, and C. J. Backhouse, "Integration of combined heteroduplex/restriction fragment length polymorphism analysis on an electrophoresis microchip for the detection of hereditary haemochromatosis," *Analyst*, vol. 129, no. 1, pp. 25–31, 2004.

[75] T. Footz, M. J. Somerville, R. Tomaszewski, K. A. Sprysak, and C. J. Backhouse, "Heteroduplex-based genotyping with microchip electrophoresis and dHPLC," *Genetic Testing*, vol. 7, no. 4, pp. 283–293, 2003.

[76] T. Footz, S. Wunsam, S. Kulak, H. J. Crabtree, D. M. Glerum, and C. J. Backhouse, "Sample purification on a microfluidic device," *Electrophoresis*, vol. 22, no. 18, pp. 3868–3875, 2001.

[77] M. B. Wabuyele, S. M. Ford, W. Stryjewski, J. Barrow, and S. A. Soper, "Single molecule detection of double-stranded DNA in poly(methylmethacrylate) and polycarbonate microfluidic devices," *Electrophoresis*, vol. 22, no. 18, pp. 3939–3948, 2001.

[78] S. M. Clark and R. A. Mathies, "Multiplex dsDNA fragment sizing using dimeric intercalation dyes and capillary array electrophoresis: Ionic effects on the stability and electrophoretic mobility of DNA-dye complexes," *Analytical Chemistry*, vol. 69, no. 7, pp. 1355–1363, 1997.

[79] C. J. Backhouse, A. Gajdal, L. M. Pilarski, and H. J. Crabtree, "Improved resolution with microchip-based enhanced field inversion electrophoresis," *Electrophoresis*, vol. 24, no. 11, pp. 1777–1786, 2003.

[80] "http://www.probes.com/handbook/sections/0801.html," .

[81] I. V. Kourkine, C. N. Hestekin, S. O. Magnusdottir, and A. E. Barron, "Optimized sample preparation for tandem capillary electrophoresis single-stranded conformational polymorphism/heteroduplex analysis," *Biotechniques*, vol. 33, no. 2, pp. 318–322, 2002.

[82] Z. Ronai, C. Barta, M. Sasvari-Szekely, and A. Guttman, "DNA analysis on electrophoretic microchips: Effect of operational variables," *Electrophoresis*, vol. 22, no. 2, pp. 294–299, 2001.

[83] D. Manage, Y. Zheng, M. Somerville, and C. Backhouse, "On-chip HA/SSCP for the Detection of Hereditary Haemochromatosis," *Microfluidics and Nanofluidics*, 2004, Submitted November 2004.

[84] H. J. Tian, A. Jaquins-Gerstl, N. Munro, M. Trucco, L. C. Brody, and J. P. Landers, "Single-strand conformation polymorphism analysis by capillary and microchip electrophoresis: A fast, simple method for detection of common mutations in brca1 and brca2," *Genomics*, vol. 63, no. 1, pp. 25–34, 2000.

[85] I. L. Medintz, B. M. Paegel, R. G. Blazej, C. A. Emrich, L. Berti, J. R. Scherer, and R. A. Mathies, "High-performance genetic analysis using microfabricated capillary array electrophoresis microplates," *Electrophoresis*, vol. 22, no. 18, pp. 3845–3856, 2001.

[86] G. A. Thomas, D. L. Williams, and S. A. Soper, "Capillary electrophoresis-based heteroduplex analysis with a universal heteroduplex generator for detection of point mutations associated with rifampin resistance in tuberculosis," *Clinical Chemistry*, vol. 47, no. 7, pp. 1195–1203, 2001.

[87] Y. W. Lin, T. C. Chiu, and H. T. Chang, "Laser-induced fluorescence technique for DNA and proteins separated by capillary electrophoresis," *Journal of Chromatography B-Analytical Technologies in the Biomedical and Life Sciences*, vol. 793, no. 1, pp. 37–48, 2003.

[88] D. B. Craig and N. J. Dovichi, "Multiple labeling of proteins," *Analytical Chemistry*, vol. 70, no. 13, pp. 2493–2494, 1998.

[89] S. L. McIntosh, T. G. Deligeorgiev, N. I. Gadjev, and L. B. McGown, "Mono- and bis-intercalating dyes for multiplex fluorescence lifetime detection of DNA restriction fragments in capillary electrophoresis," *Electrophoresis*, vol. 23, no. 10, pp. 1473–1479, 2002.

[90] C. Carlsson, M. Jonsson, and B. Akerman, "Double Bands in DNA Gel-Electrophoresis Caused by Bis-Intercalating Dyes," *Nucleic Acids Research*, vol. 23, no. 13, pp. 2413–2420, 1995.

[91] Y. S. Kim and M. D. Morris, "Separation of nucleic-acids by capillary electrophoresis in cellulose solutions with mono-intercalating and bis-intercalating dyes," *Analytical Chemistry*, vol. 66, no. 7, pp. 1168–1174, 1994.

[92] H. P. Zhu, S. M. Clark, S. C. Benson, H. S. Rye, A. N. Glazer, and R. A. Mathies, "High-Sensitivity Capillary Electrophoresis of Double-Stranded DNA Fragments Using Monomeric and Dimeric Fluorescent Intercalating Dyes," *Analytical Chemistry*, vol. 66, no. 13, pp. 1941–1948, 1994.

[93] S. Rossetti, S. Corra, M. O. Biasi, A. E. Turco, and P. F. Pignatti, "Comparison of heteroduplex and single-strand conformation analyses, followed by ethidium fluorescence visualization, for the detection of mutations in 4 human genes," *Molecular and Cellular Probes*, vol. 9, no. 3, pp. 195–200, 1995.

[94] H. J. Tian, L. C. Brody, and J. P. Landers, "Rapid detection of deletion, insertion, and substitution mutations via heteroduplex analysis using capillary- and microchip-based electrophoresis," *Genome Research*, vol. 10, no. 9, pp. 1403–1413, 2000.

[95] H. J. Tian, L. C. Brody, S. J. Fan, Z. L. Huang, and J. P. Landers, "Capillary and microchip electrophoresis for rapid detection of known mutations by combining allele-specific DNA amplification with heteroduplex analysis," *Clinical Chemistry*, vol. 47, no. 2, pp. 173–185, 2001.

[96] N. Kaji, M. Ueda, and Y. Baba, "Direct measurement of conformational changes on DNA molecule intercalating with a fluorescence dye in an electrophoretic buffer solution by means of atomic force microscopy," *Electrophoresis*, vol. 22, no. 16, pp. 3357–3364, 2001.

[97] R. C. Habbersett and J. H. Jett, "An analytical system based on a compact flow cytometer for DNA fragment sizing and single-molecule detection," *Cytometry Part A*, vol. 60A, no. 2, pp. 125–134, 2004.

[98] A. N. Glazer and H. S. Rye, "Stable Dye-DNA Intercalation Complexes as Reagents for High-Sensitivity Fluorescence Detection," *Nature*, vol. 359, no. 6398, pp. 859–861, 1992.

[99] Q. Gao, L. D. Williams, M. Egli, D. Rabinovich, S. L. Chen, G. J. Quigley, and A. Rich, "Drug-Induced DNA-Repair - X-Ray Structure of a DNA-Ditercalinium Complex," *Proceedings of the National Academy of Sciences of the United States of America*, vol. 88, no. 6, pp. 2422–2426, 1991.

[100] P. S. Andersen, C. Jespersgaard, J. Vuust, M. Christiansen, and L. A. Larsen, "Capillary electrophoresis-based single strand DNA conformation analysis in high-throughput mutation screening," *Human Mutation*, vol. 21, no. 5, pp. 455–465, 2003.

[101] R. Ma, K. Kaler, and C. Backhouse, "A rapid performance assessment method for microfluidic chips," in *ICMENS (The international conference on MEMES, NANO, and Smart Systems)*, W. Badaway and W. Moussa, Eds., Banff, Canada, 2004, pp. 680–686, IEEE Computer Society, Los Alamitos.

[102] T. T. Soong, *Fundamentals of Probability and Statistics for Engineers*. Hoboken, NJ John Wiley and Sons, Ltd. (UK), 2004.

[103] D. R. Johns, "Seminars in Medicine of the Beth-Israel-Hospital, Boston - Mitochondrial-DNA and Disease," *New England Journal of Medicine*, vol. 333, no. 10, pp. 638–644, 1995.

[104] D. C. Wallace, "Mitochondrial diseases in man and mouse," *Science*, vol. 283, no. 5407, pp. 1482–1488, 1999.

[105] S. Anderson, A. T. Bankier, B. G. Barrell, M. H. L. Debruijn, A. R. Coulson, J. Drouin, I. C. Eperon, D. P. Nierlich, B. A. Roe, F. Sanger, P. H. Schreier, A. J. H. Smith, R. Staden, and I. G. Young, "Sequence and Organization of the Human Mitochondrial Genome," *Nature*, vol. 290, no. 5806, pp. 457–465, 1981.

[106] D. A. Clayton, "Structure and Function of the Mitochondrial Genome," *Journal of Inherited Metabolic Disease*, vol. 15, no. 4, pp. 439–447, 1992.

[107] A. Mansouri, I. Gaou, C. De Kerguenec, S. Amsellem, D. Haouzi, A. Berson, A. Moreau, G. Feldmann, P. Letteron, D. Pessayre, and B. Fromenty, "An alcoholic binge causes massive degradation of hepatic mitochondrial DNA in mice," *Gastroenterology*, vol. 117, no. 1, pp. 181–190, 1999.

[108] S. Hajizadeh, J. DeGroot, J. M. TeKoppele, A. Tarkowski, and L. V. Collins, "Extracellular mitochondrial DNA and oxidatively damaged DNA in synovial fluid of patients with rheumatoid arthritis," *Arthritis Research and Therapy*, vol. 5, no. 5, pp. R234–R240, 2003, Article.

[109] A. Mansouri, D. Haouzi, V. Descatoire, C. Demeilliers, A. Sutton, N. Vadrot, B. Fromenty, G. Feldmann, D. Pessayre, and A. Berson, "Tacrine inhibits topoisomerases and DNA synthesis to cause mitochondrial DNA depletion and apoptosis in mouse liver," *Hepatology*, vol. 38, no. 3, pp. 715–725, 2003.

[110] I. J. Holt, A. E. Harding, and J. A. Morganhughes, "Deletions of Muscle Mitochondrial-DNA in Patients with Mitochondrial Myopathies," *Nature*, vol. 331, no. 6158, pp. 717–719, 1988.

[111] D. C. Wallace, G. Singh, M. T. Lott, J. A. Hodge, T. G. Schurr, A. M. S. Lezza, L. J. Elsas, and E. K. Nikoskelainen, "Mitochondrial-DNA Mutation Associated with Lebers Hereditary Optic Neuropathy," *Science*, vol. 242, no. 4884, pp. 1427–1430, 1988.

[112] N. Fukuhara, S. Tokiguchi, K. Shirakawa, and T. Tsubaki, "Myoclonus epilepsy associated with ragged-red fibers (mitochondrial abnormalities) - disease entity or a syndrome - light-microscopic and electron-microscopic studies of 2 cases and review of literature," *Journal of the Neurological Sciences*, vol. 47, no. 1, pp. 117–133, 1980.

[113] H. S. Rosing, L. C. Hopkins, D. C. Wallace, C. M. Epstein, and K. Weidenheim, "Maternally inherited mitochondrial myopathy and myoclonic epilepsy," *Annals of Neurology*, vol. 17, no. 3, pp. 228–237, 1985.

[114] S. G. Pavlakis, P. C. Phillips, S. Dimauro, D. C. Devivo, and L. P. Rowland, "Mitochondrial myopathy, encephalopathy, lactic-acidosis, and strokelike episodes - a distinctive clinical syndrome," *Annals of Neurology*, vol. 16, no. 4, pp. 481–488, 1984.

[115] R. Marotta, J. Chin, A. Quigley, S. Katsabanis, R. Kapsa, E. Byrne, and S. Collins, "Diagnostic screening of mitochondrial DNA mutations in Australian adults 1990-2001," *Internal Medicine Journal*, vol. 34, no. 1-2, pp. 10–19, 2004.

[116] H. Ahmadzadeh, R. D. Johnson, L. Thompson, and E. A. Arriaga, "Direct sampling from muscle cross sections for electrophoretic analysis of individual mitochondria," *Analytical Chemistry*, vol. 76, no. 2, pp. 315–321, 2004.

[117] A. Wong, L. Cavelier, H. E. Collins-Schramm, M. F. Seldin, M. McGrogan, M. L. Savontaus, and G. A. Cortopassi, "Differentiation-specific effects of LHON mutations introduced into neuronal NT2 cells," *Human Molecular Genetics*, vol. 11, no. 4, pp. 431–438, 2002.

[118] A. Guttman, H. G. Gao, and R. Haas, "Rapid analysis of mitochondrial DNA heteroplasmy in diabetes by gel-microchip electrophoresis," *Clinical Chemistry*, vol. 47, no. 8, pp. 1469–1472, 2001.

[119] D. B. Seifer, V. DeJesus, and K. Hubbard, "Mitochondrial deletions in luteinized granulosa cells as a function of age in women undergoing in vitro fertilization," *Fertility and Sterility*, vol. 78, no. 5, pp. 1046–1048, 2002.

[120] C. A. Piggee, J. Muth, E. Carrilho, and B. L. Karger, "Capillary electrophoresis for the detection of known point mutations by single-nucleotide primer extension and laser-induced fluorescence detection," *Journal of Chromatography A*, vol. 781, no. 1-2, pp. 367–375, 1997.

[121] M. A. Marino, K. R. Weaver, L. A. Tully, J. E. Girard, and P. Belgrader, "Characterization of mitochondrial DNA using low-stringency single specific primer amplification analyzed by laser induced fluorescence - Capillary electrophoresis," *Electrophoresis*, vol. 17, no. 9, pp. 1499–1504, 1996.

[122] K. Srinivasan, J. E. Girard, P. Williams, R. K. Roby, V. W. Weedn, S. C. Morris, M. C. Kline, and D. J. Reeder, "Electrophoretic Separations of Polymerase Chain Reaction-Amplified DNA Fragments in DNA Typing Using a Capillary Electrophoresis Laser-Induced Fluorescence System," *Journal of Chromatography A*, vol. 652, no. 1, pp. 83–91, 1993.

[123] A. Guttman, "Automated DNA fragment analysis by high performance ultrathin-layer agarose gel electrophoresis," *Lc Gc North America*, vol. 17, no. 11, pp. 1020–+, 1999.

[124] L. Ding, K. Williams, W. Ausserer, L. Bousse, and R. Dubrow, "Analysis of plasmid samples on a microchip," *Analytical Biochemistry*, vol. 316, no. 1, pp. 92–102, 2003.

[125] J. Bednar, P. Furrer, A. Stasiak, J. Dubochet, E. H. Egelman, and A. D. Bates, "The Twist, Writhe and Overall Shape of Supercoiled DNA Change During Counterion-Induced Transition from a Loosely to a Tightly Interwound Superhelix - Possible Implications for DNA-Structure in-Vivo," *Journal of Molecular Biology*, vol. 235, no. 3, pp. 825–847, 1994.

[126] N. C. Meisner, P. Hammerl, and K. Pittertschatscher, "High performance capillary gel electrophoresis as a method to separate plasmid-DNA cloning vectors with very high resolution (below 100 bp) and its application in molecular biology," *Journal of Microcolumn Separations*, vol. 12, no. 2, pp. 75–86, 2000.

[127] S. Nathakarnkitkool, P. Oefner, G. Bartsch, M. A. Chin, and G. K. Bonn, "High-Resolution Capillary Electrophoretic Analysis of DNA in Free Solution," *Electrophoresis*, vol. 13, no. 1-2, pp. 18–31, 1992.

[128] B. R. McCord, J. M. Jung, and E. A. Holleran, "High-Resolution Capillary Electrophoresis of Forensic DNA Using a Non-Gel Sieving Buffer," *Journal of Liquid Chromatography*, vol. 16, no. 9-10, pp. 1963–1981, 1993.

[129] H. J. Tian and J. P. Landers, "Hydroxyethylcellulose as an effective polymer network for DNA analysis in uncoated glass microchips: optimization and application to mutation detection via heteroduplex analysis," *Analytical Biochemistry*, vol. 309, no. 2, pp. 212–223, 2002.

[130] H. Oana, R. W. Hammond, J. J. Schwinefus, S. C. Wang, M. Doi, and M. D. Morris, "High-speed separation of linear and supercoiled DNA by capillary electrophoresis. Buffer, entangling polymer, and electric field effects," *Analytical Chemistry*, vol. 70, no. 3, pp. 574–579, 1998.

[131] D. T. Mao, J. D. Levin, L. Y. Yu, and R. M. A. Lautamo, "High-resolution capillary electrophoretic separation of supercoiled plasmid DNAs and their conformers in dilute hydroxypropylmethyl cellulose solutions containing no intercalating agent," *Journal of Chromatography B*, vol. 714, no. 1, pp. 21–27, 1998.

[132] S. Gurrieri, S. B. Smith, and C. Bustamante, "Trapping of megabase-sized DNA molecules during agarose gel electrophoresis," *Proceedings of the National Academy of Sciences of the United States of America*, vol. 96, no. 2, pp. 453–458, 1999.

[133] I. Ohsugi, Y. Tokutake, N. Suzuki, T. Ide, M. Sugimoto, and Y. Furuichi, "Telomere repeat DNA forms a large non-covalent complex with unique cohesive properties which is dissociated by Werner syndrome DNA helicase in the presence of replication protein A," *Nucleic Acids Research*, vol. 28, no. 18, pp. 3642–3648, 2000.

[134] G. Singh, W. W. Hauswirth, W. E. Ross, and A. H. Neims, "A Method for Assessing Damage to Mitochondrial-DNA Caused by Radiation and Epichlorohydrin," *Molecular Pharmacology*, vol. 27, no. 1, pp. 167–170, 1985.

[135] M. Vazquez-Acevedo, M. E. Vazquez-Memije, O. M. Mutchinick, J. J. Morales, G. Garcia-Ramos, and D. Gonzalez-Halphen, "A case of kearns-sayre syndrome with the 4,977-bp common deletion associated with a novel 7,704-bp deletion," *Neurological Sciences*, vol. 23, no. 5, pp. 247–250, 2002.

[136] "www.gen.emory.edu/mitomap.html," .

[137] K. Helmle, "mtDNA polymorphisms as genetic cancer markers," M.S. thesis, University of Alberta, Edmonton, 2004.

[138] T. Vanecek, F. Vorel, and M. Sip, "Mitochondrial DNA D-loop hypervariable regions: Czech population data," *International Journal of Legal Medicine*, vol. 118, no. 1, pp. 14–18, 2004.

[139] B. Parfait, P. Rustin, A. Munnich, and A. Rotig, "Coamplification of nuclear pseudogenes and assessment of heteroplasmy of mitochondrial DNA mutations," *Biochemical and Biophysical Research Communications*, vol. 247, no. 1, pp. 57–59, 1998.

[140] A. Eon-Duval and G. Burke, "Purification of pharmaceutical-grade plasmid DNA by anion-exchange chromatography in an RNase-free process," *Journal of Chromatography B-Analytical Technologies in the Biomedical and Life Sciences*, vol. 804, no. 2, pp. 327–335, 2004.

[141] A. Eon-Duval, R. H. MacDuff, C. A. Fisher, M. J. Harris, and C. Brook, "Removal of RNA impurities by tangential flow filtration in an RNase-free plasmid DNA purification process," *Analytical Biochemistry*, vol. 316, no. 1, pp. 66–73, 2003.

[142] H. Enzmann, C. Kuhlem, E. Loser, and P. Bannasch, "Damage to Mitochondrial-DNA Induced by the Hepatocarcinogen Diethylnitrosamine in Ovo," *Mutation Research-Fundamental and Molecular Mechanisms of Mutagenesis*, vol. 329, no. 2, pp. 113–120, 1995.

[143] M. S. Levy, I. J. Collins, J. T. Tsai, P. A. Shamlou, J. M. Ward, and P. Dunnill, "Removal of contaminant nucleic acids by nitrocellulose filtration during pharmaceutical-grade plasmid DNA processing," *Journal of Biotechnology*, vol. 76, no. 2-3, pp. 197–205, 2000.

[144] Z. J. Wang, G. W. Le, Y. H. Shi, and G. Wegrzyn, "Purification of plasmid DNA using a multicompartment electrolyser separated by ultrafilter membranes," *Biotechnology Letters*, vol. 24, no. 2, pp. 121–124, 2002.

[145] E. Stellwagen, "Gel-filtration," *Methods in Enzymology*, vol. 182, pp. 317–328, 1990.

[146] L. Fischer, *Gel filtration chromatography*, 2nd ed., vol. 1. Amsterdam : Elsevier/North-Holland Biomedical Press, 1980.

[147] S. Uchiyama, T. Imamura, S. Nagai, and K. Konishi, "Separation of Low-Molecular Weight RNA Species by High-Speed Gel-Filtration," *Journal of Biochemistry*, vol. 90, no. 3, pp. 643–648, 1981.

[148] D. S. Burgi and R. L. Chien, "Optimization in sample stacking for high-performance capillary electrophoresis," *Analytical Chemistry*, vol. 63, no. 18, pp. 2042–2047, 1991.

[149] P. R. Cook, "A General-Method for Preparing Intact Nuclear-DNA," *Embo Journal*, vol. 3, no. 8, pp. 1837–1842, 1984.

[150] C. J. Backhouse, H. J. Crabtree, and D. M. Glerum, "Frontal analysis on a microchip," *Analyst*, vol. 127, no. 9, pp. 1169–1175, 2002.

[151] M. Levy, P. Lotfian, R. O'Kennedy, M. Lo-Yim, and P. Shamlou, "Quantitation of supercoiled circular content in plasmid DNA solutions using a fluorescence-based method," *Nucleic Acids Research*, vol. 28, no. 12, pp. E57–e57, 2000.

APPENDIX : List of the samples used in chapter 4

Sample	DNA Stock Conc.	Orig. Vol./Remained Vol.
mtDNA (untreated)	300ng/μL	6 μL/0μL
Diluted mtDNA (untreated)	15ng/μL	20μL/3μL
mtDNA plus RNAse	30ng/μL	10 μL/3μL
Rho0 DNA	15ng/μL	NA/100μL
MDL template DNA	15ng/μL	NA/50μL
mtDNA purified by gel filtration	20ng/μL	50μL/30μL
Supercoiled DNA Ladder	250ng/μL	25μL/20μL

All the samples are stored frozen at -20°C in a box labeled as "mtDNA BOX".